SANDIA REPORT

SAND2016-4293
Unlimited Release
Printed April 2015 for internal review, revised April 2016 for public release

A comparison of WEC control strategies

David Wilson, Giorgio Bacelli, Ryan G. Coe, Diana L. Bull
Ossama Abdelkhalik, Umesh A. Korde, Rush D. Robinett III

Prepared by
Sandia National Laboratories
Albuquerque, New Mexico 87185 and Livermore, California 94550

Sandia National Laboratories is a multi-program laboratory managed and operated by Sandia Corporation, a wholly owned subsidiary of Lockheed Martin Corporation, for the U.S. Department of Energy's National Nuclear Security Administration under contract DE-AC04-94AL85000.

Sandia National Laboratories

Issued by Sandia National Laboratories, operated for the United States Department of Energy by Sandia Corporation.

Available to DOE and DOE contractors from
U.S. Department of Energy
Office of Scientific and Technical Information
P.O. Box 62
Oak Ridge, TN 37831

Telephone: (865) 576-8401
Facsimile: (865) 576-5728
E-Mail: reports@adonis.osti.gov
Online ordering: http://www.osti.gov/bridge

Available to the public from
U.S. Department of Commerce
National Technical Information Service
5285 Port Royal Rd
Springfield, VA 22161

Telephone: (800) 553-6847
Facsimile: (703) 605-6900
E-Mail: orders@ntis.fedworld.gov
Online ordering: http://www.ntis.gov/help/ordermethods.asp?loc=7-4-0#online

SAND2016-4293
Unlimited Release
Printed April 2015 for internal review, revised
April 2016 for public release

A comparison of WEC control strategies

David G. Wilson
Sandia National Laboratories
P.O. Box 5800, MS 1152
Albuquerque, NM 87185
dwilso@sandia.gov

Giorgio Bacelli
Sandia National Laboratories
P.O. Box 5800, MS 1124
Albuquerque, NM 87185
gbacell@sandia.gov

Ryan G. Coe
Sandia National Laboratories
P.O. Box 5800, MS 1124
Albuquerque, NM 87185
rcoe@sandia.gov

Diana L. Bull
Sandia National Laboratories
P.O. Box 5800, MS 1124
Albuquerque, NM 87185
dlbull@sandia.gov

Ossama Abdelkhalik
Michigan Technological University
1400 Townsend Dr
Houghton, MI 49931
ooabdelk@mtu.edu

Umesh A. Korde
South Dakota School of Mines and Technology
501 E St Joseph St
Rapid City, SD 57701
Umesh.Korde@sdsmt.edu

Rush D. Robinett III
Michigan Technological University
1400 Townsend Dr
Houghton, MI 49931
rdrobine@mtu.edu

Acknowledgment

This study was supported by the Department of Energy (DOE), Office of Energy Efficiency and Renewable Energy (EERE), Wind and Water Power Technologies Office (WWPTO). Sandia National Laboratories is a multi-program laboratory managed and operated by Sandia Corporation, a wholly owned subsidiary of Lockheed Martin Corporation, for the U.S. Department of Energy's National Nuclear Security Administration under contract DE-AC04-94AL85000.

Contents

Appendix

List of Figures

List of Tables

Executive Summary

The operation of Wave Energy Converter (WEC) devices can pose many challenging problems to the Water Power Community. A key research question is how to significantly improve the performance of these WEC devices through improving the control system design. This report summarizes an effort to analyze and improve the performance of WEC through the design and implementation of control systems. Controllers were selected to span the WEC control design space with the aim of building a more comprehensive understanding of different controller capabilities and requirements. To design and evaluate these control strategies, a model scale test-bed WEC was designed for both numerical and experimental testing (see Section 1.1). Seven control strategies have been developed and applied on a numerical model of the selected WEC. This model is capable of performing at a range of levels, spanning from a fully-linear realization to varying levels of nonlinearity. The details of this model and its ongoing development are described in Section 1.2.

In Chapter 3.1 of this report, six advanced control strategies and baseline resistive control are tested using a linear performance model. Average annual power (AAP) predictions for each strategy (given a Newport, OR deployment site) are shown in Table 1. Additionally, percent increases in AAP over the baseline Resistive controller are shown. In general, the chosen controllers are capable of increasing the average annual power production by more than 100% (300% improvements in power absorption were predicted in individual sea-states; see example in Figure 1). These results not only corroborate the improvements seen in literature [2], they actually instill a higher level of confidence in controls making meaningful impacts since: the device studied innately possesses broad absorption characteristics, these results represent average annual increases (as opposed to point increases), and the incorporation of initial nonlinearities has not significantly altered the percentage increase. Results employing a nonlinear version of the Performance Model are presented in Section 3.2.

Table 1: Average annual power (AAP) production in a Newport, OR deployment climate for various control strategies implemented on a linear system. Similar results are found when implemented on the nonlinear system studied (see Section 3.2).

Strategy	**AAP [kW]**	**Increase [%]**
Resistive	15.5	—
MPC	46.1	197
DP	38.4	148
SB	22.6	46
LQ	39.8	157
PDC3	26.3	73
Latching	28.8	86

These results confirm the project expectation that control strategies can increase the power absorption by a significant margin, beyond a factor of two. Although encouraging, there are

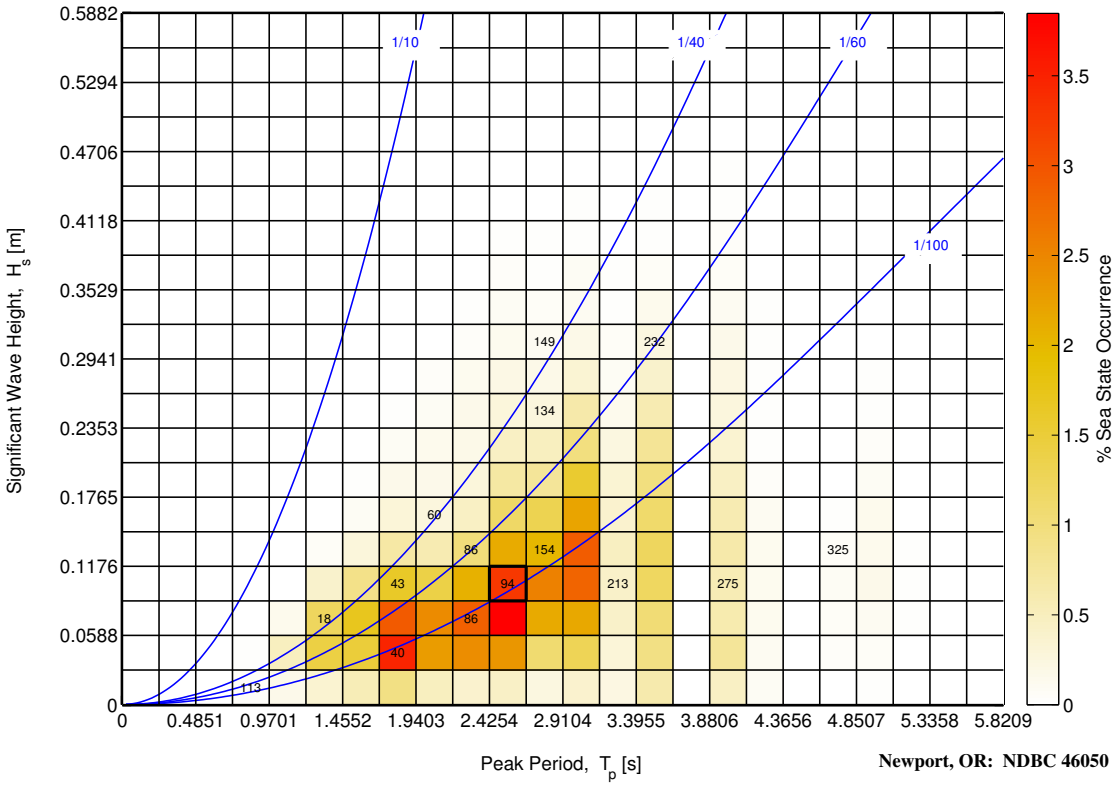

Figure 1: Percentage increase in power obtained with the LQ control strategy.

many significant steps remaining before such gains can be realized by full scale WEC devices. These steps fundamentally revolve around an upgraded performance model, capable of realistic and physical nonlinear predictions in 5DoF, as well as controllers targeted to work in this more complex/realistic system.

Chapter 1

System Description and Modeling

This chapter describes the system on which this control study was completed. Specifically, a discussion of the test-bed WEC and its design process is presented. Next, the numerical model used to represent this WEC is introduced. Lastly, the wave environments used for control evaluation are summarized.

1.1 T3R2 Design

An initial parametric shape study was completed on 6 fundamental float geometries with varying radii and drafts. A total of 54 device profiles were studied. For each of these shapes, higher-order panels representing the three-dimensional wetted surface were used to model the submerged geometry in a BEM potential flow solver [3]. Utilizing the shapes' planes of symmetry ($x = 0$ and $y = 0$), one quarter of each shape was modeled. For each of the shapes, the excitation and radiation hydrodynamic coefficients (both in the frequency domain (FD) and in the time domain (TD)) were compared as functions of parameters that characterize each geometry.

This study highlighted the superior radiation properties of cones in relation to the other shapes. Since all good wave absorbers are good wavemakers, this device will naturally have better wave absorption characteristics (without control augmentation) than most other control comparisons previously published. In order to allow for systematic testing stages to occur in mostly linear conditions, the project required that the wetted profile around the equilibrium free surface have a constant water plane area (i.e. a vertical side-wall). These considerations led to the selection of a truncated cone as the basic shape of the device. For the selected truncated cone design, more in depth analysis was completed to determine the device's performance in the MASK basin. A total of 37 devices were studied by varying the following aspect ratios

- Ratio of the top radius to the total draft
- Ratio of the top radius to the bottom radius
- Ratio of the draft to the vertical wall draft.

In addition to the hydrodynamic analysis, a FD model [4], which incorporated the T3R2's dynamics with the hydrostatic/hydrodynamic parameters determined via WAMIT, was used to predict

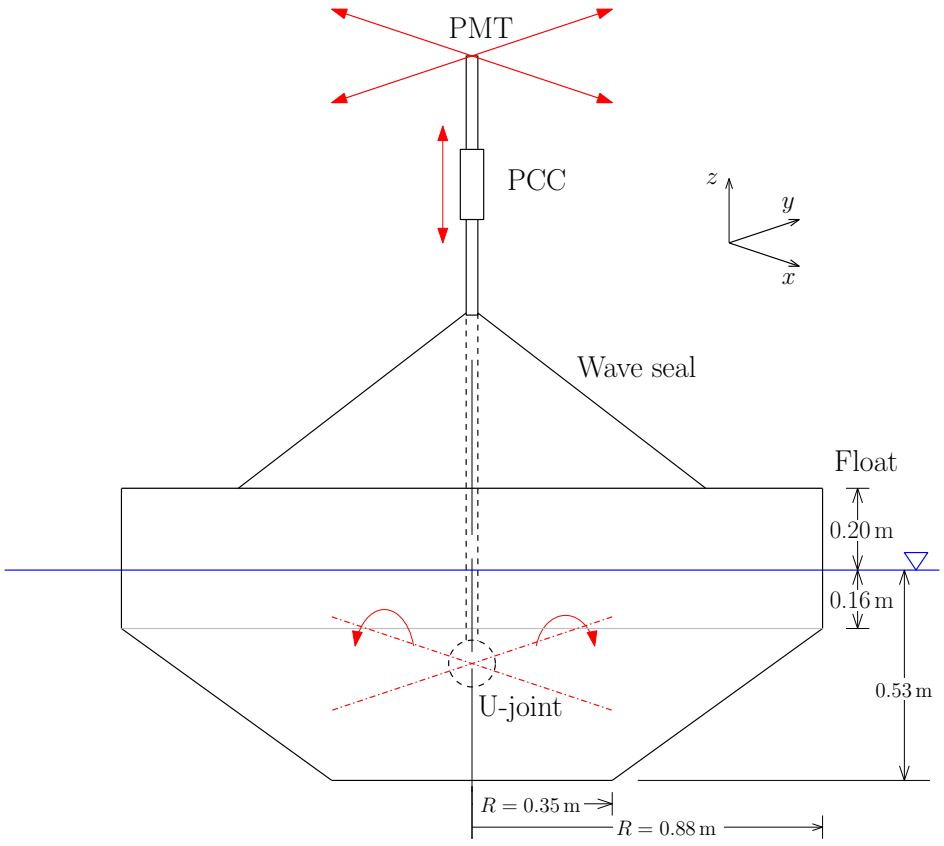

Figure 1.1: T3R2 final design with dimensions.

performance of the device within the MASK basin. Additional considerations that influenced the final shape selection will be presented in an upcoming conference publication (not yet determined when / where). The final T3R2 ("three-translations, two-rotations") design is illustrated in Figure 1.1.

Figure 1.2 illustrates the absorption capabilities in regular waves, when resistive control is applied (baseline), of the T3R2 compared to the set of geometries depicted in Figure 1.3, which is a subset of the geometries studied. All the shapes have been selected to resonate for waves with period $T_{res} = 1.6$ s; therefore, at resonance and in ideal conditions[1], they all absorb the same amount of power (all the curves in Figure 1.2 take the same value for $T = 1.6$ s, which is equal to the amount of power transported by the wave, denoted by the curve J/k). A sphere and two cylinders have been used for comparison because they are the most commonly used shapes for the study of wave energy converters (see for example [5–8]). The sphere, at equilibrium, is semi-submerged as in [9] and the radius has been determined by imposing the resonance period. Two cylinders have been included in the comparison to highlight the striking difference in their absorption characteristics, when changing the ratio between draft and radius. The narrow cylinder has a ratio draft/radius = 1.5 and a draft approximately equal to the draft of the T3R2, whereas the wide cylinder has a ratio draft/radius = 0.3 and a radius approximately equal to the radius of the T3R2.

[1] ideal conditions: no viscous effects, linear models are valid

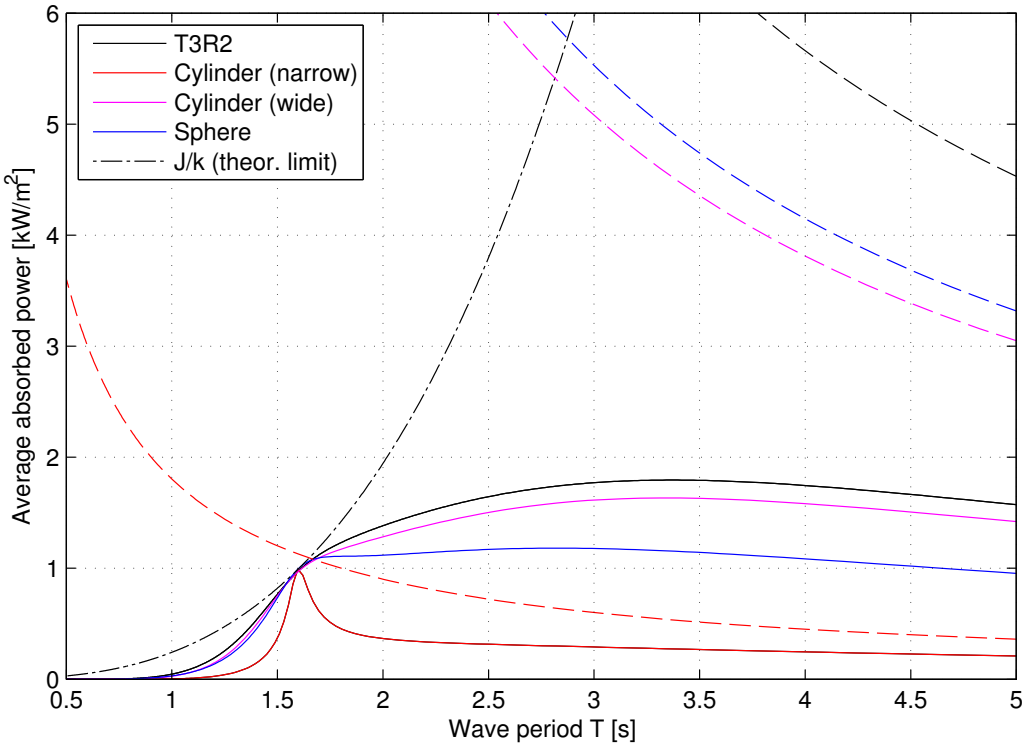

Figure 1.2: Average absorbed power normalized over square of wave amplitude. The dash-dotted curve is the upper bound due to the power transported by waves (e.g. wave energy transport). For each solid curve of any given color denoting the average absorbed power of a specific shape, there is a corresponding dashed curve of the same color denoting the Budal upper bound for that shape (i.e. the device-specific limit).

Figure 1.2 shows that the T3R2 outperforms all the other shapes in terms of power absorption over the entire range of wave periods. Additionally, the T3R2 shape has the largest radiation damping among all the shapes and, as a consequence, the largest power absorption is obtained with the smallest oscillation amplitude, as shown in Figure 1.4. Furthermore, the T3R2 has the largest Budal upper bound[2] (black dashed curve) due to the fact that it has the largest volume. In practice, due to to the superior performance of the T3R2 when compared to the other simpler shapes, like cylinders or spheres, the selected geometry is the most suitable for experimental testing.

The value of the resonance period has been selected based on the capability of the wave basin that will be used for experimental testing. In particular, the resonance period has been chosen to be within the range of wave periods that can be generated by the wavemakers, thus allowing the control strategies to be tested for waves both above and below the resonance of the device.

[2]Upper bound for the average absorbed power in heave, due to the maximum amount of displaced water

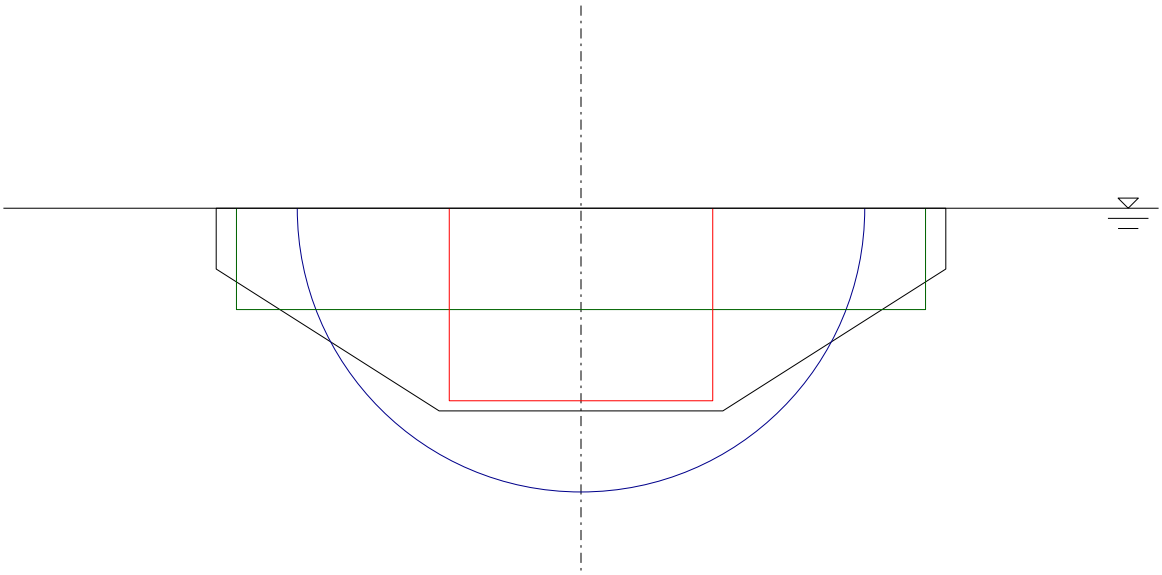

Figure 1.3: Sections of the floating bodies considered for the comparison: T3R2 (black); wide cylinder (green); narrow cylinder (red); sphere (blue)

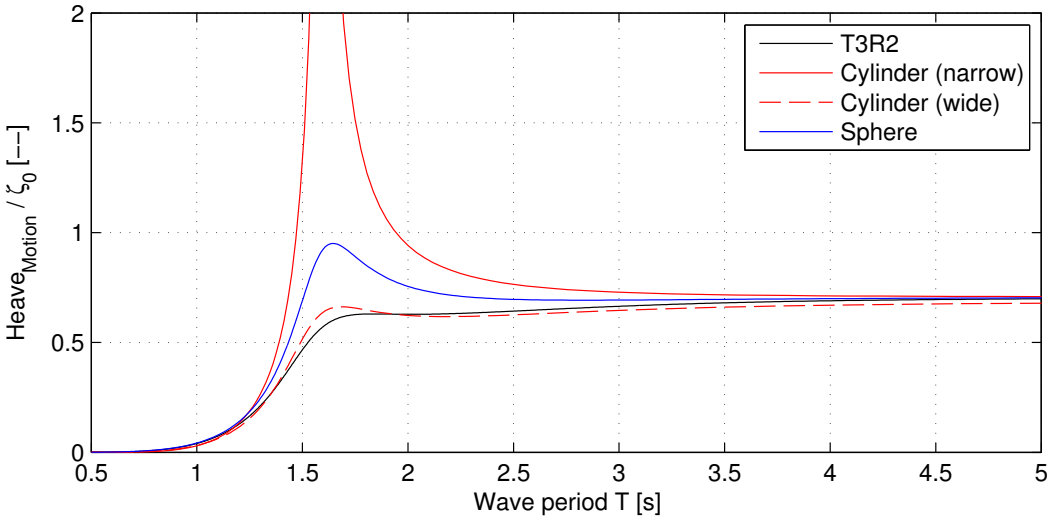

Figure 1.4: Normalized heave motion

1.2 Performance Model

A numerical "Performance Model," has been developed to simulate the performance and dynamics of the T3R2. This Performance Model serves a number of needs:

- **Assessment of control strategies** - the model can be used to assess the performance of control strategies (i.e. as a "numerical experiment")
- **Feed-forward control** - the model or a version of the model can be used as the controller model in feed-forward control strategies to provide dynamic predictions
- **Wave tank test preparation** - the model can be used to inform the design of the physical model and experimental testing

1.2.1 Model Description

A detailed description of the model has been documented in two papers [4, 10]; a brief description will be given here. The Performance Model, which is based on the formulation suggested by Cummins [11], uses superposition to combine the effects of different physical phenomena including:

- **Hydrostatics and gravitational** - Stiffness effects due to the hydrostatic/gravitational couple
- **Wave radiation** - Damping due to the creation of waves
- **Wave diffraction** - Excitation due to incident waves
- **Viscous damping** - Damping due to viscous effects in water
- **PCC input** - Reactions due to PCC force; these may be either control input or end-stop reactions
- **Mooring system** - Reactions due to the T3R2's mooring system, including restoring and frictional components

These components are combined, along with inertial effects, via nonlinear kinematic coupling in a numerical model capable of predicting T3R2's motion in all 5 degrees of freedom. The equations for the motion for the T3R2 are given by

$$\left[\underbrace{\mathbf{M}_{RB}}_{\substack{\text{rigid-body}\\ \text{mass of float}}} + \underbrace{\mathbf{A}_{\infty}}_{\substack{\text{added mass}\\ \text{of float}}} + \mathbf{J}^{\mathrm{T}}(\vartheta)\underbrace{(\mathbf{M}_{PCC}+\mathbf{M}_{PMT})}_{\substack{\text{rigid-body}\\ \text{mass of}\\ \text{PCC and PMT}}}\mathbf{J}^{-1}(\vartheta)\right]\ddot{\xi}$$

$$+\underbrace{\left[\mathbf{J}^{\mathrm{T}}(\vartheta)\left(\mathbf{M}_{PCC}+\mathbf{M}_{PMT}\right)\dot{\mathbf{J}}\left(\vartheta,\dot{\vartheta}\right)+\mathbf{C}(\dot{\xi})\right]\dot{\xi}}_{\substack{\text{Coriolis-centripetal}\\ \text{effects}}} \tag{1.1}$$

$$+\underbrace{\int_0^t \mathbf{K}_r(t-\lambda)\dot{\xi}(\lambda)\,d\lambda}_{\substack{\text{radiation}\\ \text{damping}}} + \mathbf{J}(\vartheta)^{\mathrm{T}}\left[\underbrace{\tau_h(\eta)}_{\substack{\text{hydrostatic-}\\ \text{gravitational}}} + \underbrace{\tau_m(\eta)}_{\text{mooring}}\right] + \underbrace{\tau_v(\dot{\xi})}_{\substack{\text{viscous}\\ \text{damping}}} = \underbrace{\tau_e}_{\substack{\text{wave}\\ \text{excitation}}} + \underbrace{\tau_u}_{\substack{\text{control}\\ \text{input}}}.$$

A full explanation of (1.1) and its nomenclature is given in [4, 10].

1.2.2 Model Configurations

The Performance Model was designed to allow for a high degree of reconfigurability, enabling the model to assume forms ranging from fully-linear to highly nonlinear. Three model configurations were considered to assess controller performance in this study. The first of these configurations, referred to as CONFIG-B, gives a fully-linear, single DoF model. This model reduces to the classic linear state-space formulation (i.e. $\dot{x} = \mathbf{A}x + \mathbf{B}u$; $y = \mathbf{C}x + \mathbf{D}u$) (see, e.g., [4, 5]). Results and analysis conducted with this model are discussed in Section 3.1. CONFIG-D4 is a single DoF model that includes some nonlinearities inherent to the actual T3R2 (quadratic viscous damping, end-stops to limit PCC extension and a saturation limit on the force supplied by the PCC). CONFIG-D3 is the same as D4, except the PCC force saturation level is much larger. Results from simulations conducted with CONFIG-D4 and D3 are discussed in Section 3.2. The specific submodels that make up each of these configurations are summarized in Table 1.1.

The methodology for determining the linear and quadratic viscous damping coefficients in CONFIG-B and CONFIG-D3/D4 respectively were:

- Linear - The linear viscous damping coefficient was chosen to be 2% of the critical damping factor [4, 12].
- Quadratic - Based on some empirically reported values for similar shapes [13], a drag coefficient of $C_d = 1$ was taken for the vertical mode of motion. The viscous drag force in the

Table 1.1: Performance Model configuration details.

Configuration	DOF	Potential flow	Radiation Treatment	Viscous damping	End-stops	PCC force saturation
CONFIG-B	1	Linear	State-space	Linear	∞	∞
CONFIG-D4	1	Linear	State-space	Quadratic	± 0.25 m	2.7 kN
CONFIG-D3	1	Linear	State-space	Quadratic	± 0.25 m	8.0 kN
CONFIG-G	5	Mixed-order	State-space	Quadratic	± 0.75 m	∞

vertical mode due to vertical velocity is given by

$$\tau_{v,3} = \frac{1}{2}\rho S C_d u^2. \tag{1.2}$$

Here, ρ and S are the fluid density and body frontal area respectively. Combining terms, we can include this effect in (1.1) as

$$\begin{aligned} \tau_v &= \mathbf{B}_v \left|\dot{\xi}\right| \dot{\xi} \\ \text{where} \quad \mathbf{B}_{v,3} &= \frac{1}{2}\rho S C_d \end{aligned} \tag{1.3}$$

A fourth model configuration (CONFIG-G) has also been studied to better understand the process of developing higher-order versions of the Performance Model in the future. This model includes fully nonlinear hydrostatic restoring [10].

1.3 Environment

This section describes the ocean wave environments used to assess the performance of control strategies in this report. Regular wave assessments were conducted to allow for a resource-agnostic view on control performance. Irregular wave assessments, based on a deployment location of Newport, OR, were conducted to allow for comparisons of average annual performance.

1.3.1 Regular Waves

A series of regular waves of intermediate steepness ($H/\lambda = \frac{1}{50}$) were simulated; these waves are specified in Table 1.2. The regular wave simulation allows readily allows for comparison to linear

theoretical upper bounds. Hence, monochromatic waves are an important step towards developing a resource-independent assessment of the efficacy of a particular control strategy. As the devices operation becomes dominated by nonlinearities, it is possible that this analysis will no longer hold the same importance.

Table 1.2: List of the regular waves simulated; all waves are for a steepness of $H/\lambda = \frac{1}{50}$.

Period, T [s]	**Height, H [m]**
0.95	0.0282
1.07	0.0357
1.50	0.0702
1.66	0.0860
2.00	0.1249
2.50	0.1949
3.00	0.2787
3.50	0.3704
4.00	0.4640
4.50	0.5565
5.00	0.6469
6.00	0.8222
7.00	0.9920
8.00	1.1580

1.3.2 Irregular Waves

Initial analysis of the control strategies was completed assuming a deployment climate of Newport, OR. A Joint-Probability-Distribution (JPD) is used to assign probabilities of a particular sea-state occurring. With knowledge of the probability and the performance of the device in each sea-state, it is possible to represent the expected average annual performance of the device with a single number. Although this representation loses the fidelity to describe the device performance in great detail, it is still extremely useful in understanding the expected global performance.

According to IEC recommended practices, the significant wave height and period parameter binning must be no larger than 0.5 m and 1 sec when producing a JPD. A full description in this manner results in hundreds of distinct sea-states. For each sea-state, a distinct simulation will be required to predict the performance of the device. In general this is only practical with the use of fast-running, linear, analytically optimized, frequency domain performance models.

Thus, there is a need to evaluate the performance of a device utilizing only a subset of sea-states. Following the work of [14], a cluster analysis was applied to a full JPD in order to determine a subset of sea-states that could be weighted to find the average annual performance value. This

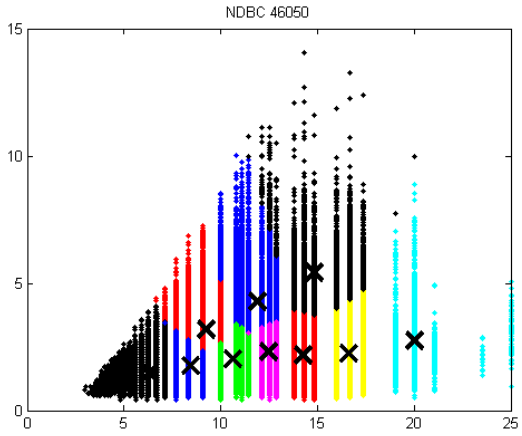

Figure 1.5: Example of k-means clustering results for Newport, OR. Each color set represents the points that are included in determination of the centroid (represented by an X) probability.

subset is found via minimization of the squared Euclidean distance between each point and a cluster centroid. This *k*-means clustering procedure is a built-in MATLAB algorithm within the Statistics Toolbox; the user defines the number of clusters over which the optimization should take place. An iterative partitioning method optimizes the centroid of each cluster and the cluster size by minimizing the sum of point-to-centroid distances, summed over all k clusters. Hence, each sea-state is assigned to an optimally determined cluster centroid that has the minimum point-to-centroid cluster distance. The probability that is then associated with each cluster centroid is the sum of the all of the probabilities within that cluster. Figure 1.5 illustrates the results of this analysis at the Newport, OR deployment site.

These optimally determined values were then evaluated to determine the steepness associated with the sea-state. The mean wave height H_m and average period T_m were used in the determination of the steepness parameter. Slight adjustments were then made to the wave heights in order to obtain the desired steepness values.

With these adjustments, new cluster centroids were selected. Hence, a recalculation of the points to be associated with each centroid was required. The points were again selected through minimization of the squared Euclidean distance using the built in MATLAB function `pdist2`. The probability that was then associated with each cluster centroid was the sum of the all of the probabilities within that cluster.

The weighted power flux from each centroid was then computed by calculating the omnidirectional power flux of the centroid multiplied by the sum of all of the probabilities within the cluster. This value was then compared to the sum of the omnidirectional power flux of each sea-state multiplied by the probability of that sea-state for all members of a particular cluster. The ratio of these two was then multiplied by the probability associated with each cluster centroid so that this cluster methodology would result in an exact replication of the average annual incident wave power flux.

Finally, the total average annual incident wave power flux was calculated using the omnidirec-

Table 1.3: The 10 sea-states that represent the deployment climate and for which average annual metrics will be calculated.

Peak period, T_p [s]	**Significant wave height, H_s [m]**	**Steepness, (H_m,T_m) [-]**	**Occurrence, Ξ [%]**
1.53	0.0871	40	18.5
2.05	0.1039	60	17.2
2.25	0.1875	40	11.3
2.58	0.1194	82	21.1
2.89	0.2523	49	7.6
3.03	0.1363	100	12.8
3.46	0.1283	138	9.2
3.60	0.3195	60	4.9
4.02	0.1320	180	5.8
4.86	0.1617	206	1.6

tional power produced for the cluster centroids and the adjusted probability (Ξ) associated with each centroid. Table 1.3 lists the 10 sea-states chosen through this k-means methodology along with the steepnesses and adjusted weights.

In addition to these 10 sea-states which will define average annual metrics, 7 sea-states were also chosen to lie along constant steepness isolines. By working with constant steepness seas, the power growth is proportional to cubic of the wave period. Although not yet completed, this allows for interpolation of the power across period for a set of constant steepness isolines.

All 17 of the simulated sea-states are shown in Figure 1.6. In this figure, the probability distribution of the Newport OR climate is shown via shading in the background and the indexing number of each sea-state identified in Table 1.4 is associated with the corresponding bin in the JPD. Results for each sea-state will be shown in a scatter diagram following this same format, for instance: average power $< P >$ for each sea-state, the RMS heave motion in each sea-state, the RMS PCC force, etc. Further, in the upper left hand corner, all average annual metrics (calculated from the 10 sea-states in Table 1.3) for the displayed variable will be given.

Table 1.4: Full list of the 17 irregular sea-states simulated.

Sea-State index	**Peak period, T_p [s]**	**Significant wave height, H_s [m]**	**Steepness, (H_m,T_m) [-]**	**Occurrence, Ξ [%]**
1	1.00	0.0247	60	0
2	1.00	0.0148	100	0
3	1.00	0.0370	40	0
4	1.53	0.0871	40	18.5
5	2.00	0.0594	100	0
6	2.05	0.1039	60	17.2
7	2.25	0.1875	40	11.3
8	2.50	0.1545	60	0
9	2.50	0.0927	100	0
10	2.58	0.1194	82	21.1
11	2.89	0.2523	49	7.6
12	3.00	0.3337	40	0
13	3.03	0.1363	100	12.8
14	3.46	0.1283	138	9.2
15	3.60	0.3195	60	4.9
16	4.02	0.1320	180	5.8
17	4.86	0.1617	206	1.6

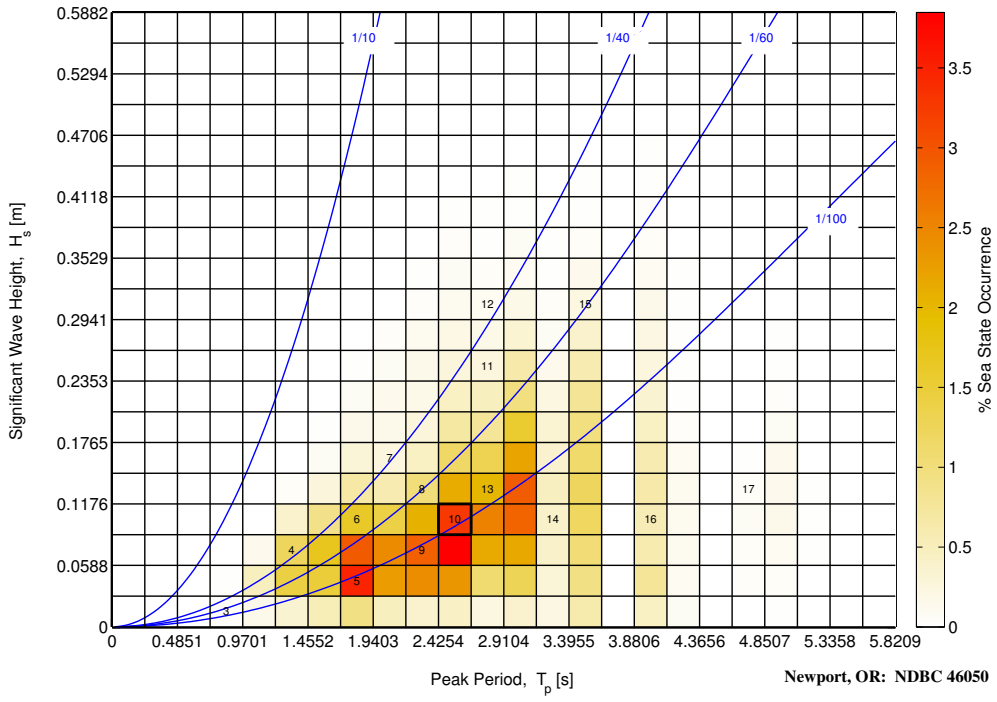

Figure 1.6: Numbering of the sea-state. NOTE: sea-states 1,2 and 3 fall in the same bin.

Chapter 2

Control System Component Descriptions

The majority of power produced by WEC devices occurs during resonant absorption when the excitation force is in phase with device velocity. When the wave climate does not match the structurally defined resonance of the device, the power produced is significantly smaller. A WEC's excitation force and natural resonance are completely dictated by device geometry and the incident wave field. This leaves PTO control as the only mechanism to influence device motion. The primary objective of this project is to extend the "structural-based absorption" (i.e. that defined by device geometry) to a broader controls-based absorption bandwidth. At resonance, the velocity of the device is in phase with the excitation force, thus velocity (both phase and amplitude in the linear sense) is the primary quantity of interest.

2.1 Control Terminology

Identifying particular attributes of the distinct control strategies is necessary in order to understand the advantages, limitations, and intricacies associated with implementation. Classifying control strategies is difficult because there are a myriad of ways to actually develop and implement an individual strategy. The RNLC project has attempted to distill the key characteristics of implementing control strategies on WEC devices. Below, as each of the individual strategies are explained, they will attempt to describe the characteristics of the controller and its implementation.

Figure 2.1 depicts a typical structure of a control system applied, in this particular case, to a WEC. The main purpose of a controller is to alter the dynamic behavior of a given system (WEC) in order to pursue a specific objective (e.g. maximize absorbed power). In general, the architecture of a control system is composed of two main blocks: a feedback (FB) and a feedforward (FF). The name feedback derives from the fact that an output signal (or a set of output signals) is measured and fed back to the control system which continuously reacts, based on the current and past measurements, according to the control objective. Conversely, a controller implemented in feedforward mode generates a control signal based on a reference r which can be pre-determined or calculated from some quantities not related to the state of the system (e.g. incident wave elevation), and it does not react to the instantaneous state of the system (no signal is fed back to the controller). In practice, it is common for control systems to be built by combining both feedback and feedforward.

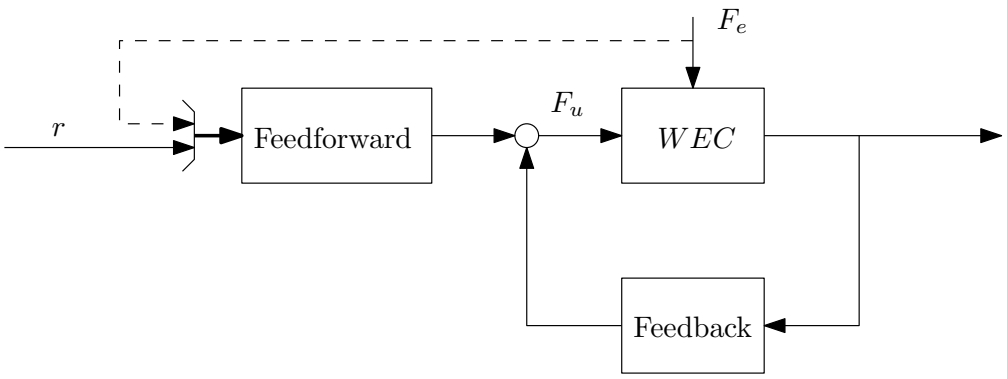

Figure 2.1: High level diagram of controller structure

The design of a controller (either feedback or feedforward) is usually based on a model of the system to be controlled (WEC); this model may be a simplified version of the model used to simulate the behavior of the device (i.e. the "performance model" described in Section 1.2). This model is known as the *controller model* and it may not incorporate complete information about the device dynamics, by either neglecting or approximating part of the "high fidelity model" (performance model). For example, the controller model may describe the WEC only on a reduced set of degrees of freedom (e.g. 1, 3 or 5 DoFs), or it may contain partial information about the hydrodynamics of the WEC by using a Reduced Order Model (ROM) for the radiation force.

Referring to Figure 2.1, both the feedback and the feedforward blocks are control functions relating the input to the output. The feedforward function calculates the control signal from the reference r and the feedback function calculates the control signal form the state x. The design of the control system consists of developing the control functions (FF and FB) by using the controller model with respect to some desired performance objective. This performance is optimized to determine the controller parameters, part of the control functions. Examples of control functions can range from simple gains, in case of a pure feedback strategy, to cost functions, in case the control algorithm is based on an optimization carried out during the implementation (e.g. MPC, further details below). The environment conditions may change during the course of the operation, hence the control functions may need to be updated to reflect these changes. For example varying sea-states may require control function updates. The frequency of these updates are specific to each control strategy. Specifically, the MPC updates the control policy on a wave-to-wave basis (e.g. $\approx 1/10$ of a second), whereas LQ utilized spectral information of the sea-state and the gains are updated at much lower rate (e.g. $\approx$ 30min).

In some cases, the feedback controller is designed to include internal states (x), which are not accessible through output (y) measurements. In these cases, the state estimator is required in the control design (as for the LQ strategy, sec. 2.2.5), to provide an estimate of the internal states and reduce the effect of noisy measurements. Estimator design can be developed following the principles in [15].

The functioning of a control system involves any number of operations or actions that can be carried out online or offline. The distinction between these two terms is based on the subject carrying out the operation and the moment at which is executed. An operation that is performed by

the controller during its active mode is generally called online; an example of an online operation is the periodical optimization of the optimal reference velocity and force carried out by the controller as done in MPC (2.2.2) and DP (2.2.3). However, if the action is carried out before the controller is "turned on" (e.g. design stage), or it is carried out independently from the normal operation of the controller, then it is defined as offline. Examples of offline operations are the calculation of the feedback gain for the PDC3 (Section 2.2.6) and LQ (Section 2.2.5) strategies during controller design.

The calculation of the control signal (PCC force) can be the results of an optimization, which can be done online or offline. In the offline case, for example, the result of the optimization can be the parameters of the controller allowing maximum absorption as in the LQ case (Section 2.2.5). The optimization can also be performed online, as it is done in MPC (Section 2.2.2) and DP (Section 2.2.3), however, requiring more computational resources. Online optimization based algorithms generally require *foreknowledge* of the incoming waves or excitation force for a given prediction time, and the length of the horizon affects the controller's performance. Some insight into the relation between the prediction horizon and the control performance may be gained by examining the dynamics of the WEC (also including the wave-body interaction).

Besides wave foreknowledge, some control strategies, such as LQ (Section 2.2.5) and PDC3 (Section 2.2.6), may require a different type of information, in the form of spectral characteristics of the current sea state (i.e. the significant wave height and the peak period of a Brestchneider spectral distribution).

Optimization based controllers for WECs generally optimize the absorbed power, which is the product of force and velocity. As a byproduct, the optimization produces optimal motion and, as a consequence, these feedforward control strategies can be seen as optimal velocity generators. In turn, these optimal reference velocities can be used as the input to a feedback velocity tracking controller.

The *control variable(s)* in most cases will be the control effort or commanded PTO force that is determined by each specific control strategy and is related to the object being optimized, such as increasing the absorbed power (force times velocity), and the state variable of interest is most commonly selected as the velocity. In general the *control parameter(s)* are those quantities affecting the performance of the controller which are normally determined offline. Tuning these parameters may require some level of heuristics.

The optimal force calculated by the controller is updated regularly; however a feedback control strategy generally has a faster update rate than a feedforward or online optimization based technique. When deploying the controller to a real hardware application, the controller needs to be run in *real-time*. In this context, real-time is defined as the capability of the algorithm to execute within a prescribed update rate.

2.2 Control Strategies

This section introduces the initial control strategies created to improve power for WEC devices. The baseline control strategy is resistive control. All the initial control strategies will be compared to the baseline strategy.

2.2.1 Baseline: Resistive Control

2.2.1.1 General description

Net power capture from a wave-excited oscillating body is a resistive process. The baseline strategy used here is resistive control, consisting of a force proportional to the velocity. Therefore, this control strategy is a pure feedback.

This strategy has been chosen as the baseline strategy because:

- An ability to provide resistive loading is the basic capability built into all power conversion chains,
- Most power conversion chains can also control the amount of resistive loading.

In resistive loading control the constant of proportionality between the force and velocity determines the 'resistance' offered, which is also the power absorption rate. The main drawback is that only the amplitude and not the phase of the velocity can be controlled with this strategy. Power conversion without reactive loading is maximized when the "system" resistance is matched by the power take off resistance. The system resistance equals the sum of (i) the radiation damping in the energy absorbing oscillation mode, and (2) the approximate viscous damping coefficient acting on the oscillation velocity. The strategy is therefore suboptimal at best.

Given that almost any PCC can implement this strategy and that there is no reactive power, there are no special requirements for the PCC, and no foreknowledge of the excitation force is required.

2.2.1.2 Controller Optimization

Optimization of the controller for irregular waves occurs off-line through a numeric approach whereas there is an analytic solution for regular waves. It is straightforward to implement resistive match in regular waves using the radiation damping variation plots and a viscous damping approximation for the oscillation mode of interest. A single control parameter is applied across all frequencies for irregular waves, and hence true optimization cannot occur. Thus the control parameter is selected through numeric optimization routines that are completed offline.

The offline numeric optimization uses as its base the controller model, and multiple controller models were used in this study: CONFIG-B, D4, D3, and G.

2.2.1.3 Controller Model Characteristics

Multiple controller models were used in the design of the controller and the offline optimization of the parameters. The controller model used for the calculation of the optimal damping for both regular and irregular waves is the linear frequency domain version of the CONFIG-B model, which includes frequency dependent radiation. The other controller models, CONFIG-D4, D3, and G, were also used in the calculation of the optimal damping for the irregular waves.

2.2.1.4 Controller Parameter

The controller parameter is the resistive constant of proportionality (damping) that multiplies velocity to give the PCC force at each instant. Additionally, the update rate of the resistive value is another parameter that can be optimized.

2.2.1.5 Improvements - how to move forward

- Update the controller parameter at a faster time scale.

2.2.2 Model Predictive Control (MPC)

2.2.2.1 General description

Model Predictive Control is an optimization based control strategy. It is primarily a feedforward strategy targeting both amplitude and phase implemented in a receding horizon fashion (see Figure A.2). The current state of the system is taken into account at every optimization step and hence there is a feedback loop present (see Figure A.2) in which these states are passed directly to the optimization. The current implementation is valid for a single DOF system using deterministic and perfect wave prediction 8 seconds into the future.

The MPC control strategy has been selected because:

- The control signal is optimal for the predicted excitation force for a linear system. If the prediction is perfect, the control algorithm provides the maximum energy absorption. Hence, this strategy is able to give the theoretical upper bound for a linear model.

- The control algorithm is capable including constraints (force and position) when calculating the optimal control signal; the current implementation only allows constraints defined as linear functions of state and control.

The main drawbacks are the requirement of excitation force prediction and, in some cases (e.g. when the prediction horizon is very long and/or constraints are very stringent), the large computational power required for solving the optimization problem in a timely manner suitable for real-time implementation. An MPC control strategy has been tested experimentally in [16]. This experiment resulted in improved experimental performance, by $\approx$20%, over linear damping in one irregular sea state despite considerable experimental complications.

The control algorithm requires the WEC to use reactive power; therefore, the algorithm requires high efficiency and 4-quadrant capabilities from the PCC. Additionally, MPC is suitable for real-time implementation as the quadratic programming problem, if convex, can be solved very efficiently (quickly). The control signal resulting from the optimization is the force required to control the PCC optimally.

Although this strategy is not novel with respect to its implementation on a WEC, it's ability to provide the theoretical upper limit for a linear system with linear constraints makes its implementation important.

2.2.2.2 Controller Optimization

MPC is an optimization based control strategy that is derived from attempting to solve a Quadratic Program (QP) in an online optimization. The QP is composed of a cost function, which is quadratic in the state (i.e. position, velocity and radiation) and in the control (i.e. PCC force), and of a set of constraints which are linear in the state and control. The control signal (PCC force) is updated periodically by solving the QP. Since the cost function depends on the current state of the system and on the future values of the excitation force, this control strategy requires both a state estimator and predictor for the excitation force.

2.2.2.3 Controller model characteristics

The controller model, CONFIG-B, is a linear, state space model described in the standard matrix form (A,B,C,D) for a 1 DoF heaving buoy. The frequency-dependent radiation is included into the controller model in state space form.

2.2.2.4 Parameters

The control algorithm allows the specification of a number parameters, namely the weighting matrices Q, H and R of the Linear Quadratic optimization problem. Additionally, the particular im-

plementation described in [7] includes weights to penalize 2-norm of the control signal and its derivative.

The control strategy has been upgraded to include constraints on the maximum allowed PCC force and oscillation amplitude, and additional penalties on the 2-norm of the mean value of the position and of the PCC force.

For the particular implementation, the weighting matrices Q, H and R are completely defined by the problem specification, that is the controller model and the objective of the optimization (see Section A.1). However, the Q and R matrices can be used to approximate the constraints on the position and on the PCC force, resulting in an unconstrained quadratic optimization problem which is faster to solve and less computationally demanding.

An additional parameter is the prediction horizon.

2.2.2.5 Improvements - how to move forward

- Design and implement excitation force predictor.
- Include improved model of the PCC
- Design controller using multi DoF controller model.

2.2.3 Dynamic Programming (DP)

2.2.3.1 General description

Dynamic programming is a useful mathematical technique for making a sequence of interrelated decisions. It provides a systematic procedure for determining the optimal combination of decisions [17]. There is no standard mathematical formulation of the dynamic programming problem; unlike other techniques like linear programming, DP is a general approach to problem solving. Hence the implementation of DP requires developing a tailored algorithm and equations for the particular application. In this WEC optimal control problem, the space-time domain is discretized. At each time node, the problem can be thought of as searching for the optimal control (decision) at that time such that the extracted energy is maximized over a given future horizon.

Dynamic Programming (DP) is primarily a feedforward strategy targeting both amplitude and phase implemented in a receding horizon fashion (see Figure A.2). Like MPC, the current state of the system is used to initialize the optimization process and hence there is a feedback loop in which these states are passed directly to the optimization. This current implementation requires a deterministic foreknowledge (the prediction block in Figure A.2). The length of the foreknowledge horizon ranges from 1 to 3 wave peak periods.

The DP control strategy has been selected because:

- DP can be used on highly nonlinear systems and it will always search for the optimal solutions. Hence, this strategy is capable of defining the upper bound for the achievable power for a non-linear WEC device. Stochastic optimization techniques, such as genetic algorithms, also search for global optimal solutions. Unlike DP, these stochastic methods do not guarantee finding the optimal solutions even when sufficient computational resources are available [18]. Hence, DP is the best strategy for producing the the upper bound for a nonlinear system.
- DP is capable of handling constraints. In particular in the current implementation, constraints on the states boundaries and control are forced.

The control algorithm requires the WEC to use reactive power.

Implementation of this strategy on a WEC system, with radiation states included, is novel. It is not likely that DP will be a candidate for a real-time control strategy to be implemented in the wave tank due to its high computational costs. Expansion of the strategy to multi-DoF's and more nonlinear cases is essential in order to provide an upper bound to the nonlinear control problem.

2.2.3.2 Controller Optimization

The basis of the dynamic programming approach is the Bellman's principle of optimality [19]. An optimal sequence of decisions has the property that at any stage (time) the remaining decisions

must be optimal for the remaining problem with the decision and state resulting from the previous decision considered as initial conditions.

In DP the states, time and control, are discretized. The DP optimization approach searches for the global optimal solution through online numeric optimization, i.e. each step is evaluated for given set of states and compared with one another. DP requires a priori knowledge about the states and control boundaries. For instance, in the current implementation, maximum and minimum boundaries on the buoy's position and velocity are needed so that the domain between these boundaries can be discretized. The size of the grid affects the obtained accuracy, optimality of the solution, as well as the required computational time and resources. Finer grids result in better solutions, yet they require long computational times.

The online numeric optimization uses as its base the controller model, and only one controller model was used in this study: CONFIG-B. However, theoretically, any controller model can be used for online optimization with computational efficiency the only drawback.

2.2.3.3 Controller model characteristics

In the current implementation, the controller model is CONFIG-B; it is the state space model described in the standard matrix form (A,B,C,D) for a linear 1 DoF heaving buoy. The controller model is composed of a linear model of the WEC and a linear model of the spectral characteristics of the sea. The frequency-dependent radiation is included into the controller model in state space form.

2.2.3.4 Parameters

The control algorithm allows the specification of six parameters that can be tuned to optimize the performance of the dynamic programming approach. These parameters are: 1) the grid size of each of the states, 2) the grid size of the control force range, 3) the upper and lower bounds on each of the states, 4) the upper and lower bounds on the control force range, 5) the number of control nodes in the peak period, and 6) the prediction horizon length.

2.2.3.5 Improvements - how to move forward

- Upgrade controller for a multi-DoF dynamic model.
- Design controller using a nonlinear dynamic model.
- Improve computational speed. The propagation in time in the current DP implementation uses the full controller model. It is possible to work with a reduced order model to increase computational speed.

2.2.4 Shape-Based (SB) Control

2.2.4.1 General description

The SB approach was recently developed for space trajectory optimization [20–23], and has its roots in pseudo spectral optimal control [24, 25]. In pseudo spectral methods, the system dynamics are approximated by function series. The derivative of the state vector is approximated by the analytic derivative of the corresponding approximating function of the state.

This SB approach differs from the pseudo spectral optimal control approach in that it approximates only one state (buoy's vertical velocity) using Fourier series as opposed to approximating all the system's states and the control in pseudo spectral methods; hence the SB method is computationally faster. The SB approach benefits from a priori knowledge about the shape of one of the states to generate a good initial guess for the optimization process. In this development, the buoy's vertical velocity is selected to be the approximated state since the shape of the wave vertical velocity can be used as initial guess for the buoy's vertical velocity. In this development, a Fourier series expansion is used for approximation.

The Shape-Based control approach is primarily feedforward computing control over a future horizon (hence receding horizon, see Figure A.2) and it targets both amplitude and phase. Like MPC and DP, the current state of the system is used to initialize the optimization process and hence there is a feedback loop in which these states are passed directly to the optimization. This current implementation requires a deterministic foreknowledge (the prediction block in Figure A.2). The length of the foreknowledge horizon ranges from 3 to 7 wave peak periods.

This strategy has been chosen as the baseline strategy because:

- it approximates only one state (buoy's vertical velocity) using Fourier series; hence the SB method is computationally faster then DP.
- it can be implemented with both linear and nonlinear system models.

It is possible that SB may not be a candidate for a real-time control strategy to be implemented in the wave tank due to its high computational costs.

The control algorithm requires the WEC to use reactive power.

Implementation of this strategy on a WEC system, with radiation states included, is novel.

2.2.4.2 Controller Optimization

The controller model is approximated by a Fourier series representing the heave velocity thus converting the optimal control problem into a mathematical programming problem. Hence existing, well-developed optimization algorithms may be used to solve the transformed problem [24].

The SB approach performs a search for the optimal Fourier coefficients that maximize the extracted energy over the prediction horizon. The optimization of the buoy's vertical velocity shape is carried out using a sequential quadratic programming optimization method. This process is repeated at each control time step online using this Fourier series. The SB solution is suboptimal due to the use of Fourier series for approximating the buoy's vertical velocity.

The online numeric optimization uses as its base the controller model, and only one controller model was used in this study: CONFIG-B. However, theoretically, any controller model can be used for online optimization with computational efficiency the only drawback.

2.2.4.3 Controller model characteristics

The SB approach utilizes the system's equations of motion to compute the PCC control that would result in the optimized buoy's vertical velocity over the prediction horizon. The controller model in the current implementation is linear, CONFIG-B; it is the state space model described in the standard matrix form (A,B,C,D) for a 1 DoF heaving buoy. The state space model includes the frequency-dependent radiation. The control model is composed of a linear model of the WEC and a linear model of the spectral characteristics of the sea. For nonlinear systems, the dynamic model in the SB needs to model the system nonlinearities, and can be used to compute the PCC control.

2.2.4.4 Parameters

The control algorithm allows the tuning of a number parameters to improve the performance of the SB approach. These parameters are: the number of Fourier terms representing the buoy's vertical velocity, the prediction horizon length, the control time step, and the control calculations update frequency. The PCC control will updated each control time step, while the control calculations may be performed at a different rate (the control calculations update frequency).

2.2.4.5 Improvements - how to move forward

- A proper choice of trial functions and the distribution of collocation points is crucial to the accuracy of the approximating solution [26]. In this project, Fourier series are used for approximation with equally spaced collocation points. Using Legendre-Gauss-Lobatto points for approximation provides spectral accuracy for smooth problems [25], and hence is expected to significantly enhance the performance of the SB method if they were used as collocation points. It is planned to switch to Legendre-Gauss-Lobatto approximations to improve the current software code.

- Nonlinear dynamic models: the use of nonlinear controller dynamic models is possible in the SB approach to generate PCC controls suitable for nonlinear WEC systems. There are a number of nonlinearities that can be included in the dynamic model. The SB approach re-

quires a separate development for each combination of these nonlinearities. These nonlinear terms will be investigated with SB approach for PCC control.

- Improve computational speed. The propagation in time in the current SB implementation uses the full controller model. It is possible to work with a reduced order of the controller model to increase the computational speed. This will result in a degraded accuracy and balance between accuracy and computational cost is to be investigated.

- The SB method can be used with nonlinear systems. In addition to developing the SB method to compute the PCC control, it is crucial to understand the behavior of the WEC nonlinear system. This deeper understanding for the WEC nonlinear system enables the development of more efficient control, especially when deling with the multi-DoF coupled system. To that effect, a nonlinear analysis or the WEC system is needed.

2.2.5 Linear Quadratic (LQ) Control

2.2.5.1 General description

Linear Quadratic control is a pure feedback control strategy in which the feedback gain is obtained by solving an optimization problem. This is a feedback strategy targeting amplitude and phase.

This strategy also includes a state estimator; the control signal is obtained by multiplying the estimated state by the gain matrix calculated offline. In the current implementation the entire state vector is being estimated, that is position, velocity and radiation states.

The LQ control strategy has been selected because:

- it is the "simplest" strategy based on optimization,

- being based on feedback, is known for its robustness.

The LQ strategy is also suitable for real-time time implementation because it is not computationally demanding; in fact, the only operations that are being carried are the vector-matrix multiplications used to update the state estimate and to calculate the control signal.

The control algorithm requires the WEC to use reactive power and, based on a few preliminary results, provides output power very similar to model predictive control (the two strategies are actually based on the same cost function and WEC model). Therefore, the algorithm requires high efficiency and 4-quadrant capabilities from the PCC.

Implementation of this strategy on a WEC system is not novel.

2.2.5.2 Controller Optimization

The cost function is quadratic in both the state and control, and it has the same form as the cost function used for the definition of the MPC optimization problem (Section 2.2.2). If the dynamic of the system is described by a linear model and no constraints are being considered, then the quadratic optimization problem can be solved analytically. Furthermore, the solution (control signal) can be expressed as function of the current state (feedback). For this reason, the LQ control strategy requires a state estimator.

The feedback gain is calculated offline as a result of the optimization problem, which is sea-state dependent. Therefore, the feedback gain needs to be updated whenever the spectral properties of the sea change. The spectral characteristics of the sea are approximated by a linear filter, the parameters of which are calculated assuming a Bretschneider distribution. The filter is then converted to a state space form and it is combined with the dynamics of the WEC to form an augmented state space model. This augmented state space model is then used to build the Riccati equation, the solution of which is the feedback gain [27]. The optimization problem has an analytical solution (the feedback gain matrix) because the problem is Linear Quadratic (LQ), that is the model is linear and the cost function is quadratic. With this control strategy is not possible to include constraints in the problem formulation.

2.2.5.3 Controller model characteristics

The control model is a linear (CONFIG-B), state space model described in the standard matrix form (A,B,C,D) for a 1 DoF heaving buoy. The frequency-dependent radiation is included into the control model in state space form. The control model is composed of a linear model of the WEC and a linear model of the spectral characteristics of the sea. The order of the WEC model has not been reduced, while the order of the sea spectral model has been reduced. The control algorithm also requires a simple model of the PCC for its implementation, which has been implemented as an ideal electrical motor/generator with a resistor connected in series.

2.2.5.4 Parameters

The control algorithm allows the specification of three parameters, namely the weighting matrices Q, H and R. Given the controller model described above, all the control parameters are completely specified. In particular, the R matrix corresponds to the resistance in the PCC model, the H matrix is the transpose of the output matrix of the controller model C, and the Q matrix is zero.

The Q and R matrices act as penalty terms that can be used to approximate constraints. The R matrix penalizes the 2-norm of the control effort, while the Q matrix penalizes the 2-norm of the state components, therefore force and position constraints can be approximated by "soft" constraints introduced by choosing appropriate values of the matrices Q and R.

An additional parameter is the spectral estimate of the sea-state.

2.2.5.5 Improvements - how to move forward

- Improve estimator to use sensors available for the "real" device.
- Include improved model of the PCC
- Design controller using multi DoF controller model.

2.2.6 PD Version of CC Control (PDC3)

2.2.6.1 General description

This control strategy suboptimally realizes Complex Conjugate (CC) control via a feedback strategy (Figure A.1) by creating a resonate generator. The theoretical underpinnings of complex conjugate control are fundamentally linear, and hence this is also linear. It targets both amplitude and phase through feedback that is constructed from individual frequency components that come from the excitation input signal. Each individual frequency uses a Proportional-Derivative (PD) control to provide both optimal resistive and reactive elements. By resonating each frequency component and summing them together the controller feedback effort that maximizes the amount of absorbed power is provided.

This control strategy has been developed because:

- Demonstrates actual realization of a CC control design.
- The wave foreknowledge is not required.
- This method is computationally fast and hence potentially easy to implement.

The controller model consists of a linear transfer function with individual feedback for a bank of filters that isolate primary frequencies associated with a given sea-state irregular wave input profile. The goal is to have the filters resonate for frequencies that are off-resonance which will require reactive power to help boost total energy capture width and absorbed power. The control algorithm will require the WEC to use reactive power, with energy storage, with prerequisite high efficiency and 4-quadrant capabilities from the PCC.

Implementation of this strategy on a WEC system is fundamentally novel and the first practical approximation of an optimal CC based concept. Expansion of the strategy to multi-DoF's and more nonlinear cases is essential in order to understand how well this strategy can work on real world systems.

2.2.6.2 Controller Optimization

The controller gains are selected to optimize resistive feedback characteristics and to match off-resonance conditions with position feedback similar to an ideal CC design. The filters are designed offline; the design process includes selection of the number of filters, the peak frequencies, and their corresponding Q-factor[1]. The filters are manually optimized or tuned with respect to a complex-conjugate transfer function baseline. With simple peaking filters proof-of-concept was demonstrated. It is expected that with the utilization of higher-resolution filters that larger improvements in absorbed power are expected for irregular wave conditions.

2.2.6.3 Controller model characteristics

A linearized transfer function was used as the controller model and validation was performed with the performance model set to CONFIG-B.

2.2.6.4 Parameters

The parameters of interests are primarily associated with the filter design parameters, such as the Q factor and the primary frequency of interest, for a peaking filter design. A range of $1-3$ peaking filters where used during this study for each Bretschnieder spectrum.

Currently, the filter sets are sea-state specific. As development work continues on this strategy, the filter set is expected to become sea-state independent.

2.2.6.5 Improvements - how to move forward

- Investigate higher resolution filters, such as, Bessel or Elliptic filters.
- Further optimize existing peaking filters to help improve energy capture for irregular wave sets.
- Design controller with filters using multi DoF controller model (may require nonlinear filter implementation, such as Volterra type).
- The PDC3 design can be simplified to an resistive control realization by only considering the Derivative portion of the individual filter designs (i.e., the reactive portion would be set to zero).

[1]The Q-factor is a parameter related to the bandwidth of the filter

2.2.7 Latching

2.2.7.1 General description

Latching is a type of switching control, the origins of which in wave energy conversion can be traced back to early studies on small heaving point absorber buoys with short natural resonant periods. The technique consisted of locking the buoy displacement until the approach of a crest (or a trough) and releasing it so it achieved full velocity at the crest (or trough) and then re-locking the displacement until the approach of a crest or trough. The presence or absence of a full-valued braking force was thus the only control required. A formal theoretical foundation was established in the mid-eighties through the work of Hoskin and Nichols [28]. In practice, the objective of latching control can be seen as to maximize the absorbed power by "keeping" the velocity of the buoy in phase with the excitation force. The strategy is most effective when the incoming wave has a period greater than the resonance period of the oscillating body because by holding the device in a latched state for a given amount of time, the net result can be understood as "shifting" the resonance period of the device to a larger value.

Latching is a mixed feedback/feedforward control strategy targeting phase, and its implementation is based on the prediction of the excitation force caused by the incident wave. Rather than the exact profile of the excitation force, latching requires the prediction of the next peak in the excitation force. Although the design of the latching control strategy has been based on a single DOF device, it can be also be implemented with additional DOFs[2].

The latching control strategy has been selected because:

- It is conceptually simple to implement, at least in its basic form.
- Latching control does not require reactive power, which has significant implications, such as:
  - No risk of obtaining negative average absorbed power: in the case of "bad" predictions, malfunctioning in the sensors or control algorithm, the control strategies that require reactive power may result in a net loss of energy, while this is not possible with latching control. In the case of latching control the worst case scenario is zero absorption.
  - The required PCC simpler and components efficiency is less critical.

Latching is a type of nonlinear control because the control variable can only assume two values, 1 or 0. Typically, latching involves application of resistive loads only, so it is a sub-optimal control in the hydrodynamics sense. The entire formulation is developed in the time domain, and is framed as an optimal switching control problem.

The calculation of the latching control law can be carried out online in both the Hoskin and Nichols [28] approach, where the implementation is based on Pontryagin Max/Min principle, and

[2]Examples of latching control applied to multi-body WECs is available in the literature [29]

in the empirical approach [30]. The Hoskin and Nichols approach, however, may not be suitable for real-time implementation due to the required intensive computation. On the opposite side, the empirical approach requires the prediction of the incoming excitation force and the resonance period of the device (T_{res})[3], but it is generally suitable for real-time implementation.

Implementation of this strategy on a WEC system is not novel.

2.2.7.2 Controller Optimization

The optimal switching sequence is one that leads to maximum power absorption over a duration of time T, subject to the constraints imposed by the converter dynamic model and limits on PCC force and stroke-length. In the framework of Hoskin and Nichols [28], the switching sequence is derived using the Pontryagin Max/Min principle. Implicit in the procedure is the need to solve a two-point boundary value problem in the time domain, where the boundary extends from the current instant to T time units into the future. Therefore, prediction of the exciting force is required even though the control leads to suboptimal velocities. Early solutions evaluated the optimal switching sequence using an iterative procedure.

More expedient approaches have evolved in recent years, among which empirical rules to calculate the switching sequence [30]. In this case, the device is latched whenever the buoy reaches zero velocity and it is released approximately $T_{res}/4$ s before the next predicted peak in the excitation force, where T_{res} is the resonance period of the device.

2.2.7.3 Controller model characteristics

The current implementation of latching is based on a the linear model of the WEC (CONFIG-B).

Because no Fourier transformation is involved in the control sequence determination, the dynamic model for the converter can incorporate certain types of nonlinearities (for instance, viscous friction, actuator saturation, etc.).

2.2.7.4 Parameters

Power absorption is obtained by a linear damper during the time interval in which the device is unlatched. The damping coefficient used for power absorption is a parameter that is currently optimized offline.

2.2.7.5 Improvements - how to move forward

- Implement model-based real-time estimation of latching time.

[3]The resonance period is fixed once the structural/hydrodynamical properties of the device have been set

- Implement optimization of the damping coefficient.
- Implement “multi-period” latching to improve performance when wave periods are below resonance.

Chapter 3

Detailed Results

3.1 Linear Results

3.1.1 Regular Waves and associated Capture Ratios

This section reports simulation results where the control strategies have been tested using regular waves, meaning that, for each simulation, the water surface elevation is described by a single sinusoid with a prescribed period and amplitude. Before presenting the simulation results, it is useful to introduce a brief discussion to understand the bounds to which a WEC is limited in terms of absorbed energy. Clearly, a WEC cannot absorb more power than the amount carried by the incident wave; this quantity is generally known as wave energy flux, denoted by the symbol J, and it gives the transported wave power per unit width of of the wave front. The quantity J/k [31] has been introduced in Figure 1.2, where it is shown that in ideal conditions, any linear wave energy converter can absorb all the energy transported by waves at resonance with the simple resistive controller. In practice, however, dissipative effects will reduce the amount of power available to be absorbed by the WEC (see Section2.3.2 in [32]). An additional limitation is due to the shape of the device; in particular to the maximum amount of water that the floating body is capable to displace, and it is known as Budal upper bound [31].

Since average absorbed power is quadratically dependent upon the wave-height for a linear hydrodynamic model, it is more insightful to evaluate a devices performance in a normalized manner. For this reason, the performance of the control strategies will be compared in terms of capture ratio χ. The capture ratio is the average absorbed power divided by the theoretical maximum that can be absorbed by the device (J/k).

The plot in Figure 3.1 illustrates this approach for the shape T3R2. When the capture ratio is 1 (dotted line), the absorbed power is the maximum predicted by the linear models in ideal conditions (note: this line corresponds to the dashed-dotted curve in Figure 1.2). However, when taking into account dissipation as shown by the dash-dot line in Figure 3.1, due to viscous losses for example, then the amount of power available is reduced as described by eq.2.83 in [32]. And finally, when accounting for the finite volume of the device, and hence finite stroke length, using the Budal bound for several wave steepnesses, as shown in Figure 3.1, there are further limitations to the available power. In this analysis the draft of the device, 0.53 m, is used to define the finite stroke length.

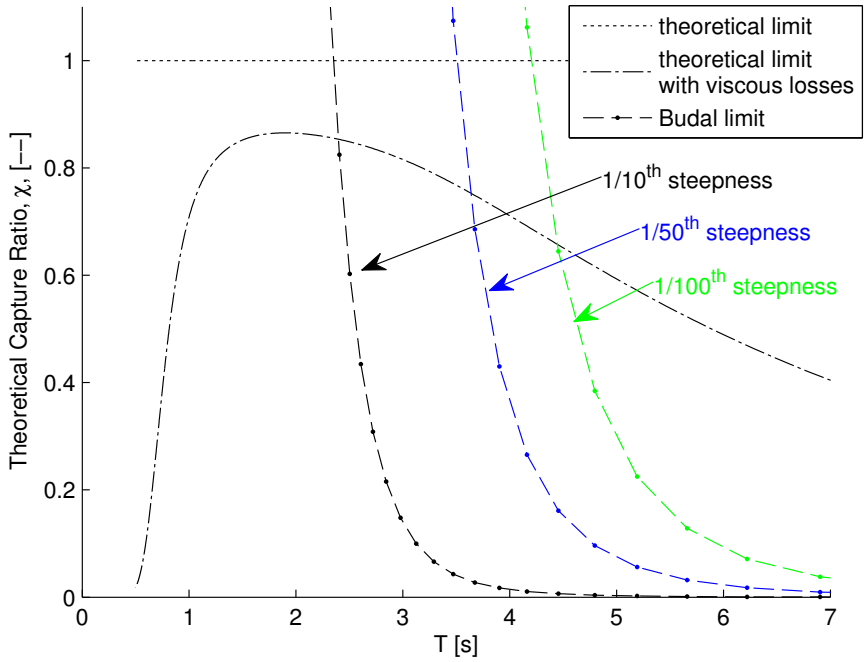

Figure 3.1: Theoretical absorption bounds for a 1DOF device.

The area between the theoretical maximum absorption with viscous losses and the Budal upper bound is the theoretical maximum absorption for this device with the acknowledgment of physical limitations (e.g. viscous losses and the physical size of the device). As a direct consequence of the previous discussion, the potential improvements are bounded in the following ways, each adding a level of realism:

- the theoretical maximum absorbed power for a 1-DoF WEC (this is the straight line at χ=1),
- the theoretical incident wave energy decreased by the viscous losses that will occur due to the motions of the device (this is the dashed line on the originating from zero), and
- the Budal upper bound, which describe the maximum amount of power that can be absorbed by a heaving buoy based on the maximum displaced water (these are the dash-dot lines decaying to zero).

Clearly, each layer of realism negatively effects the maximum capture ratio area for the device. Additionally both the viscous losses and the Budal limit depend on the geometry of the floating body. Table 3.1 details the percentage decrease in area as each layer of realism is added to the analysis.

By superimposing the baseline performance of the device on this capture ratio comparison, as shown in Figure 3.2, it is clear that the control strategies will influence the performance of the device most strongly for longer periods. Further, the difference in area between the Resistive

Table 3.1: Percentage decrease in area (over the identified period range) from lossless theoretical maximum capture ratio to the identified bounds.

Bound	**Decrease in Area,%**
Viscous Losses	32
Viscous Losses & $\frac{1}{100}$ Budal limit	48
Viscous Losses & $\frac{1}{50}$ Budal limit	57
Viscous Losses & $\frac{1}{10}$ Budal limit	75

Control capture ratio and the area defined by the various theoretical limits including loss are given in Table 3.2. Note: although the Resistive Control is shown capturing more then the Budal limit for the $\frac{1}{10}$ case, this is an artifact from not modeling the resistive control with stroke limitations. The tabulated value in Table 3.2 assumes that the resistive control would lie along the limit for the $\frac{1}{10}$ steepness case.

Table 3.2: Percentage increase in area (over the identified period range) from the baseline resistive control strategy to the loss accounting theoretical limits.

Bound	**Increase in Area,%**
Viscous Losses	111
Viscous Losses & $\frac{1}{100}$ Budal limit	59
Viscous Losses & $\frac{1}{50}$ Budal limit	50
Viscous Losses & $\frac{1}{10}$ Budal limit	36

The capture ratios obtained by simulating the control strategies with incident waves having a constant steepness of $\frac{1}{50}$ are shown in Figure 3.3. A few items of note regarding these results:

- theoretical limits only valid for linear governing equations of motion
- these results use CONGFIG-B (the 1-DOF performance model with linear hydrostatics, linear viscous losses, and state-space radiation without stroke limitations).

For a linear device, complex conjugate control (CC) provides the theoretical upper bound on power absorption [33]. The current state-of-the-art control strategy is constant coefficient '"derivative" control (the D from PID) in which a single resistive damping value is applied to the velocity of the devices motion. Resistive control thus provides the lower bounds for power absorption (black solid thick line). The difference in area between these two plots is dependent upon the wave steepness (see Figure 3.1).

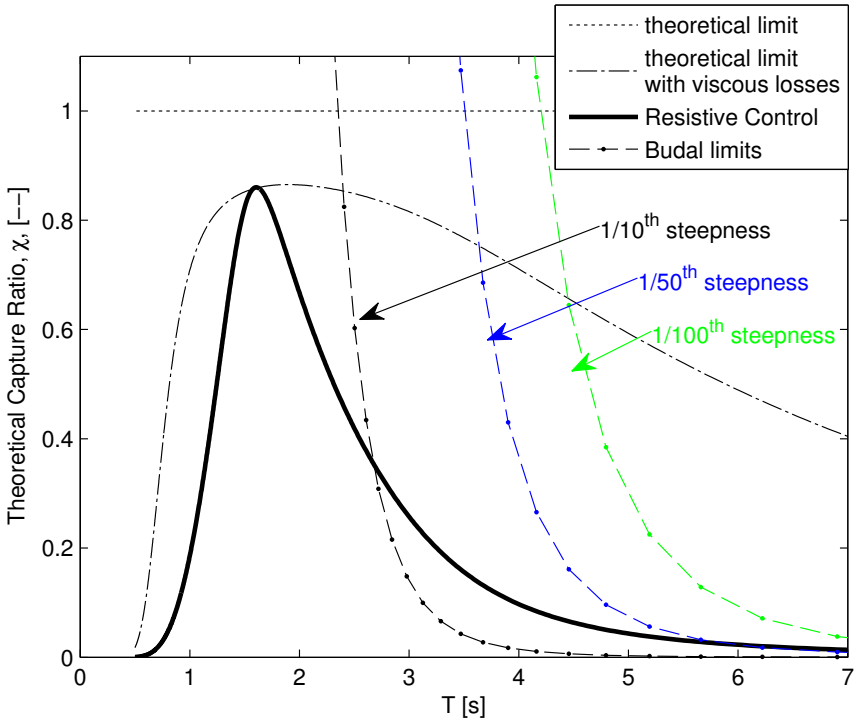

Figure 3.2: Theoretical absorption bounds for a 1DOF device compared with baseline Resistive Control.

Figure 3.3 shows the Capture ratios of the control strategies. For some sea states, some of the control strategies did not reach steady state to maximize the power, and they show higher capture ratios than the theoretical limit, at those sea states.

Each control strategy modifies the behavior of the device in a different way, thus it is also useful to compare the resulting motion. The top plot in Figure 3.4 shows the maximum heave displacement while the bottom plot shows the velocity. Since the model is linear, both displacement and velocity are a linearly proportional to the amplitude of the incident wave. For this reason the plots in Figure 3.4 have been normalized with the wave height. Again, some control strategies result in larger amplitudes or velocities then the optimal CC control. This simply implies that the device is moving more (or faster) then is required to achieve optimal absorption.

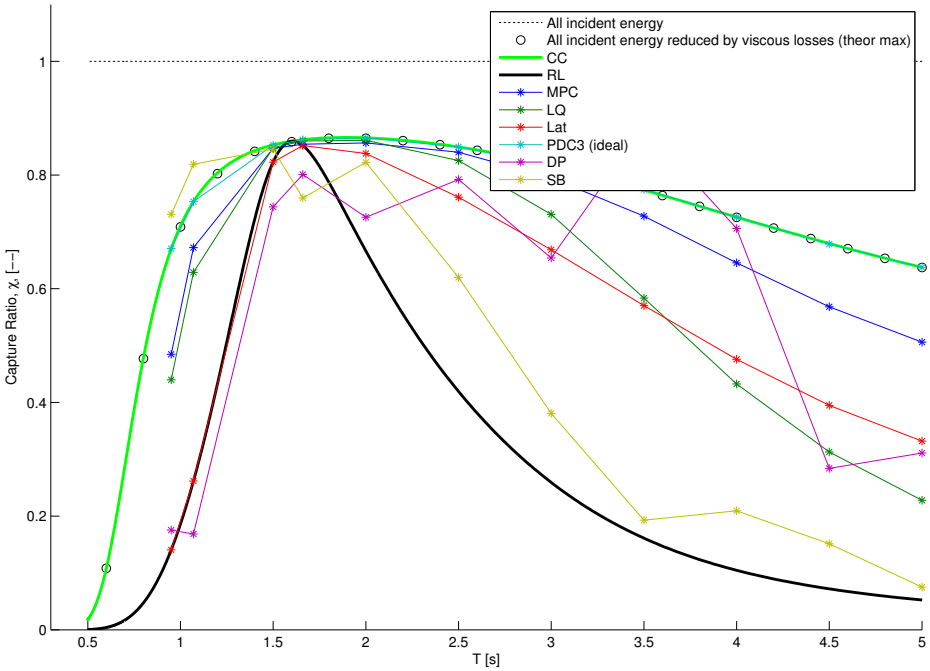

Figure 3.3: Capture ratios of the control strategies.

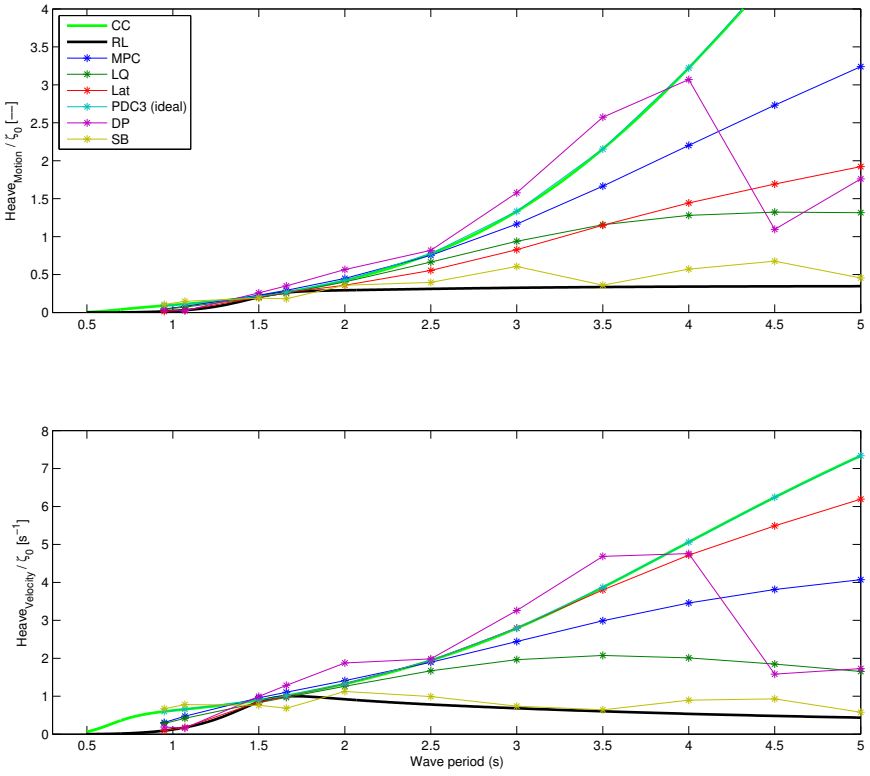

Figure 3.4: Comparative motions and velocities, normalized by height of incident wave, of the device subject to various control strategies.

3.1.2 Irregular Waves

This sections reports simulation results for irregular waves. The results are summarized in different formats: the Metric Matrix, which provides a summary of a number of metrics, is descried in Section 3.1.2.1. Section 3.1.2.2 provides an overview of the behavior of the WEC when controlled with a subset of control strategies, by means of plots depicting the motion, forces and power over a representative time interval. In Section 3.1.2.3, the control strategies are compared by using scatter diagrams (see Section 1.3).

Table 3.3 summarizes the key linear AAP results from these simulations.

Table 3.3: Average annual power (AAP) production in a Newport, OR deployment climate for various control strategies implemented on a linear system. Similar results are found when implemented on the nonlinear system studied (see Section 3.2).

Strategy	**AAP [kW]**	**Increase [%]**
Resistive	15.5	—
MPC	46.1	197
DP	38.4	148
SB	22.6	46
LQ	39.8	157
PDC3	26.3	73
Latching	28.8	86

3.1.2.1 Metric Matrix

A metric matrix, summarizing control strategy performance results is presented in Table 3.4. All values are given as the average annual value for the quantity defined. Further, all units are metric and all results are shown in model scale. Quantities presented in Table 3.4 are defined as follows:

- Power production characteristics - Quantities relevant to power production.
  - Average power-in - Average annual power used to motor the device (i.e. "reactive power").
  - Average power-net - Average annual net power from the device.
  - Average energy-stored - Average annual stored power (only necessary for reactive strategies). Storage is calculated as the amount of energy necessary to provide the reactive power required by the control strategy without absorbing power from other sources (e.g. power from the electrical network).
  - Power-in, peak†/RMS - Peak power-in divided by RMS power-in.

  - Power-net, peak†/RMS - Peak power-net divided by RMS power-net.
  - Total absolute power flow - Indication of stress on PCC. Is is calculated as the annual weighted average of the absolute value of the power flowing through the PCC.

- PCC requirement - Quantities relevant to PCC capability requirements.
  - PCC force, peak† - Peak force applied by PCC.
  - Slew rate requirements - Average annual rate change in force applied by PCC (i.e. $\frac{\partial F}{\partial t}$)
  - PCC force, RMS - RMS of force applied by PCC.
  - PCC Force, peak†/RMS - Peak PCC force divided by RMS PCC force.

- Mechanical loading - Measures of requirements for device device drive train structure (e.g., bearing surfaces, motor extension limits)
  - Oscillation amplitude, peak† - Peak of float vertical motion amplitude.
  - Oscillation amplitude, peak†/RMS - Peak of float vertical motion amplitude divided by RMS of float vertical motion amplitude.
  - Oscillation velocity, peak† - Peak of float vertical velocity.
  - Oscillation velocity, peak†/RMS - Peak of float vertical velocity divided by RMS of float vertical velocity.
  - Oscillation acceleration, peak† - Peak of float vertical velocity
  - Oscillation acceleration, peak†/RMS - Peak of float vertical acceleration divided by RMS of vertical acceleration.

†Here, the term "peak" refers to the 98$^{\text{th}}$ percentile of the identified response's peaks.

The control strategies are then divided into four main categories: the bounding cases, the cases that target phase (TP), the cases that target amplitude and phase with a predominantly feedback strategy (TAP-FB), and the cases that target amplitude and phase with a predominantly feedforward strategy (TAP-FF).

Table 3.4: Metric matrix.

	Bounding cases		**TP**	**TAP-FB**		**TAP-FF**		
	Resistive	**CCC**	**Latching**	**LQG**	**PDC3**	**Linear MPC**	**DP**	**SB**
Power production characteristics								
Average power-in	0	279	0	46.5	45.8	98.8	374.8	39.0
Average power-net	15.5	52.5	28.8	39.8	25.5	46.1	38.4	22.6
Average energy-stored	0	251	0	27.5	42.9	76.4	332.9	23.8
Power-in, peak/RMS	0.0	5.8	0.0	5.6	5.1	5.6	5.4	4.3
Power-net, peak/RMS	7.3	38.8	6.2	14.3	17.3	20.2	60.1	16.2
Total absolute power flow	15.5	313.3	28.8	76.0	91.5	131.8	384.9	54.5
PCC requirements								
PCC force, peak	739	4312	2099	1970	1854	2653	5850	2500
Slew rate requirements	2.8 E+3	1.1 E+3	1.5 E+6	5.9 E+3	4.5 E+3	7.0 E+3	1.2 E+3	5.5 E+3
PCC force, RMS	315	2367	923	915	1086	1401	2730	1010
PCC Force, peak/RMS	2.35	1.82	2.27	2.15	1.71	1.89	2.14	2.49
Mechanical loading								
Oscillation amplitude, peak	0.06	0.25	0.10	0.14	0.11	0.17	0.28	0.12
Oscillation amplitude, peak/RMS	2.52	1.97	2.05	2.27	1.89	2.09	1.99	2.52
Oscillation velocity, peak	0.14	0.47	0.30	0.31	0.22	0.35	0.50	0.22
Oscillation velocity, peak/RMS	2.63	2.20	2.77	2.43	2.30	2.33	2.17	2.6
Oscillation acceleration, peak	0.39	1.02	0.45	0.78	0.22	0.46	1.27	0.64
Oscillation acceleration, peak/RMS	2.70	2.39	1.21	2.58	2.30	1.95	2.36	2.56

3.1.2.2 Representative Time Series

Figure 3.5–3.9 show sample results from select control strategies for the irregular sea-state 15 ($H_s = 0.32\,\text{m}$, $T_p = 3.6\,\text{s}$). In Figure 3.5, the wave elevation is overlapped with the resulting excitation force in heave exerted on the T3R2. It is interesting to note the low-pass filtering effects on the WEC: it is clear from the plot that the wave elevation contains multiple harmonic components, while the excitation force looks almost sinusoidal. In practice, the hydrodynamics of the device makes it insensitive to high frequency components of the wave elevation, which carry lower amount of power, as the power decreases with the wave period as $1/T$.

Figure 3.6 shows the heave velocity of the T3R2 for several control strategies overlapped with the excitation force. It is interesting to note that all the control strategies attempt to improve the "phase matching" between velocity and excitation force, when compared to resistive control. The plots also show how the control strategies try to keep velocity in phase with excitation: latching locks the device in order to match the peaks of the velocity with the peaks of the excitation force while MPC and LQ force the device to follow excitation with a smoother profile, by using reactive power (Figure 3.9), that is by accelerating the device by means of the actuator force. The smoother motion resulting form applying MPC and LQ can be observed also by looking at the time profiles of the position (Figure 3.7) and the force exerted by the actuator (Figures 3.8).

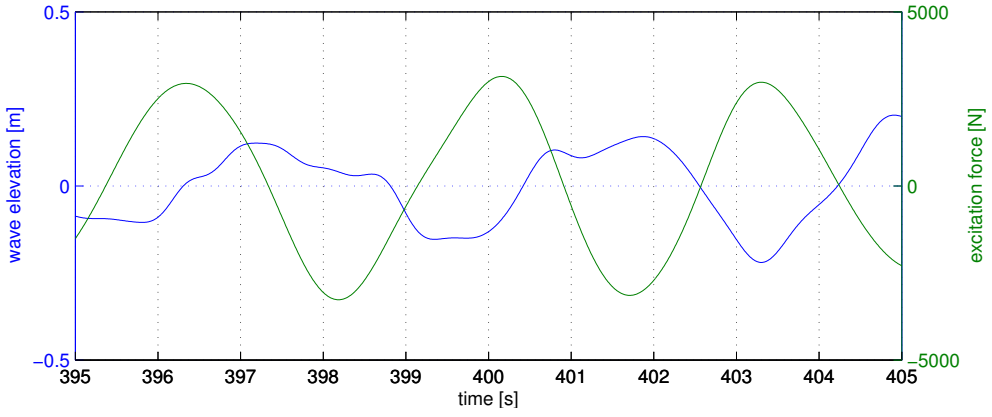

Figure 3.5: Wave elevation and the corresponding heave excitation force for the T3R2

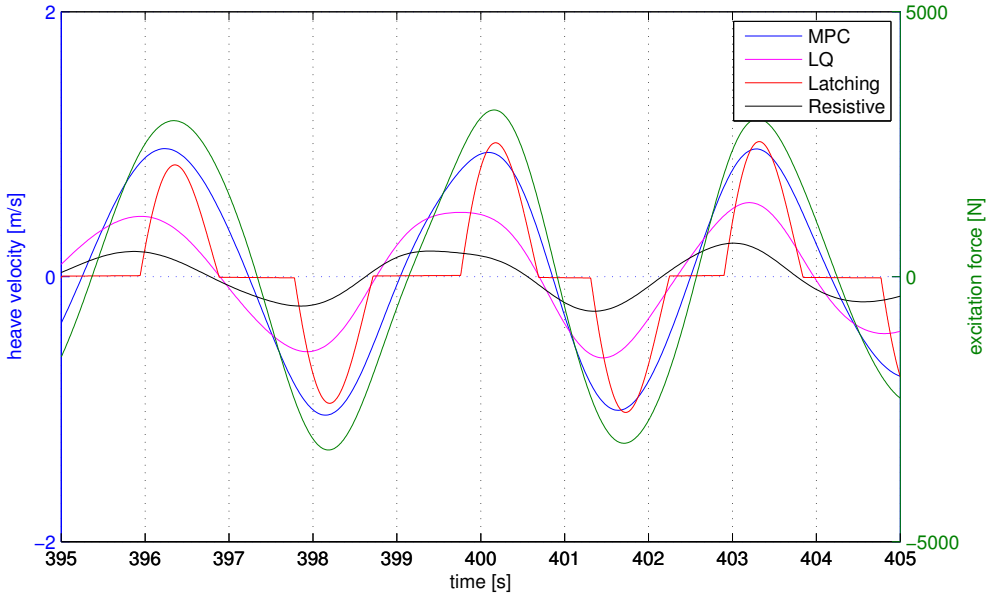

Figure 3.6: Heave velocities and excitation force

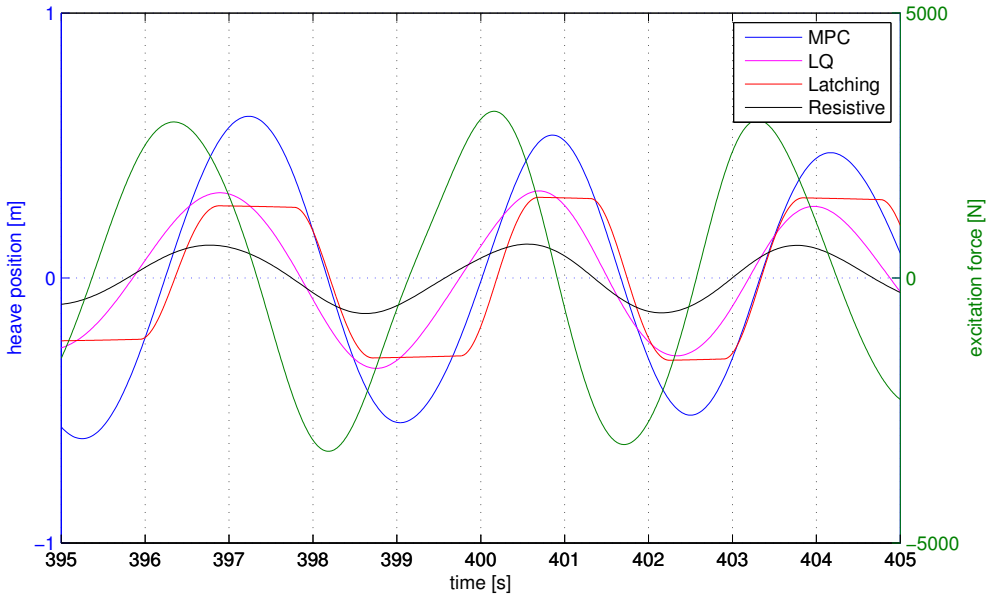

Figure 3.7: Heave position and excitation force

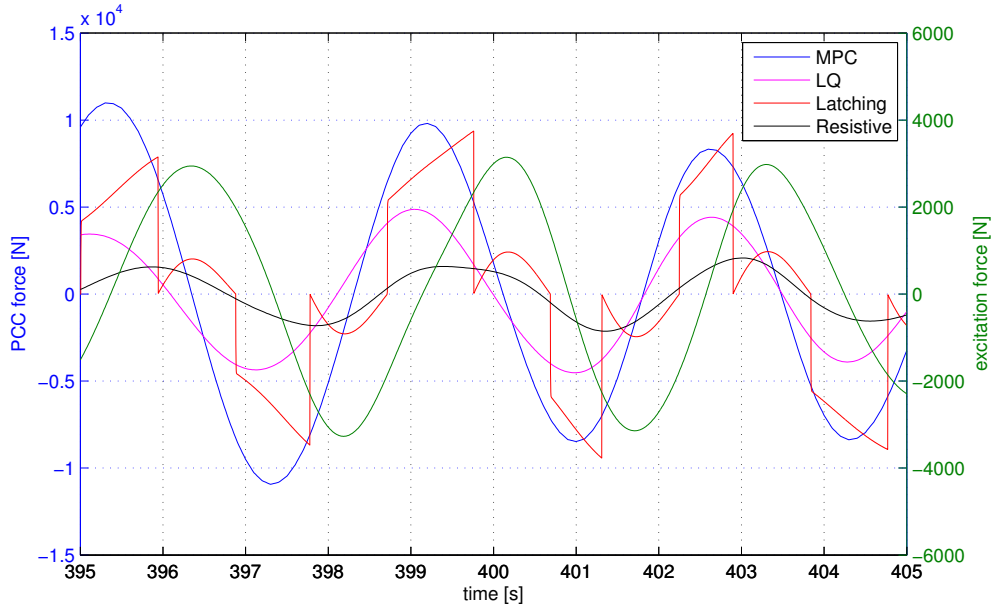

Figure 3.8: PCC and excitation forces

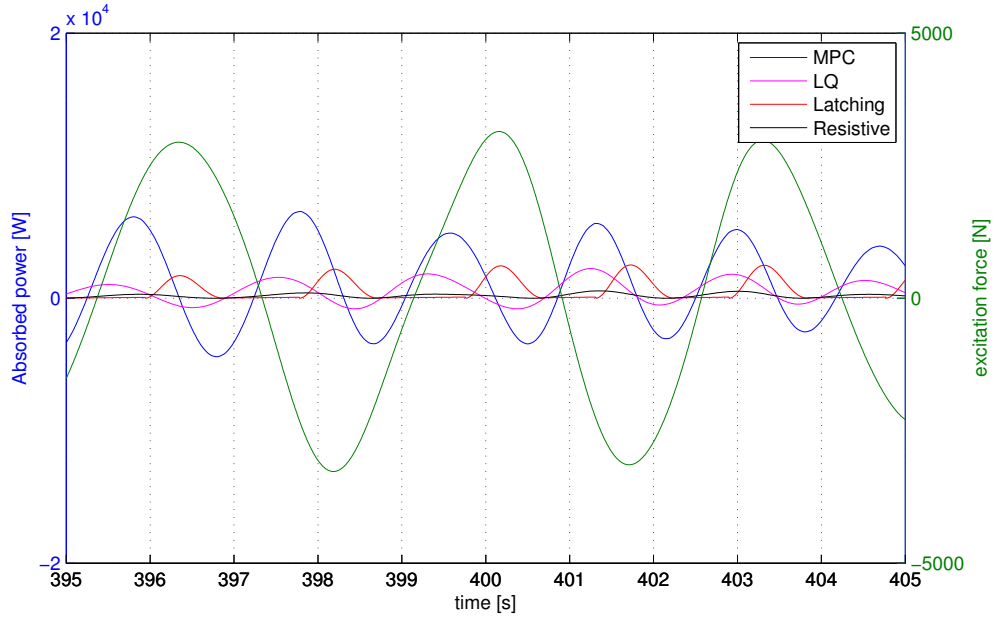

Figure 3.9: Instantaneous absorbed power and excitation force

3.1.2.3 Scatter Diagrams

This section reports simulation results in scatter diagram format (Fig. 3.10–3.29). Scatter diagrams are two-dimensional plots describing a quantity (e.g. absorbed power) as function of the two parameters describing the Bretschneider wave spectral distribution (i.e H_s and T_p). For a detailed description of scatter diagram format presented in this section, see Section 1.3.2. The objective of this section is to compare the performance of the control strategies, according to a selected number of metrics, with respect to the sea conditions.

The scatter diagrams of the absorbed power for all control strategies are presented in Figures 3.10–3.16. For each strategy, the average annual absorbed power (AAP) is plotted in the top left corner of the scatter diagram, and it is calculated as a weighted average of the power absorbed for each sea-state (see Section 1.3). From Figures 3.10–3.16 it possible to observe basic trends in power absorption with respect to the period and height of the incident waves. In particular, it is possible to observe how the amount of power absorbed for each control strategy follows, approximately, the amount of power carried by waves, which is linearly proportional to the wave period and to the square of the wave height.

The scatter diagrams in Figures 3.17–3.22 illustrate the relative performance of the control strategies in terms of average absorbed power relative to resistive control. In this case, it is possible to see how the improvement increases mostly with increasing wave period (see for example sea-states 10,14,16 and 17 in Figure 3.20 for MPC – seas state numbers are detailed in Figure 1.6). This fact is in agreement with the observation for the regular waves described in Section 3.1.1 and illustrated by Figures 3.2 and 3.3, where it is shown that the potential for improvement of a control strategy over resistive control increases with increasing wave periods.

All control strategies, except for latching (and resistive control), use reactive power to improve absorption efficacy. Figures 3.23–3.25 show the average amount of reactive power required by the control strategies, for each sea-state. The amount of reactive power increases generally with both wave period and wave height; however, in this case there are multiple reasons explaining this effect. The first most obvious reason is that the amount of reactive power increases commensurately with the amount of absorbed power: more power is carried by waves for longer periods and larger amplitudes and thus more power is absorbed by the WEC; consequently, more reactive power is required to effectively "enforce" the control strategy. A second important reason can be observed in the scatter diagram in Figure 3.26, which shows the ratio of the power flowing from the PCC into the oscillating body (reactive power) divided by the power flowing from the oscillating body into the PCC ("active power"). It can be clearly seen that the longer the waves the larger the ratio, and that this quantity is not affected by the wave height.

The last set of plots (Figures 3.27–3.29) show the average storage required for each sea-state by the control strategy. This quantity indicates the amount of energy storage that would be required to implement a control strategy that uses reactive power, in order to prevent the controller from taking the required reactive power from the grid.

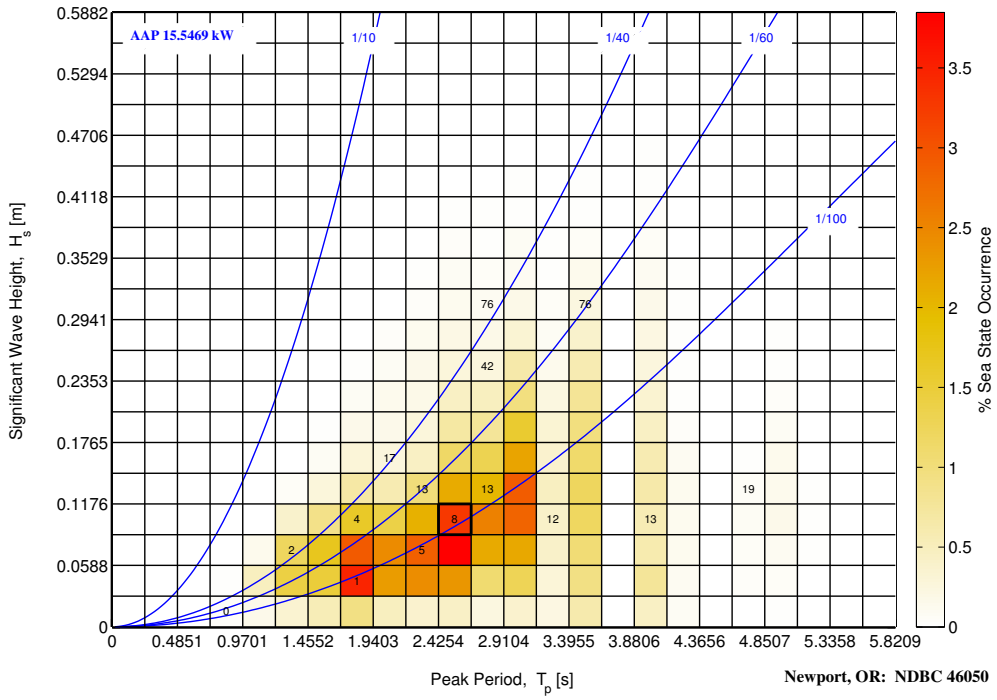

Figure 3.10: Average absorbed power for the Resistive (baseline) control strategy.

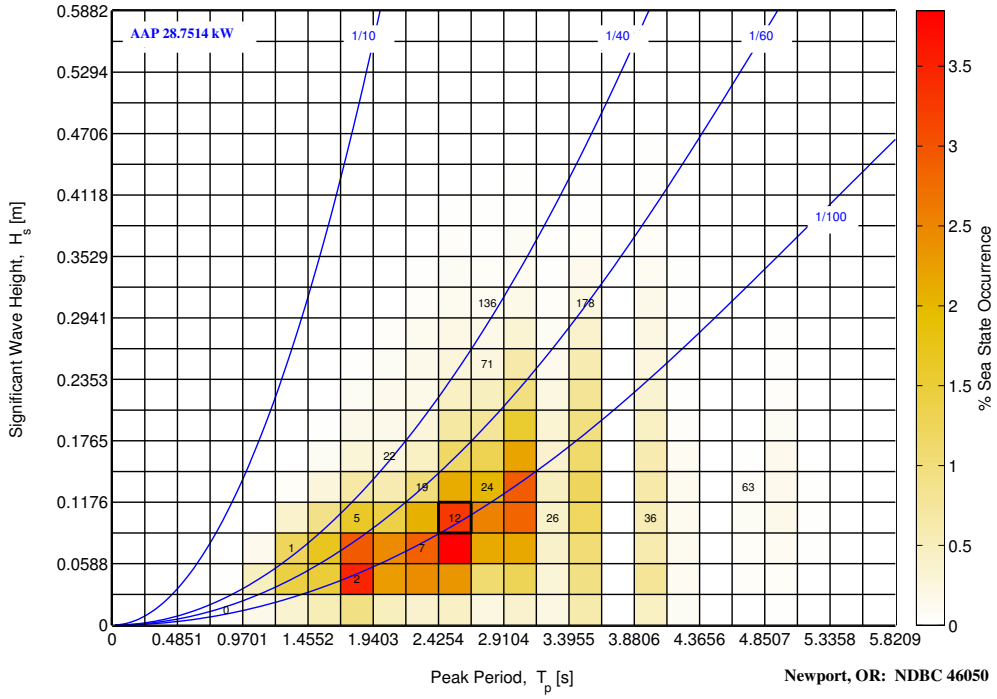

Figure 3.11: Average absorbed power for the Latching control strategy.

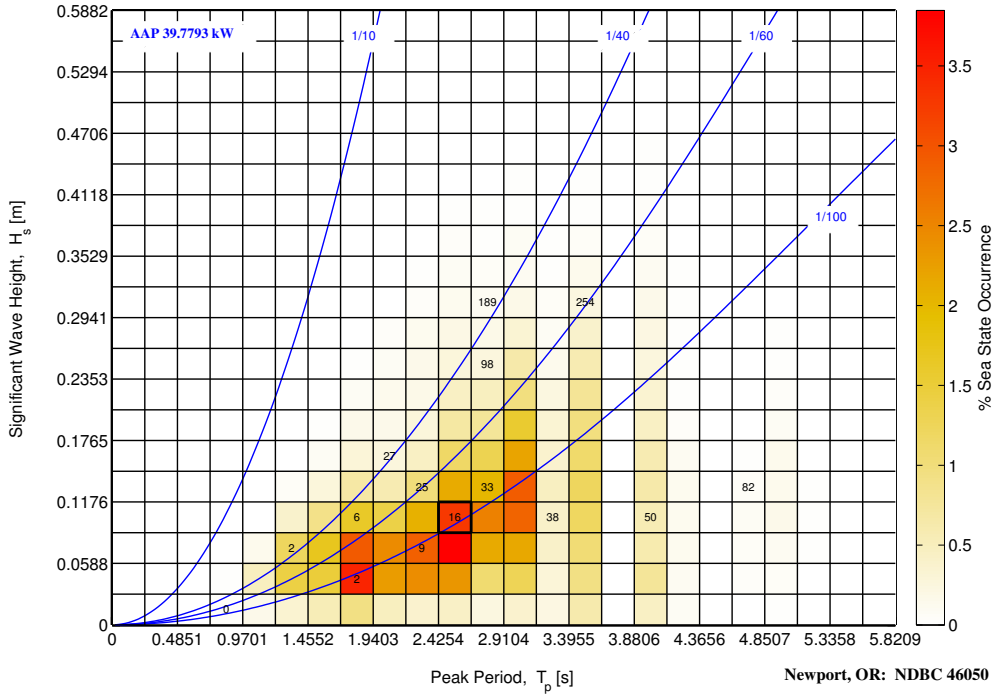

Figure 3.12: Average absorbed power for the LQ control strategy.

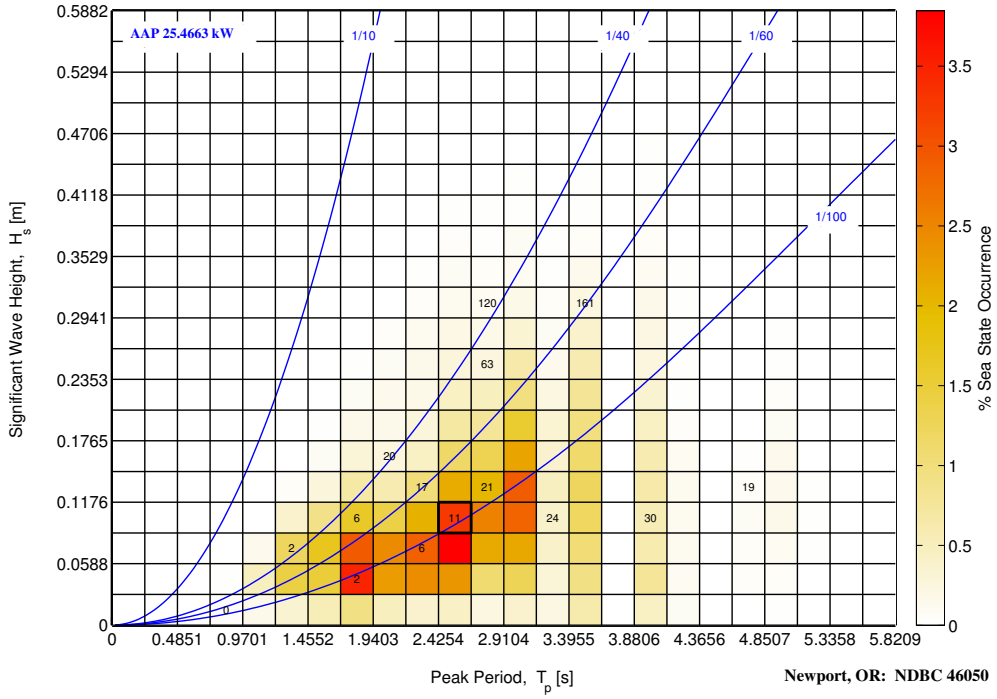

Figure 3.13: Average absorbed power for the PDC3 controls strategy.

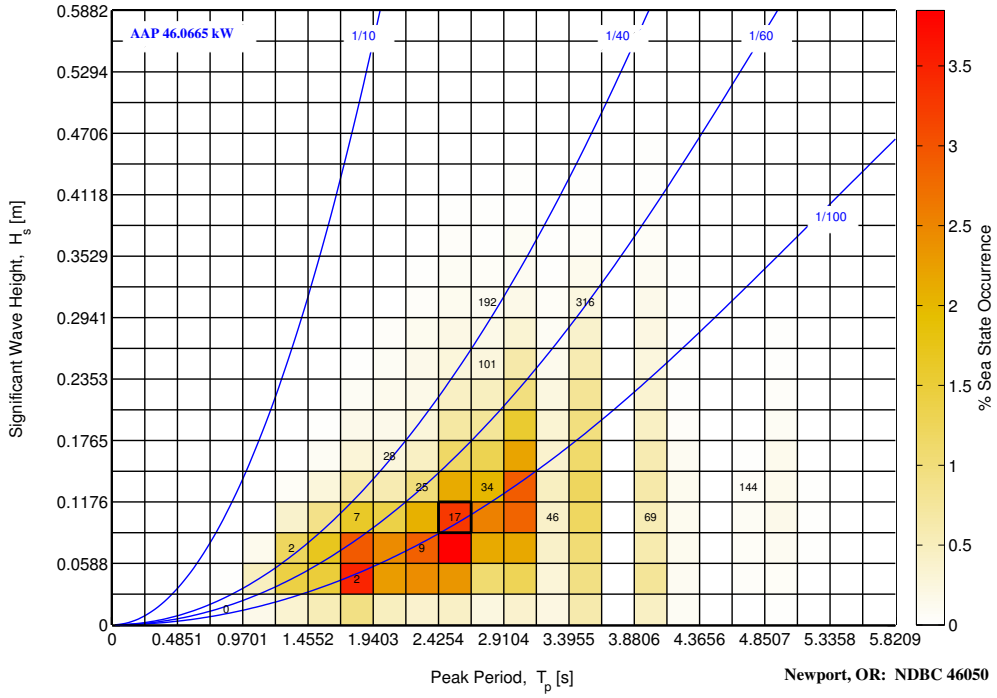

Figure 3.14: Average absorbed power for the MPC control strategy.

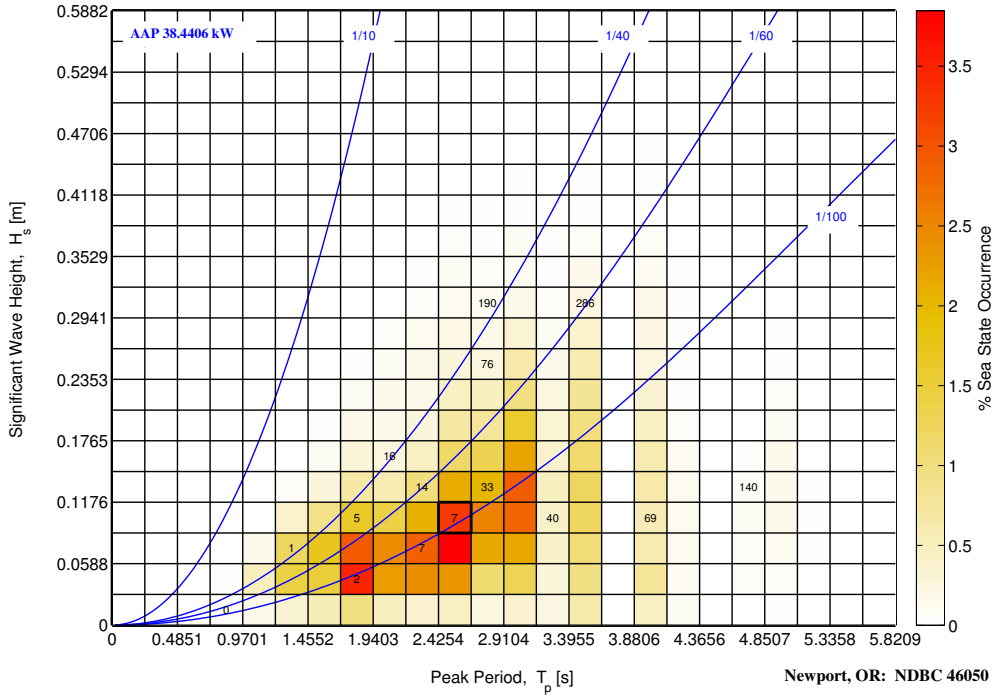

Figure 3.15: Average absorbed power for the DP control strategy.

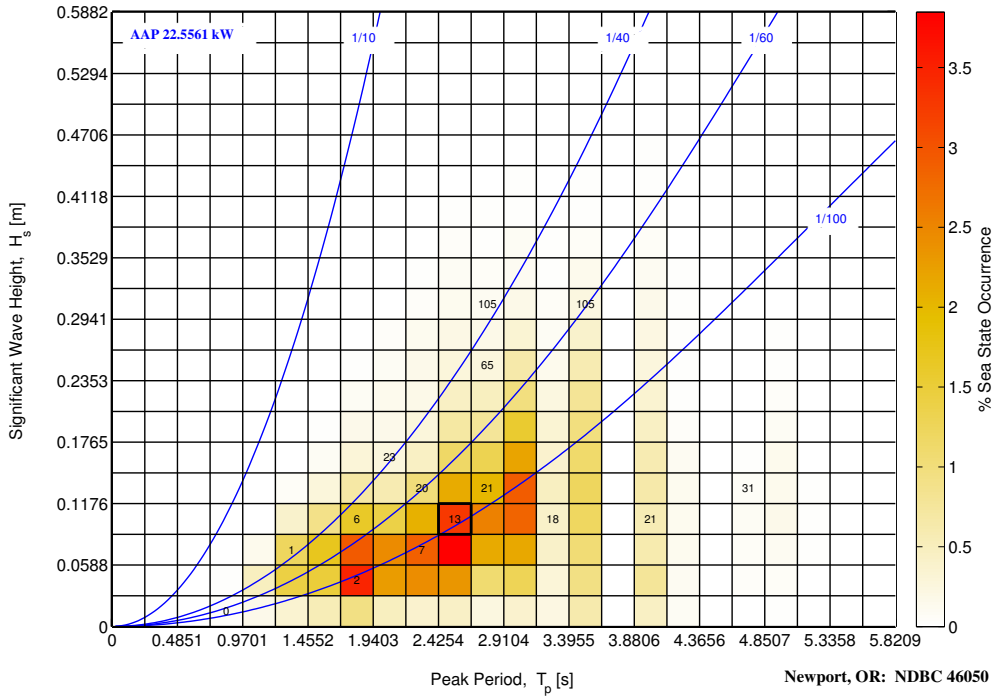

Figure 3.16: Average absorbed power for the SB control strategy.

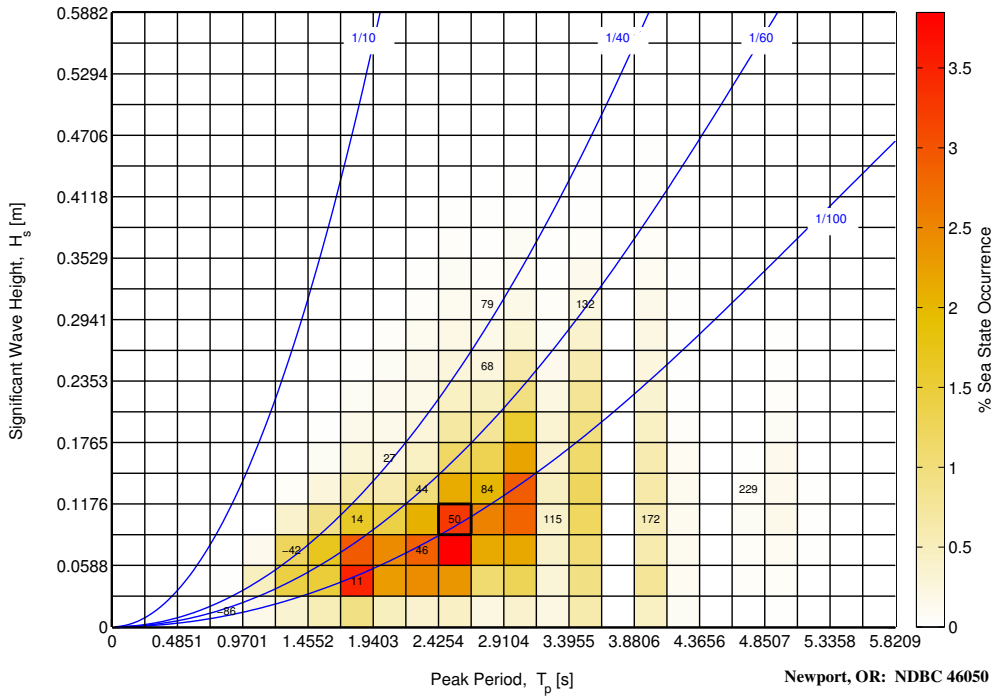

Figure 3.17: Percentage increase in power obtained with the Latching control strategy.

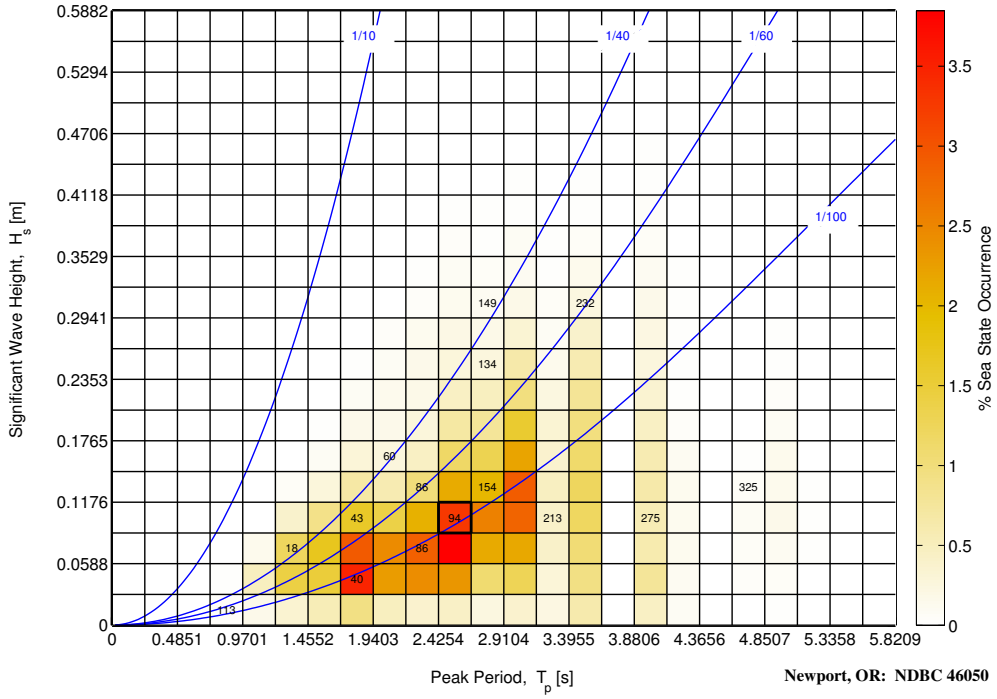

Figure 3.18: Percentage increase in power obtained with the LQ controls strategy.

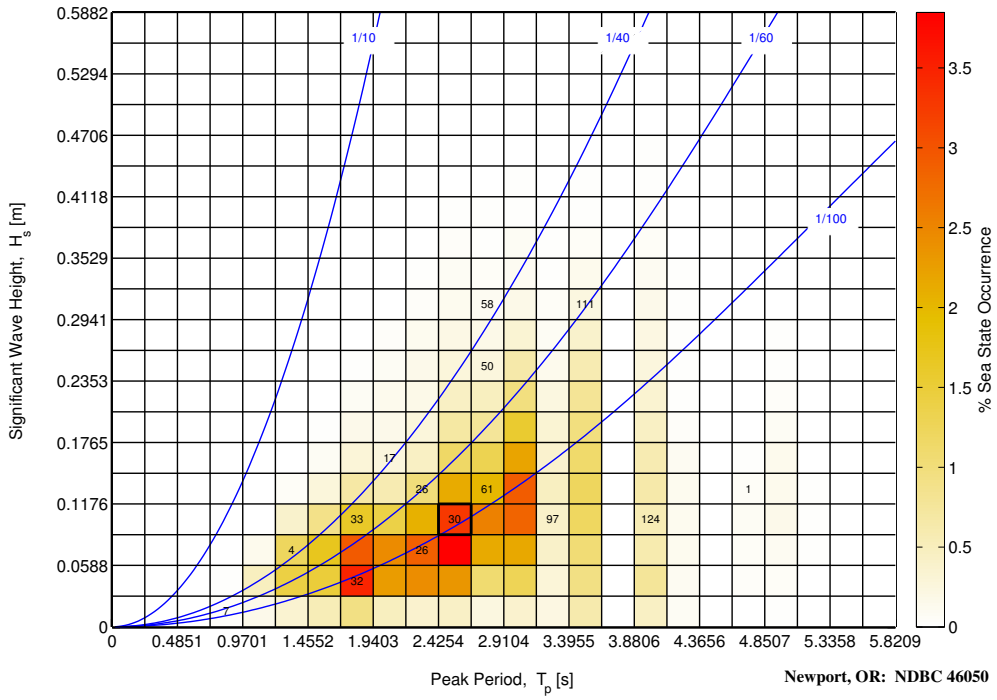

Figure 3.19: Percentage increase in power obtained with the PDC3 controls strategy.

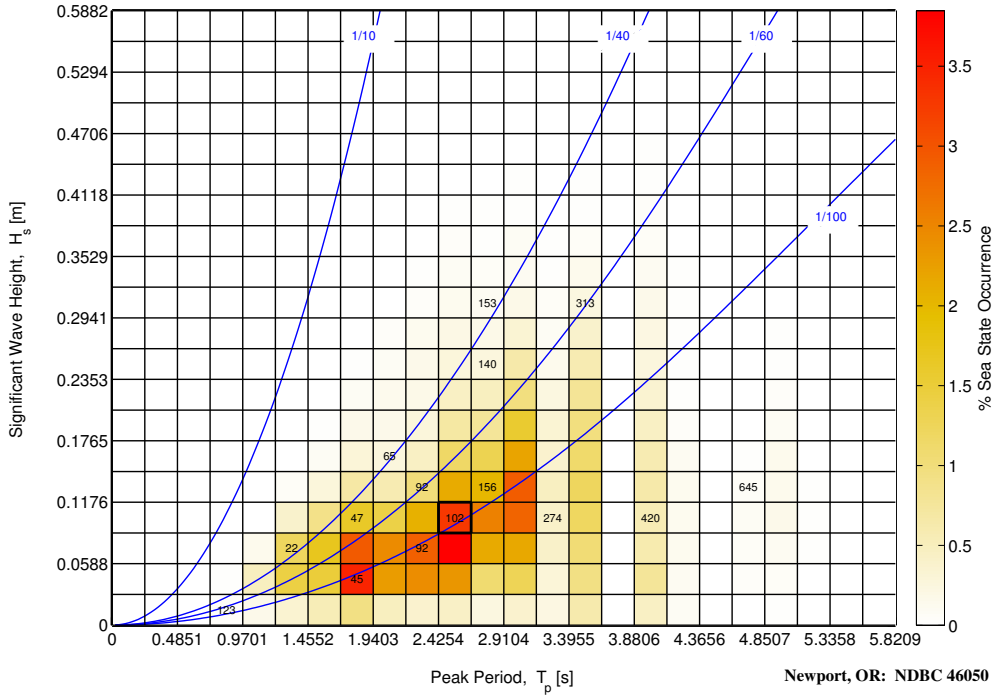

Figure 3.20: Percentage increase in power obtained with the MPC control strategy.

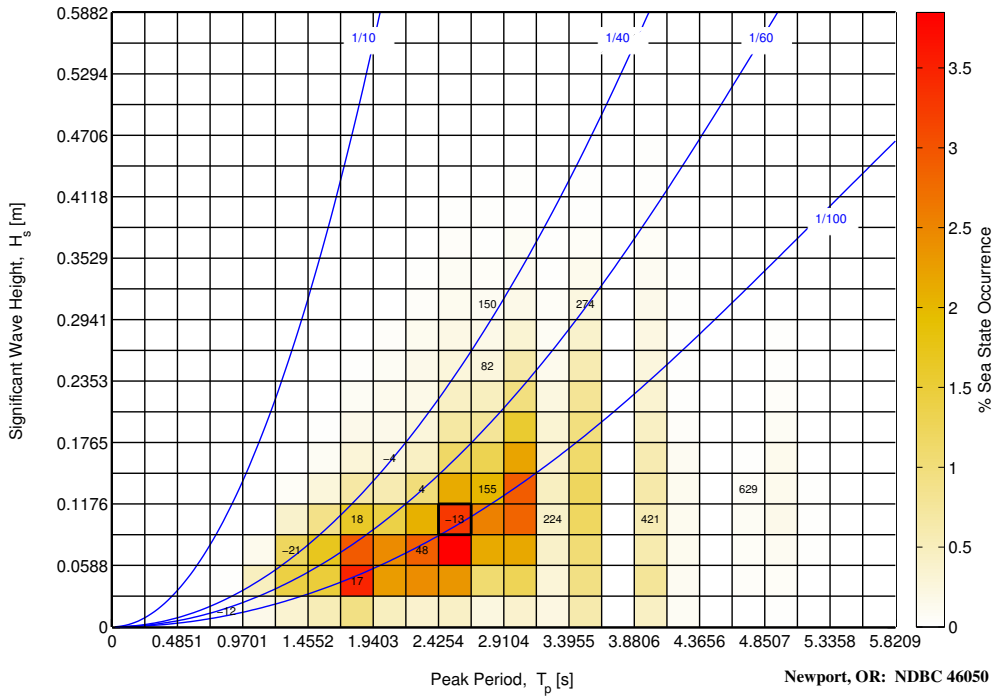

Figure 3.21: Percentage increase in power obtained with the DP controls strategy.

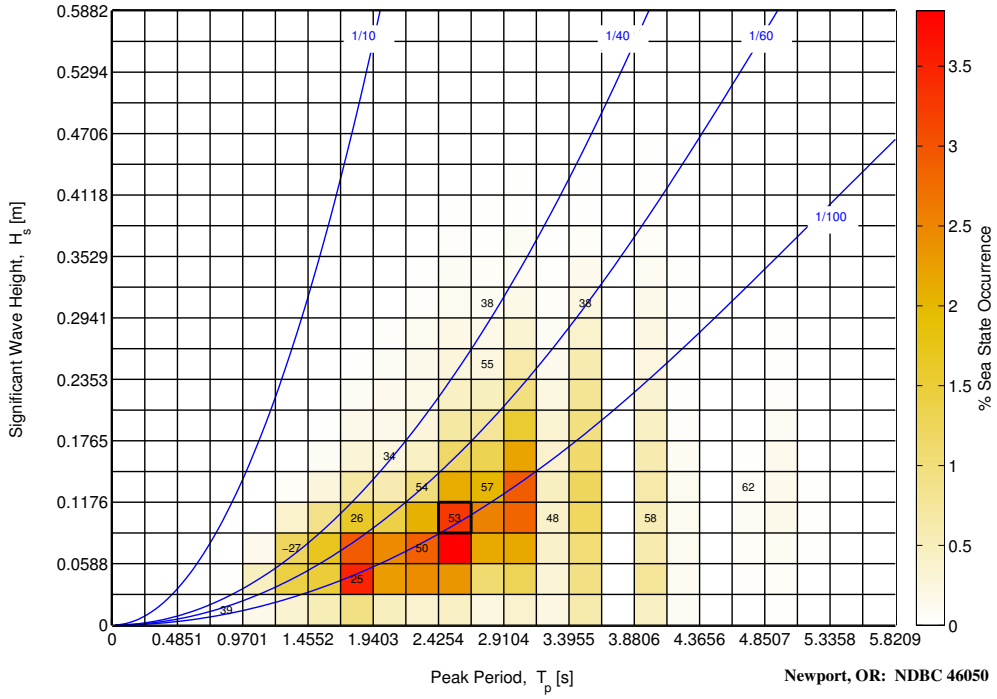

Figure 3.22: Percentage increase in power obtained with the SB controls strategy.

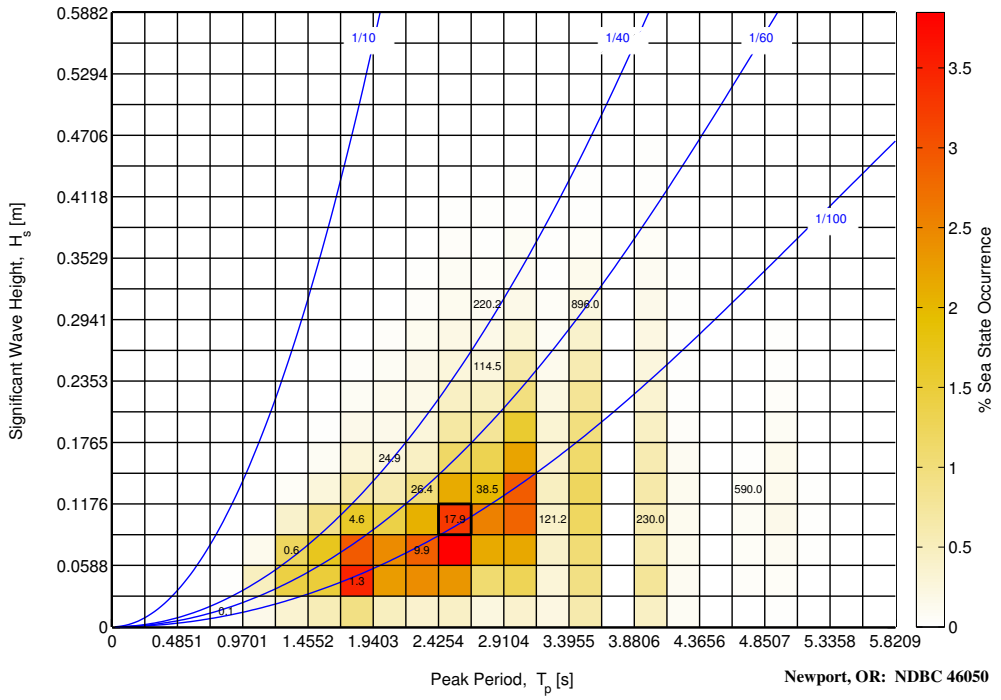

Figure 3.23: Average value of the reactive power for the MPC control strategy.

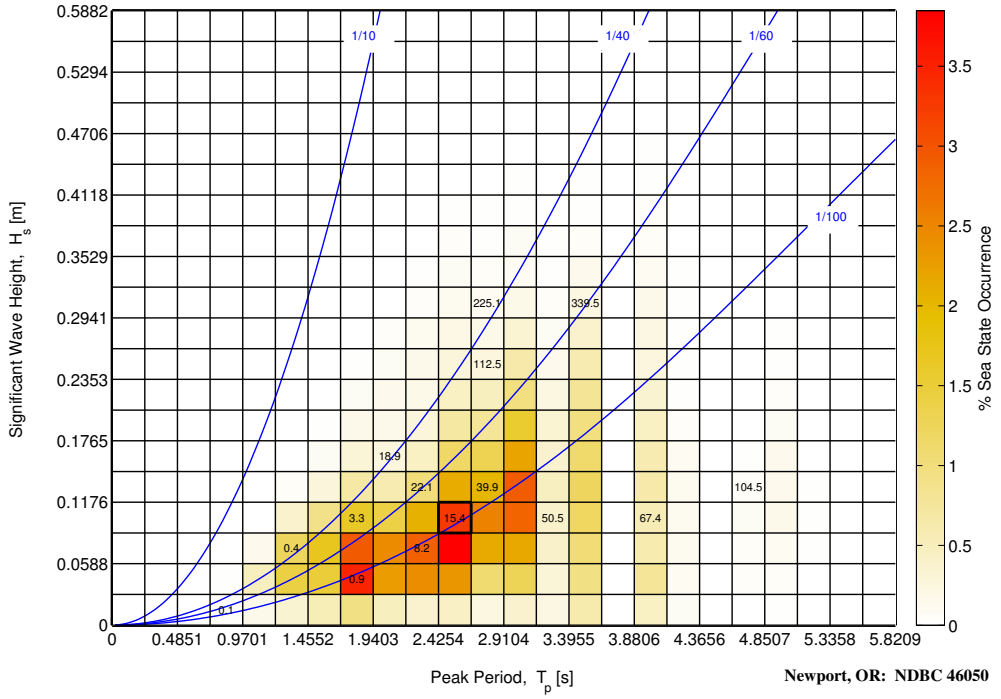

Figure 3.24: Average value of the reactive power for the LQ control strategy.

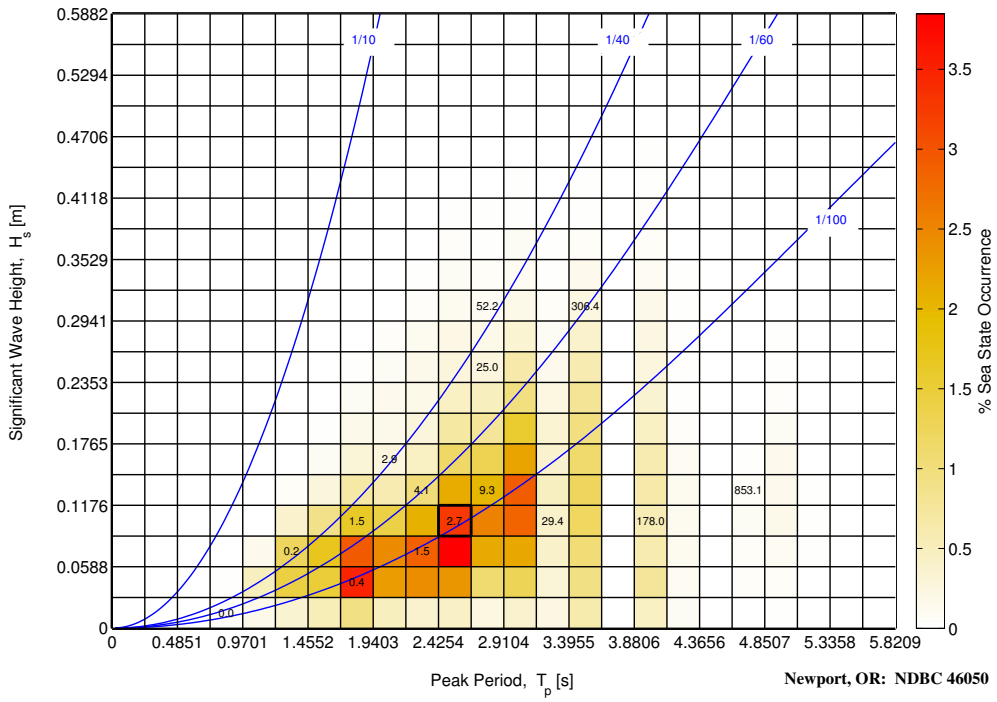

Figure 3.25: Average value of the reactive power for the PDC3 controls strategy.

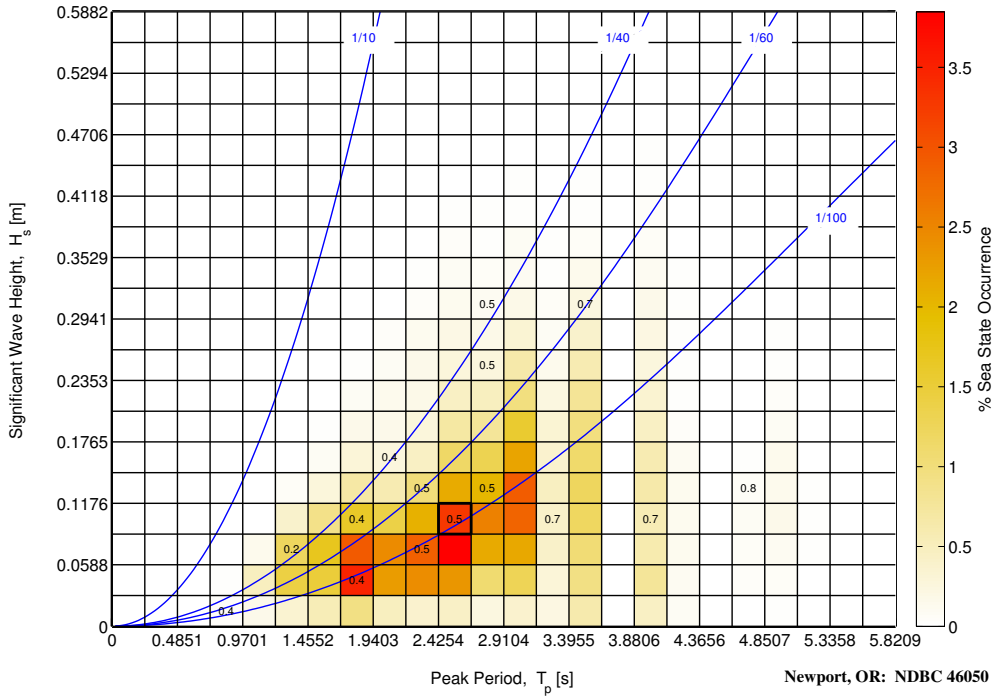

Figure 3.26: Ratio of the average reactive power needed by the MPC controller divided by the power flowing from the oscillating body into the PCC ("active power").

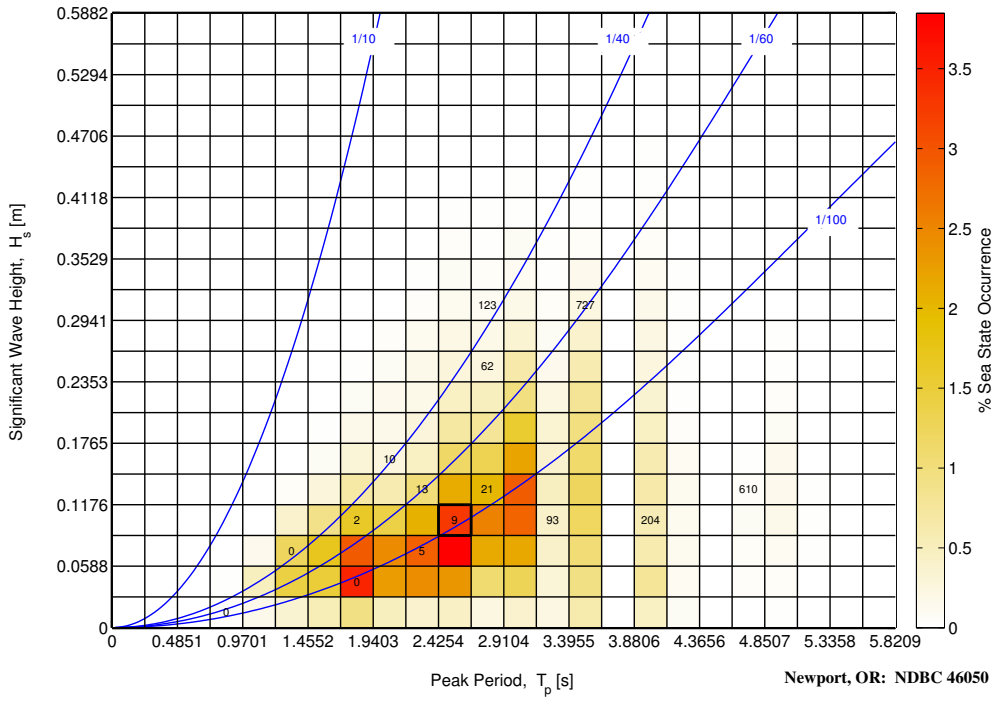

Figure 3.27: Average value of the required storage for the MPC control strategy.

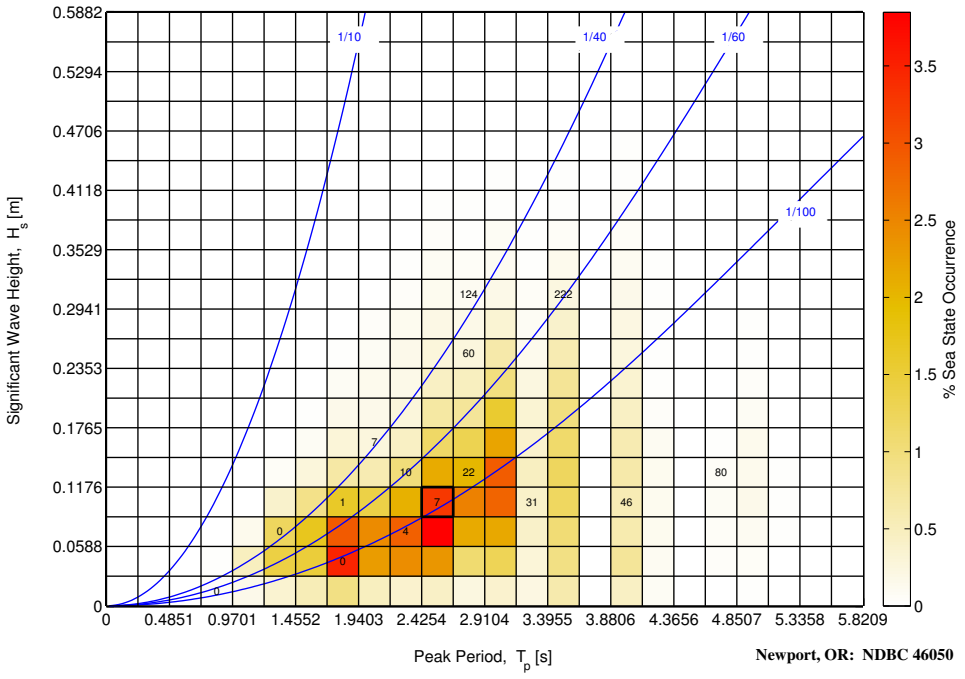

Figure 3.28: Average value of the required storage for the LQ control strategy.

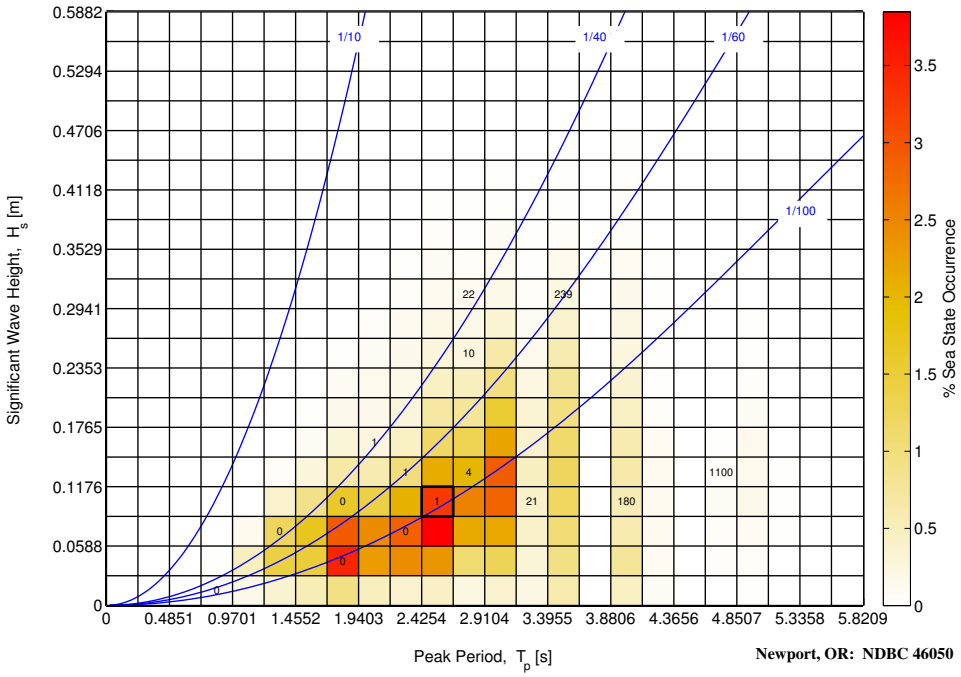

Figure 3.29: Average value of the required storage for the PDC3 controls strategy.

3.2 Nonlinear Results

The following section summarizes predictions for the T3R2's performance using CONFIG-D3 and D4, which are described in Section 1.2.2. Results are shown for the Resistive, MPC, LQ and Latching strategies. It is important to note that results shown here for CONFIG-D4 and D3 should not be compared directly with those obtained using CONFIG-B. While both models attempt to represent the same system (with different levels of fidelity), the tuning of each model is not necessarily synchronized to the other. As such, it is best to compare relative performance within each model configuration (e.g. a comparison of percent improvement over Resistive control in each configuration.)

3.2.1 Irregular Waves

Simulations were conducted using the seventeen irregular waves described in Section 1.3. A summary of the average annual power obtained from the Resistive, MPC, LQ and Latching strategies using CONFIG-D3 and D4 is shown in Table 3.5. In some cases, the results were unable to be obtained for a given controller due to its inability accommodate the nonlinear system (e.g. see discussion on constraint handling for LQ in Section 2.2.5). The most appropriate comparison is to consider relative performance for a certain control strategy with respect to Resistive for each configuration. For example, one could compare the 137% gain shown for MPC in Table 3.5 to the 197% gain shown for MPC in Table 1 (i.e., MPC appears to have performed better for the linear system than the nonlinear system). Additionally, one can observe the effect of limited PCC force by comparing the relative results for CONFIG-D3 and D4 in Table 3.5; MPC drops from an AAP increase of 151% with 8 kN of available PCC force to a 138% increase with on 2.7 kN of available PCC force. The following sections present extended discussions of the results from each of the control strategies listed in Table 3.5.

Table 3.5: Average annual power (AAP) production in a Newport, OR deployment climate for various control strategies using CONFIG-D3 and D4.

	CONFIG-D3		**CONFIG-D4**	
	AAP [kW]	Increase [%]	AAP [kW]	Increase [%]
Resistive	15.5	—	15.6	—
MPC	38.9	151	37.1	138
LQ	35.7	130	—	—
Latching	26.2	69	20.6	32.1

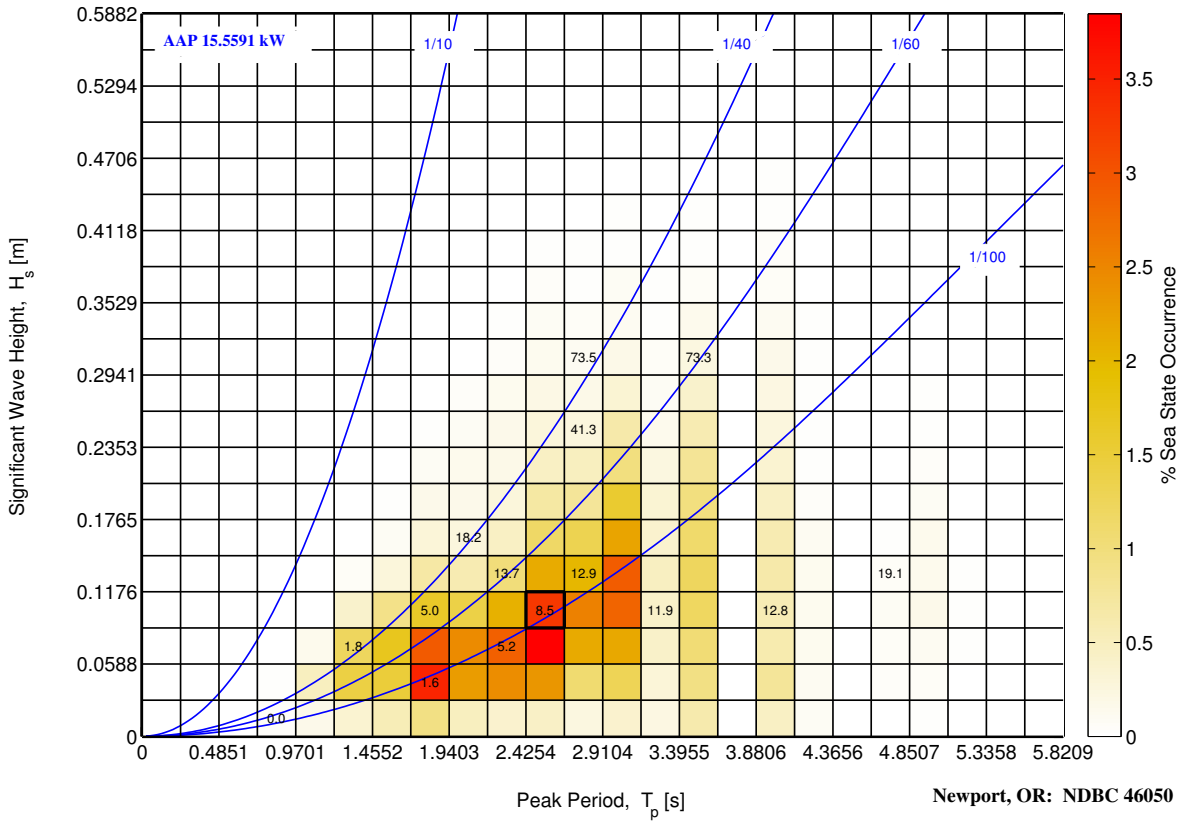

Figure 3.30: Power obtained with the Resistive control strategy using CONFIG-D4.

3.2.1.1 Resistive

Figure 3.30 shows the power obtained for Resistive control using the CONFIG-D4 Performance Model. Here, an optimal Resistive loading parameter was approximated by linearizing the quadratic viscous damping coefficient using the methodology described in [34]. The average annual power predicted from this scenario was 15.6 kW. This is similar to that predicted Resistive control using CONFIG-B (see, e.g., Table 1); however as noted in Section 3.2, direct comparison of results between CONFIG-B and CONFIG-D4 is unwise.

3.2.1.2 MPC

MPC has been implemented by approximating the quadratic dissipative term with a linear damping coefficient which dissipates the same amount of energy, as described in [34]. In practice, the controller model corresponds to CONFIG-B, where the damping coefficient has been calculated by using the linearization procedure previously described. The improvement in performance of MPC over resistive control is not as large as in the linear case (CONFIG-B); however the strategy is still producing more twice the amount power on an (averaged) annual basis (Tab 3.5).

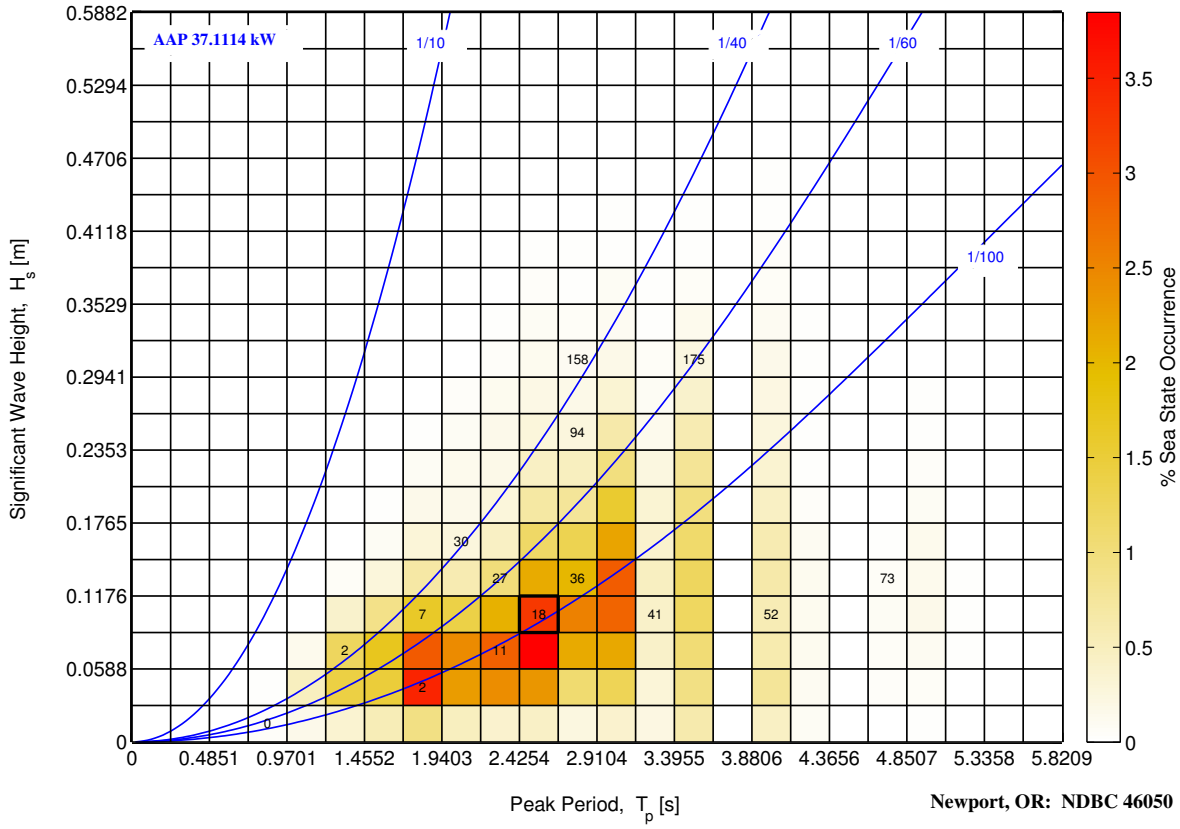

Figure 3.31: Power obtained with the MPC strategy using CONFIG-D4

By looking at the single sea-states on the scatter diagram in Figure 3.32, as expected, the improvement in absorbed power is smallest for wave periods close to the device resonance (i.e. sea-states 4–7). Conversely, for long waves, the improvement is more dramatic, reaching ≈300% for sea-states 16 and 17.

The effect of force saturation can be observed by noting that the improvement in power absorption decreases by increasing the wave height (sea-states 11, 12 and 15). For these sea-states, in fact, the optimal force required by the MPC to absorb the maximum amount of power is not available due to limitations in the PCC (see Figure 3.33).

3.2.1.3 LQ

LQ has been adapted to the nonlinear model by means of the same linearization used for MPC described in Section 3.2.1.2. LQ in the current formulation cannot include saturation in force or position, therefore the only nonlinearity included in the model is due to viscosity (CONFIG-D3). The simulation results are provided in Figure 3.34 for the average absorbed power and in Figure 3.35 for the improvement in power absorption with respect to resistive control.

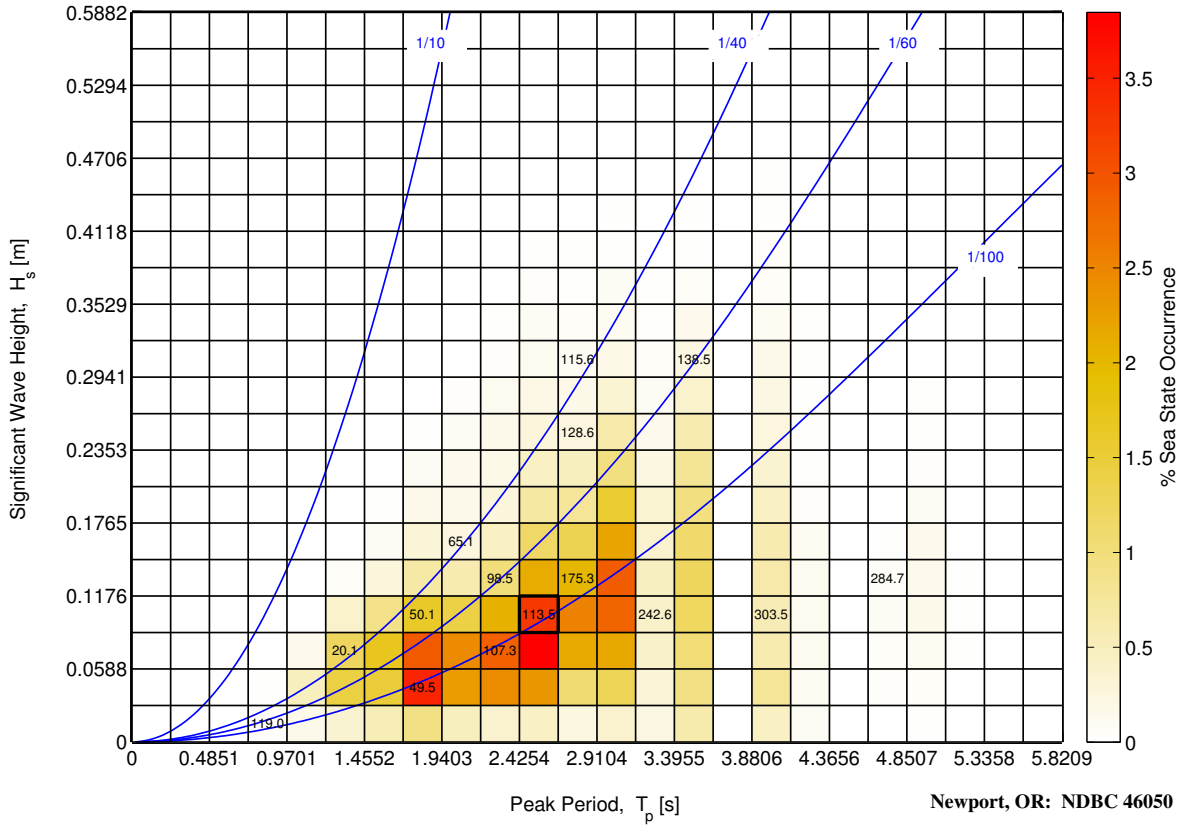

Figure 3.32: Percentage increase in power obtained with the MPC strategy using CONFIG-D4.

3.2.1.4 Latching

Latching has been adapted to the nonlinear model by means of the same linearization used for MPC described in Section 3.2.1.2. Latching cannot include saturation in force or position, therefore the only nonlinearity included in the model is due to viscosity. The simulation results are provided in Figure 3.36 for the average absorbed power and in Figure 3.37 for the improvement in power absorption with respect to resistive control.

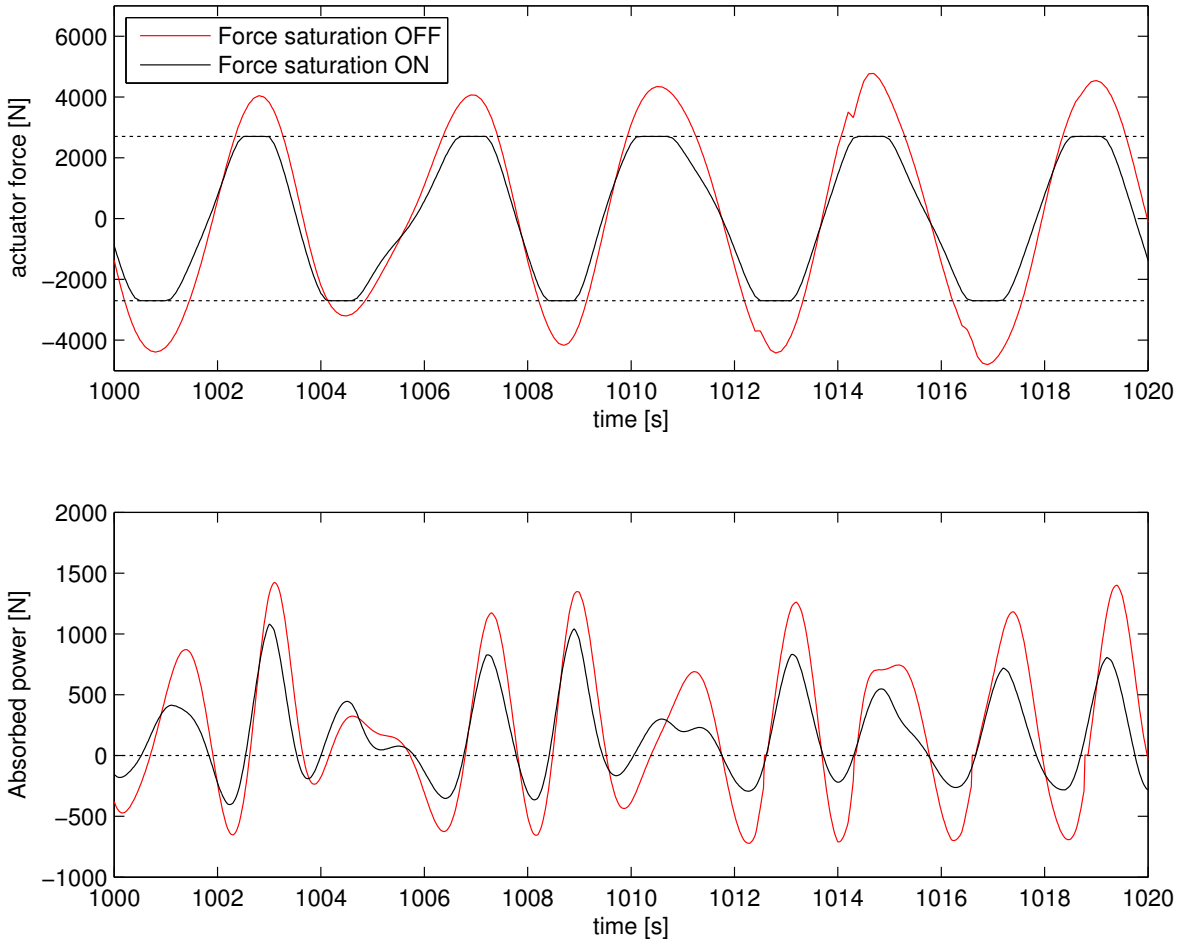

Figure 3.33: Effects of force saturation on actuator force and power for MPC (sea-state 15)

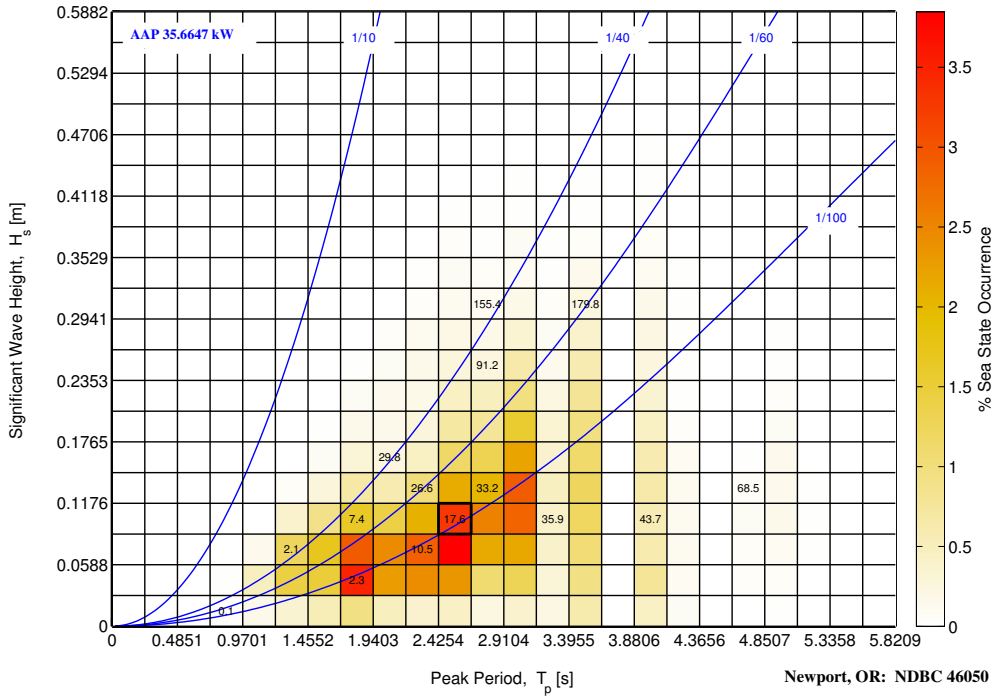

Figure 3.34: Power obtained with the LQ strategy using CONFIG-D3

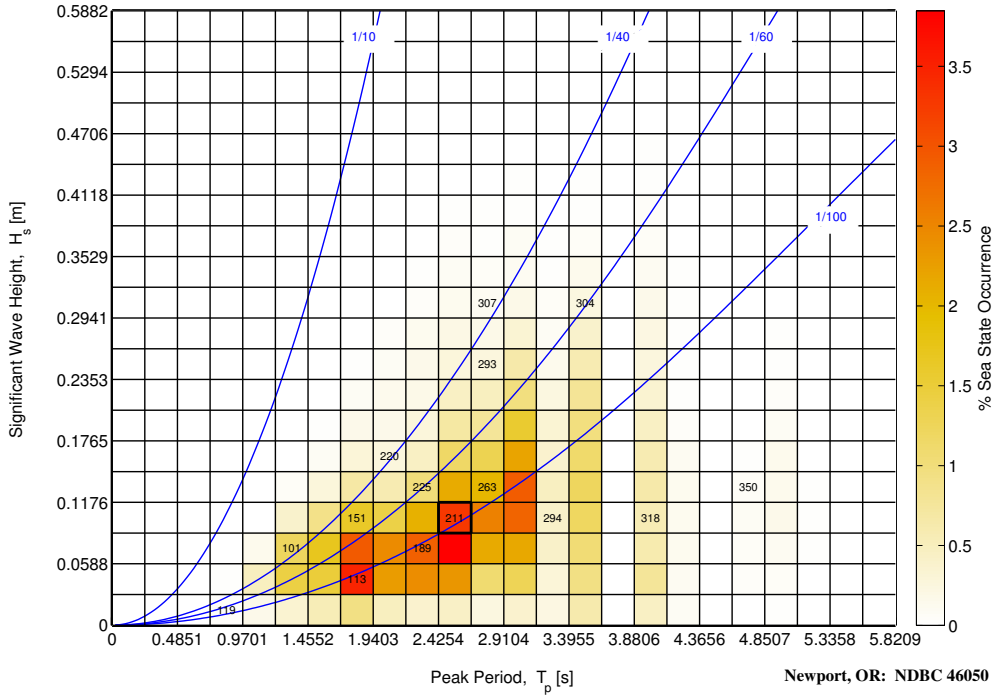

Figure 3.35: Percentage increase in power obtained with the LQ strategy using CONFIG-D3.

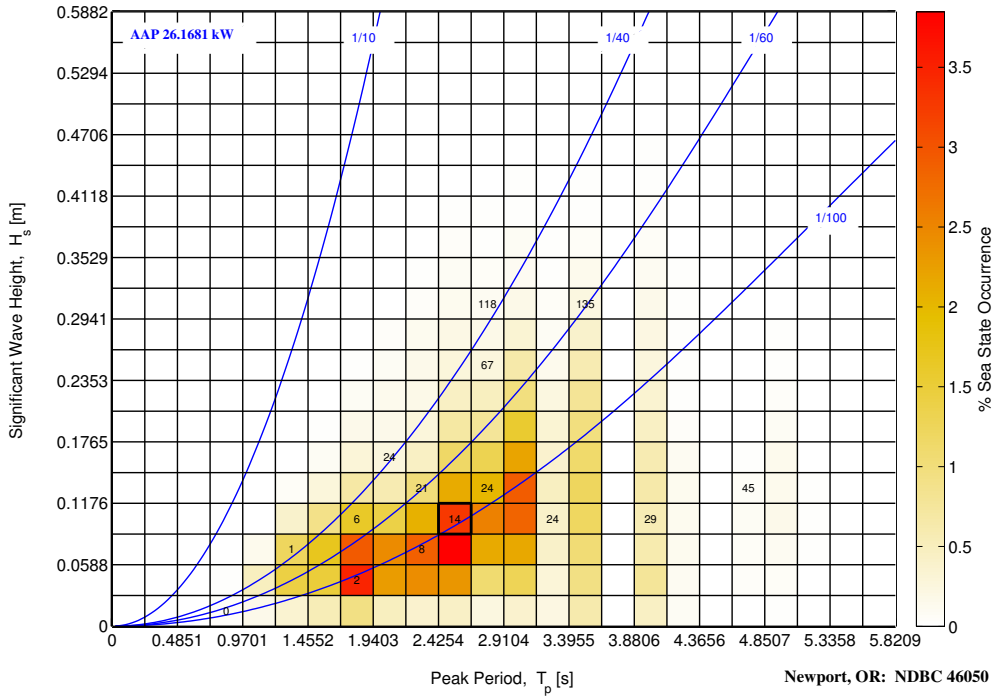

Figure 3.36: Power obtained with the Latching strategy using CONFIG-D3

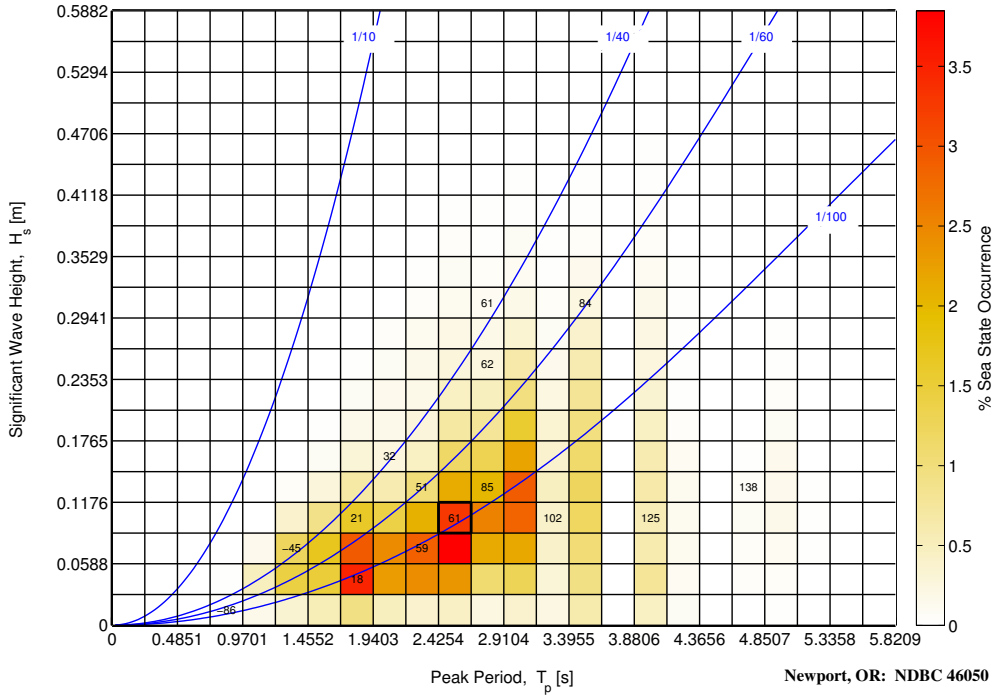

Figure 3.37: Percentage increase in power obtained with the Latching strategy using CONFIG-D3.

References

[1] K. Ogata, *Modern Control Engineering*. Prentice Hall, 2002.

[2] J. Hals, "Modelling and phase control of wave-energy converters," PhD, Norwegian University of Science and Technology, Trondheim, Norway, 2010. [Online]. Available: http://ntnu.diva-portal.org/smash/record.jsf?pid=diva2:403616

[3] WAMIT, *WAMIT User Manual*, 7th ed., Chestnut Hill, MA, 2012. [Online]. Available: http://www.wamit.com/manual.htm

[4] R. G. Coe and D. L. Bull, "Nonlinear time-domain performance model for a wave energy converter in three dimensions," in *OCEANS2014*. St. John's, Canada: IEEE, 2014.

[5] J. Hals, J. Falnes, and T. Moan, "Constrained optimal control of a heaving buoy wave-energy converter," *Journal of Offshore Mechanics and Arctic Engineering*, vol. 133, no. 1, pp. 1–15, 2011.

[6] G. Bacelli, J. Ringwood, and J.-C. Gilloteaux, "A control system for a self-reacting point absorber wave energy converter subject to constraints," in *Proceedings of 18th IFAC World Congress*, Milan, Italy, Aug. 2011. [Online]. Available: http://eprints.nuim.ie/3555/

[7] J. A. M. Cretel, G. Lightbody, G. P. Thomas, and A. W. Lewis, "Maximisation of energy capture by a wave-energy point absorber using model predictive control," in *IFAC World Congress*, 2011.

[8] R. Genest, F. Bonnefoy, A. H. Clment, and A. Babarit, "Effect of non-ideal power take-off on the energy absorption of a reactively controlled one degree of freedom wave energy converter," *Applied Ocean Research*, vol. 48, no. 0, pp. 236 – 243, 2014. [Online]. Available: http://www.sciencedirect.com/science/article/pii/S0141118714000893

[9] J. Hals, J. Falnes, and T. Moan, "A comparison of selected strategies for adaptive control of wave energy converters," *Journal of Offshore Mechanics and Arctic Engineering*, vol. 133, no. 3, p. 031101, March 2011. [Online]. Available: http://offshoremechanics.asmedigitalcollection.asme.org/article.aspx?articleid=1456895

[10] R. G. Coe and D. L. Bull, "Sensitivity of a wave energy converter dynamics model to nonlinear hydrostatic models," in *Proceedings of the ASME 2015 34th International Conference on Ocean, Offshore and Arctic Engineering (OMAE2015)*. St. John's, Newfoundland: ASME, 2015.

[11] W. E. Cummins, "The impulse response function and ship motions," Department of the Navy, David Taylor Model Basin, Bethesda, MD, Tech. Rep. DTNSDRC 1661, 1962. [Online]. Available: http://dome.mit.edu/handle/1721.3/49049

[12] D. Bull and E. Johnson, "Optimal resistive control strategy for a floating OWC device," in *Proceedings of the 10th European Wave and Tidal Energy Conference*. Aalborg, Denmark: Technical Committee of the European Wave and Tidal Energy Conference, 2013. [Online]. Available: http://energy.sandia.gov/wp/wp-content/gallery/uploads/SAND2013-6198c.pdf

[13] DNV, "Modelling and analysis of marine operations," Tech. Rep. DNV-RP-H103, 2011.

[14] J. Lavelle and J. P. Kofoed, "Representative spectra of the wave resource from sea wave measurements," in *EWTEC*, Aalborg, Denmark, 2013. [Online]. Available: http://www.researchgate.net/profile/John_Lavelle2/publication/267763888_Representative_Spectra_of_the_Wave_Resource_from_Real_Sea_Wave_Measurements/links/545a287b0cf2cf51648437dc.pdf

[15] B. D. Anderson and J. B. Moore, *Optimal Control - Linear Quadratic Methods*. Prentice-Hall International, Inc., 1989.

[16] P. Kracht, "Wave prediction and its implementation on control systems of wave-energy converters," Fraunhofer IWES, EU MaRINet Infrastructure Access Report, Tech. Rep., 2013.

[17] D. P. Bertsekas, *Dynamic Programming and Optimal Control*, 4th ed. Athena Scientific, 2012.

[18] O. Abdelkhalik, "Hidden genes genetic optimization for variable-size design space problems," *Journal of Optimization Theory and Applications*, vol. 156, no. 2, February 2013.

[19] R. D. Robinett, D. G. Wilson, G. R. Eisler, and J. E. Hurtado, *Applied Dynamic Programming for Optimization of Dynamical Systems*. Society for Industrial and Applied Mathematics, 2005.

[20] E. Taheri and O. Abdelkhalik, "Shape based approximation of constrained low-thrust space trajectories using Fourier series," *Journal of Spacecraft and Rockets*, vol. 49, no. 3, May - June 2012.

[21] ——, "Approximation of constraint low thrust space trajectories using Fourier series," in *AAS / AIAA Astrodynamics Specialist Conference*, no. AAS11-555, Girdwood, Alaska, USA, July 31 – August 4 2011.

[22] O. Abdelkhalik and E. Taheri, "Approximate on-off low-thrust space trajectories using Fourier series," *Journal of Spacecraft and Rockets, AIAA*, accepted in February 2012.

[23] E. Taheri and O. Abdelkhalik, "Constraint low-thrust trajectory planning in three-body dynamic models: Fourier series approach," in *AIAA Space and Astronautics Forum and Exposition, AAS / AIAA Astrodynamics Specialist Conference*, no. AIAA-2014-4464, San Diego, CA, USA, August 4–7 2014.

[24] G. Elnagar, M. Kazemi, and M. Razzaghi, "The pseudospectral legendre method for discretizing optimal control problems," *Automatic Control, IEEE Transactions on*, vol. 40, no. 10, pp. 1793–1796, Oct 1995.

[25] I. M. Ross and M. Karpenko, "A review of pseudospectral optimal control: From theory to flight," *Annual Reviews in Control*, vol. 36, no. 2, pp. 182 – 197, 2012. [Online]. Available: http://www.sciencedirect.com/science/article/pii/S1367578812000375

[26] D. Gottlieb and S. A. Orszag, *Numerical Analysis of Spectral Methods: Theory and Applications*. Society for Industrial and Applied Mathematics, 1977.

[27] J. T. Scruggs, S. M. Lattanzio, A. A. Taflanidis, and I. L. Cassidy, "Optimal causal control of a wave energy converter in a random sea," *Applied Ocean Research*, vol. 42, pp. 1–15, Aug. 2013. [Online]. Available: http://www.sciencedirect.com/science/article/pii/S0141118713000205

[28] R. Hoskin, B. Count, N. Nichols, and D. Nicol, "Phase control for the oscillating water column," in *Hydrodynamics of Ocean Wave-Energy Utilization*, ser. International Union of Theoretical and Applied Mechanics, D. Evans and A. de Falco, Eds. Springer Berlin Heidelberg, 1986, pp. 257–268. [Online]. Available: http://dx.doi.org/10.1007/978-3-642-82666-5_22

[29] A. F. O. Falcao, P. A. Justino, J. C. Henriques, and J. M. Andre, "Reactive versus latching phase control of a two-body heaving wave energy converter," in *Control Conference (ECC), 2009 European*, Aug 2009, pp. 3731–3736.

[30] K. Budal, J. Falnes, T. Hals, L. C. Iversen, and T. Onshus, "Model experiment with a phase controlled point absorber," in *Proc. of the Second International Symposium on Wave and Tidal Energy*. Cambridge, UK: H. S. Stephens and C. A. Stapleton, eds, BHRA Fluid Engineering (Cranford, Bedford), 1981, pp. 191–206.

[31] J. Falnes and J. Hals, "Heaving buoys, point absorbers and arrays," *Philosophical Transactions of the Royal Society A: Mathematical,Physical and Engineering Sciences*, vol. 370, no. 1959, pp. 246–277, 2012. [Online]. Available: http://rsta.royalsocietypublishing.org/content/370/1959/246.abstract

[32] G. Bacelli, "Optimal control of wave energy converters," PhD, National University of Ireland, Maynooth, Maynooth, Ireland, 2014.

[33] J. Falnes, *Ocean Waves and Oscillating Systems*. Cambridge; New York: Cambridge University Press, 2002.

[34] G. Bacelli, P. Balitsky, and J. V. Ringwood, "Coordinated control of arrays of wave energy devicesbenefits over independent control," *Sustainable Energy, IEEE Transactions on*, vol. 4, no. 4, pp. 1091–1099, 2013.

Appendix A

Detailed description of controllers

Classical feedback and feedforward architectures are shown in Figures A.1 and controllers based on some form of optimization in the loop are given in Figure A.2, and will be considered as "receding horizon" architectures.

Both architectures will employ some form of *controller model*, which is used by the controller in an online fashion (hopefully in real-time) and during the design process (offline). The performance model represents a real WEC device which is modeled as multi-DOF model with constraints and nonlinear hydrodynamics. However, the model that the controller uses for the calculation of the control signal may not be the performance model; it may be a Reduced Order Model (ROM) form that is employed. For example, the performance model could be multi-frequency models incorporating the full frequency-dependence of hydrodynamic parameters, whereas single-frequency models use constant coefficients (i.e., Constant Coefficient model (CCM)).

The main blocks composing Figure A.1 are the feedback and the feedforward: the feedback processes the output by means of the block $H_{FB}(s)$ which could describe sensors or other signal processing devices, and the output is compared to a reference signal. The resulting tracking error (e) is processed by the feedback controller ($C_{FB}(s)$) which continuously calculates a control signal output to the plant (usually the model of the WEC), and it is denoted by $G(s)$. The feedforward block ($C_{FF}(s)$), on the other hand, only processes the reference signal directly, and is summed with the feedback signal as input to the plant. The block $H_{ref}(s)$ is used to condition the reference signal, in order to be compared with the feedback signal[1]. Note all the signals are represented in the s-domain.

The main blocks composing the receding horizon architecture in Figure A.2 are the optimizer (OPTIM) and the predictor (PRED). The predictor generates a finite horizon prediction of a reference condition (e.g. wave elevation, excitation force, power, etc.). These reference conditions are used by the optimizer to calculate the optimal control signal over the finite horizon. The control signal is updated periodically and each time the initial conditions are reset to reflect the current state of the system; this is achieved by means of the feedback line (feedback from the plant $G(s)$ output y to the block OPTIM). In some cases there may be a low level feedback loop ($H_{FB}(s)$) which could be used to reduce the effect of disturbances or model mismatch.

[1] e.g., the input reference can be the excitation force, and the feedback signal can be the velocity. In this case, the block $H_{ref}(s)$ would be the force-to-velocity transfer function of the WEC.

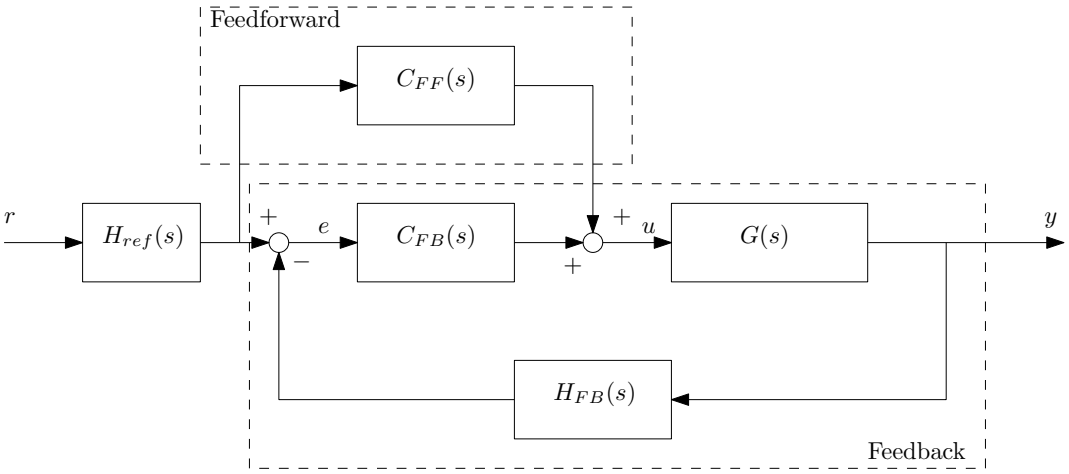

Figure A.1: Basic FF+FB controller structure [1]

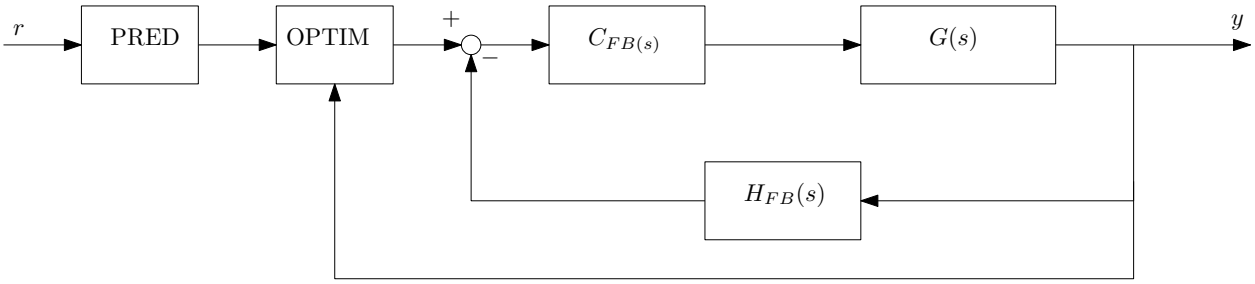

Figure A.2: Basic structure for "receding horizon"

A.1 MPC

Model Predictive Control is an optimization based control strategy that is derived from attempting to solve a Quadratic (QP) Program in a receding horizon fashion (Figure A.2). In the current implementation, the inner feedback loop has not been considered, therefore the transfer function of the feedback block is $H_{FB}(s) = 0$ and the controller is $C_{FB}(s) = 1$, however as shown in Figure A.2 the current state of the system is passed to the optimization block directly. The signal r is the excitation force and the prediction block predicts the value of the excitation force over the prediction horizon, which is used by the optimizer to calculate the optimal motion and the corresponding force maximizing the absorbed power. The procedure is repeated periodically to compensate for disturbance and imperfect modeling by updating the current state of the system every time the optimization is carried out. In the current implementation it is assumed that perfect foreknowledge of the excitation is available.

The derivation of the MPC control law begins with the specification of the WEC model used for control (controller model), which is the continuous time state space model.

$$\begin{aligned} \dot{\boldsymbol{x}}_c(t) &= A_c \boldsymbol{x}_c + B_c(u_c(t) + v_c(t)) \\ \boldsymbol{y}_c(t) &= C_c \boldsymbol{x}_c(t) \end{aligned} \tag{A.1}$$

Here, the state variable $\boldsymbol{x}_c$ and the output variable $\boldsymbol{y}_c$ are defined, respectively, as

$$\boldsymbol{x}_c = \begin{bmatrix} z \\ \dot{z} \\ \boldsymbol{x}_r \end{bmatrix} \in \mathbb{R}^{2+n} \qquad \boldsymbol{y}_c = \begin{bmatrix} z \\ \dot{z} \end{bmatrix} \in \mathbb{R}^2 \tag{A.2}$$

The vertical position of the buoy is denoted by z and $\boldsymbol{x}_r \in \mathbb{R}^n$ is the state vector of radiation dynamics. The matrices A_c, B_c and C_c are

$$A_c = \begin{bmatrix} 0 & 1 & \mathbf{0} \\ \frac{-k_h}{m+\mu} & \frac{-b_v}{m+\mu} & \frac{-1}{m+\mu} C_r \\ \mathbf{0} & B_r & A_r \end{bmatrix} \in \mathbb{R}^{(n+2)\times(n+2)}$$

$$B_c = \begin{bmatrix} 0 \\ 1 \\ \mathbf{0} \end{bmatrix} \in \mathbb{R}^{(n+2)\times 1},$$

where k_h is the hydrostatic restoring coefficient, b_v is a linear damping term describing the viscous effects of the fluid (and/or any other linear friction terms), m is the mass of the buoy and μ is the asymptotic value of the added mass. The matrices A_r, B_r and C_r, as usual, describe the dynamics of the radiation force (f_r):

$$\begin{aligned} \dot{\boldsymbol{x}}_r(t) &= A_r \boldsymbol{x}_r(t) + B_r \dot{z}(t) \\ f_r(t) &= C_r \boldsymbol{x}_r. \end{aligned} \tag{A.3}$$

The MPC algorithm requires the dynamic model to be formulated in discrete time: following [7], the discretization of the model in eq. (A.1) is carried out by means of a triangle-hold (first order-hold), which results in continuous and piecewise linear profile for the optimal PCC force. The benefit of this type of discretization is to allow for a longer update interval compared to a zero-hold discretization, which provides only a discontinuous, piecewise constant profile for the optimal control force. The state space model resulting from the discretization is:

$$\begin{aligned} \boldsymbol{x}(k+1) &= A\,\boldsymbol{x}(k) + B\,\Delta u(k+1) + F\,\Delta(k+1) \\ \boldsymbol{y}(k) &= C\,\boldsymbol{x}(k) \end{aligned}$$

where

$$A = \begin{bmatrix} \phi(h) & \Gamma & \Gamma \\ 0 & 1 & 0 \\ 0 & 0 & 1 \end{bmatrix} \in \mathbb{R}^{(n+4)\times(n+4)} \qquad B = \begin{bmatrix} \Lambda \\ 1 \\ 0 \end{bmatrix} \in \mathbb{R}^{(n+4)\times 1}$$

$$F = \begin{bmatrix} \Lambda \\ 0 \\ 1 \end{bmatrix} \in \mathbb{R}^{(n+4)\times 1} \qquad C = \begin{bmatrix} 1 & 0 & 0 & \dots & 0 & 0 & 0 \\ 0 & 1 & 0 & \dots & 0 & 0 & 0 \\ 0 & 0 & 1 & \dots & 0 & 0 & 0 \end{bmatrix} \in \mathbb{R}^{3\times(n+4)}$$

and where $\phi(h) = e^{A_c h}$

$$\Gamma = A_c^{-1}\left(\phi(h) - I\right) B_c \ \in \mathbb{R}^{(n+2)\times 1}$$
$$\Lambda = \frac{1}{h} A_c^{-1}\left(\Gamma - hB_c\right) \quad \in \mathbb{R}^{(n+2)\times 1}$$

Note: the state vector has been augmented by including the PCC force and the excitation force; also the output vector has been augmented, including only the PCC force. The state and output vectors have been augmented because the inputs has been expressed as increments with respect to its previous value $(\Delta u, \Delta v)$, therefore the dynamical system had to be augmented with two integrators corresponding to the last two rows of matrix A.

Let N denote the number of prediction steps, then the predicted output of the system can be written as function of the current state and future inputs increments as:

$$\underline{\mathbf{y}}(k) = \mathscr{P}\mathbf{x}(k) + \mathscr{T}_u \underline{\Delta \mathbf{u}}(k) + \mathscr{T}_v \underline{\Delta \mathbf{v}}(k)$$

where $\mathscr{P}$, $\mathscr{T}_u$ and $\mathscr{T}_v$ are

$$\mathscr{P} = \begin{bmatrix} CA \\ CA^2 \\ \vdots \\ CA^N \end{bmatrix} \in \mathbb{R}^{3N\times(n+4)}$$

$$\mathscr{T}_u = \begin{bmatrix} CB & 0 & 0 & \dots \\ CAB & CB & 0 & \dots \\ CA^2B & CAB & CB & \dots \\ \vdots & \vdots & \vdots & \vdots \\ CA^{N-1}B & CA^{N-2}B & CA^{N-3}B & \dots \end{bmatrix} \quad \in \mathbb{R}^{3N\times N}$$

$$\mathscr{T}_v = \begin{bmatrix} CF & 0 & 0 & \dots \\ CAF & CF & 0 & \dots \\ CA^2F & CAF & CF & \dots \\ \vdots & \vdots & \vdots & \vdots \\ CA^{N-1}F & CA^{N-2}F & CA^{N-3}F & \dots \end{bmatrix} \quad \in \mathbb{R}^{3N\times N}$$

The quantity to be maximized is the mechanical work done by the PCC over the prediction horizon T, expressed as:

$$E_{t,t+T} = -(m+\mu)\int_t^{t+T} u(\tau)\dot{z}(\tau)\,d\tau$$

By means of the discretization, this quantity can be written in matrix form as the quadratic cost function J, defined as

$$J = \frac{1}{2}\underline{\Delta \mathbf{u}}^T \mathscr{T}_u^T Q \mathscr{T}_u \underline{\Delta \mathbf{u}} + \underline{\Delta \mathbf{u}}^T \mathscr{T}_u^T Q\left(\mathscr{P}\mathbf{x} + \mathscr{T}_v \underline{\Delta \mathbf{v}}\right),$$

where Q and M are:

$$Q = \begin{bmatrix} M & & & \\ & \ddots & & \\ & & M & \\ & & & \frac{1}{2}M \end{bmatrix}, \qquad M = \begin{bmatrix} 0 & 0 & 0 \\ 0 & 0 & 1 \\ 0 & 1 & 0 \end{bmatrix}.$$

Constraints on the maximum PCC force and maximum displacement can be included in the formulation of the optimization problem using the linear inequalities

$$\begin{bmatrix} M_z \\ -M_z \end{bmatrix} \mathscr{T}_u \underline{\Delta \mathbf{u}} = \begin{bmatrix} -M_z \\ M_z \end{bmatrix} (\mathscr{P}\mathbf{x} + \mathscr{T}_v \underline{\Delta \mathbf{v}}) + z_{max}$$
$$\begin{bmatrix} M_f \\ -M_f \end{bmatrix} \mathscr{T}_u \underline{\Delta \mathbf{u}} = \begin{bmatrix} -M_f \\ M_f \end{bmatrix} (\mathscr{P}\mathbf{x} + \mathscr{T}_v \underline{\Delta \mathbf{v}}) + f_{max}$$

where M_z and M_f are

$$M_z = \begin{bmatrix} C_z & & & \\ & \ddots & & \\ & & C_z & \\ & & & C_z \end{bmatrix} \in \mathbb{R}^{N \times 3N} \quad C_z = [1\ 0\ 0],$$

$$M_f = \begin{bmatrix} C_f & & & \\ & \ddots & & \\ & & C_f & \\ & & & C_f \end{bmatrix} \in \mathbb{R}^{N \times 3N} \quad C_f = [0\ 0\ 1].$$

A.2 Dynamic Programming Control Optimization

Dynamic Programming (DP) is a receding horizon strategy (Figure A.2) targeting both amplitude and phase, and in the current implementation does not include a inner feedback loop (block $C_{FB}(s) = 1$ and feedback block $H_{FB}(s) = 0$, however as shown in Figure A.2 the current state of the system is passed to the optimization block directly). The states are discretized in space and time. This discretization is fundamental for DP operation and is crucial for computational efficiency of the DP approach. Given maximum and minimum values for each of the system states, the state space is divided into nodes of equal inter-spaces. The number of nodes for the states, $N_{x1}, N_{x2}, \cdots, N_{xn}$, are tuning parameters. An illustration for a two-dimensional discretized domain is shown in Fig. A.3. In this discretized domain, any state $\vec{x}_i$, for instance in box 1, is associated with the state vector at the node $\vec{x}_{\mathbf{a}l}$ in the same box. When the system transitions from a state $\vec{x}_i$ at time step k to a state $\vec{x}_j$, for instance in box 2, at time step $k+1$ through a control u, the two associated states for $\vec{x}_i$ and $\vec{x}_j$, $\vec{x}_{\mathbf{a}l}$ and $\vec{x}_{\mathbf{a}m}$ respectively, are computed and stored. The transition between any two other states whose associated states are also $\vec{x}_{\mathbf{a}l}$ and $\vec{x}_{\mathbf{a}m}$ (i.e. transition between

any state in box 1 to any state in box 2) at the time step k and $k+1$, respectively, is considered to have the same fitness value as the fitness of the transition between $\vec{x}_i$ and $\vec{x}_j$; hence a significant computational effort can be saved.

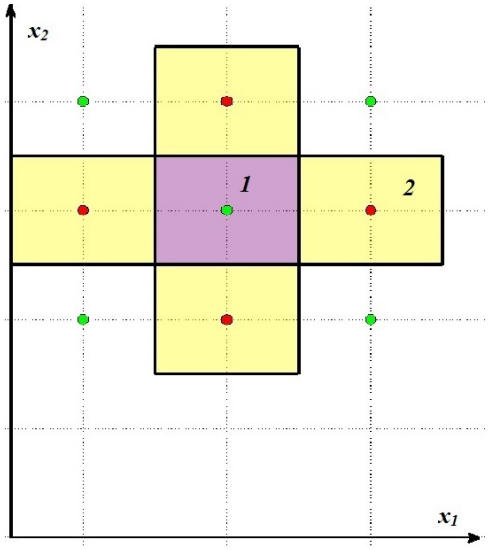

Figure A.3: Discretization of the state space for DP implementation

The process of dynamic programming for the WEC optimal control is here described. Suppose that the control is updated at a rate of u_{rate} Hz. Given a current state vector $\vec{x}_k$ and current time t_k, the optimal control over a horizon (H seconds) is computed, $u_1, u_2, ...u_N$, where $N = H \times u_{rate}$. Only the first control u_1 is used to update the current state to a new state $\vec{x}_{k+1}$. This process is repeated. To implement this process, three matrices are constructed and updated at a rate u_{rate}; also an index is given to each associated state. The three matrices are: $S_{Ind,N}$, $U_{Ind,N}$, and $I_{Ind,N}$, where $Ind = N_{x1} \times N_{x2}$ is the total number of indices. The matrix $S_{Ind,N}$ contains associated states at N different times starting from the current time until the end of the horizon H. The matrix element $S(i,k)$, for instance, includes the index of the associated states at time $k-1$ that is transitioned to the associated state i at time k. The corresponding control used for this transition is stored in $U(i,k)$. The corresponding extracted energy is stored in $I(i,k)$.

The three matrices (S, U and I) are initialized recursively. Starting from the initial state $\vec{x}_0$ at time t_0, each of the Nu discrete control values between (u_{max} and $-u_{max}$) is applied to $\vec{x}_0$ to compute a set of new states $\vec{x}_1, \cdots, \vec{x}_{Nu}$ at time t_1. The associated states of the states $\vec{x}_0, \vec{x}_1, \cdots, \vec{x}_{Nu}$ are computed ($\vec{x}_{\mathbf{a}0}, \vec{x}_{\mathbf{a}l}, \cdots, \vec{x}_{\mathbf{a}Nu}$ respectively) and stored in the S matrix.

$$\begin{aligned} S(\vec{x}_{\mathbf{a}l}, 1) &= \vec{x}_{\mathbf{a}0} \\ &\vdots \\ S(\vec{x}_{\mathbf{a}Nu}, 1) &= \vec{x}_{\mathbf{a}0} \end{aligned} \tag{A.4}$$

The corresponding controls and extracted energies are stored in U and I matrices as follows:

$$\begin{aligned} U(\vec{x}_{\mathbf{a}l},1) &= u_1 \\ &\vdots \\ U(\vec{x}_{\mathbf{a}Nu},1) &= u_{Nu} \\ I(\vec{x}_{\mathbf{a}l},1) &= u_1 \times \vec{x}_0(2) \\ &\vdots \\ I(\vec{x}_{\mathbf{a}Nu},1) &= u_{Nu} \times \vec{x}_0(2) \end{aligned} \tag{A.5}$$

Starting from each of $\vec{x}_1,\ldots,\vec{x}_{Nu}$ as initial states, the above process is repeated recursively until time t_N to initialize the three matrices. The extracted energy is accumulated in subsequent steps, e.g.:

$$I(\vec{x}_{\mathbf{a}4},2) = I(\vec{x}_{\mathbf{a}1},1) - u_1 \times \vec{x}_1(2) \tag{A.6}$$

After initialization, the last column in the I matrix is scanned for the maximum value (maximum extracted energy). This entry in the I matrix at time t_N is traced back in the U matrix to find the corresponding control at initial time u_1. This initial control is applied to the initial state to compute the new updated state. The above process repeats. It is not needed to compute the full matrices anymore; we only need to compute one additional column in each matrix, at each new time step.

A.3 Shape-Based Control

The Shape-Based control approach is a receding horizon strategy targeting both amplitude and phase, and in the current implementation does not include an inner feedback loop (block $C_{FB}(s) = 1$ and feedback block $H_{FB}(s) = 0$). However as shown in Figure A.2 the current state of the system is passed to the optimization block directly.

For the WEC optimal control problem, the SB control approach approximate the buoy's vertical velocity, $v_f(t)$, as follows:

$$v_f(t) \equiv x_2 = \frac{a_0}{2} + \Sigma_{n=1}^{N}\left(a_n \cos\left(\frac{n\pi}{H}t\right) + b_n \sin\left(\frac{n\pi}{H}t\right)\right) \tag{A.7}$$

Where H is the predication horizon time interval, and N is number of Fourier terms which is a design parameter. The coefficients a_0, a_n, and b_n are the design variables to be optimized in order to obtain the shape of $v_f(t)$ that would maximize the extracted energy. For a given set of the coefficients, $v_f(t)$ is computed using Eq. (A.7). The PCC control input associated with the obtained buoy's vertical velocity is computed using the system's dynamic model (A,B,C,D matrices).

The SB optimal control problem is formulated as: find the optimal values of the coefficients a_0, a_n, and b_n, $\forall n = 1 \cdots N$ such that the extracted energy is maximized, subject to the constraints: $u(t) < u_{max},\ 0 < t < T$. The optimal control problem is converted to a parameters optimization problem. An interior point optimization algorithm is used for optimizing the coefficients. A good initial guess for the coefficients a_0, a_n, and b_n ($\forall n = 1 \cdots N$) can be obtained if we note that the wave velocity model can be approximated using Fourier series as follows:

$$w(t) = \frac{c_0}{2} + \Sigma_{n=1}^{N} \left(c_n \cos\left(\frac{n\pi}{T} t\right) + d_n \sin\left(\frac{n\pi}{T} t\right) \right) \tag{A.8}$$

In Eq. (A.8), the coefficients c_0, c_n, and d_n can be computed given a prediction for $w(t)$. These coefficients are used as initial guesses for the coefficients a_0, a_n, and b_n, respectively.

The SB approach computes the required control at each control update step over the prediction horizon. These control updates are stored. In order to save computational time, it is possible to use these control updates at subsequent control time steps with updating the control calculations. The number of control steps that do not need control calculations is $CtrlInteg$. There are four parameters that need to be selected in order to start running the software developed in this project. These parameters are:
N_H : = an integer that represents the Horizon length in units of wave period
N_{cw} : an integer that determines the No of control updates in one wave period
N_{FFT} : the number of fourier terms
$CtrlInteg$: an integer that determines the step of updating the control calculations

The optimal selection for these parameters varies depending on the sea-state being solved. Table A.1 shows the parameters' values for some of the irregular sea-states. Table A.2 shows the parameters' values for some of the irregular sea-states.

Table A.1: Selected SB parameters for some of the regular sea-states

	N_H	N_{cw}	N_{FFT}	$CtrlInteg$
RS06	4	10	7	6
RS07	5	15	6	3
RS08	5	15	7	2
RS09	3	15	7	2
RS10	5	30	8	10
RS11	5	30	7	10
RS12	7	40	7	64
RS13	7	80	7	49

Table A.2: Selected SB parameters for some of the irregular sea-states

	N_H	N_{cw}	N_{FFT}	$CtrlInteg$
IS10	3	60	7	3
IS11	3	60	6	3
IS12	3	50	7	2
IS13	3	50	8	2
IS14	3	50	7	2
IS15	3	50	7	2
IS16	3	50	7	2
IS17	3	60	7	2

A.4 LQ

Linear Quadratic control is a pure feedback control strategy (Figure A.1), meaning that the control signal can be expressed as function of the current state by means of the controller $C_{FB}(s)$. For this reason, the LQ control strategy requires a state estimator (block $H_{FB}(s)$). LQ does not include any feedforward block ($C_{FF}(s)$) nor input conditioning block ($H_{ref}(s)$), and the reference signal r is zero.

Linear Quadratic (LQ) optimal control is an optimization based design technique for the calculation of a feedback law. The Linear Quadratic Regulator (LQR) and the Linear Quadratic Gaussian (LQG) controller are two common "special cases" of LQ optimal control problems. In particular, given the linear dynamical system (non-necessarily time-invariant)

$$\dot{x}(t) = A(t)x(t) + B(t)u(t), \tag{A.9}$$

where $u(t) \in \mathbb{R}^m$ is the input and $x(t) \in \mathbb{R}^m$ is the state, the objective of the LQR if to find a

feedback matrix $K(t)$ such that the closed-loop system with feedback[2]

$$u(t) = -K(t)\,x(t) \tag{A.10}$$

minimizes the functional J defined as:

$$J = \int_{t_0}^{t_f} x^T Q x + x^T H\,u + u^T R\,u\;dt + x(t_f)^T\,F\,x(t_f), \tag{A.11}$$

where $Q \geq 0$, $F \geq 0$ and $R > 0$ [15]. The weight matrices Q, H, R and F are in general design parameters to be tuned. The feedback gain K is calculated as $K(t) = R^{-1}B^T P(t)$, where the symmetric matrix P is the solution of the Riccati equation:

$$-\dot{P} = PA + A^T P - (PB + H)\,R^{-1}\left(B^T P + H^T\right) + Q, \tag{A.12}$$

with boundary condition $P(t_f) = F$.

A special case of the LQR problem is the infinite-time and time-invariant LQR, that is when $t_f \to \infty$ and the matrices A and B are constant. In this case, both the gain matrix K and the matrix P are constant; in particular,

$$K = R^{-1}B^T P \tag{A.13}$$

and P is the solution of

$$0 = PA + A^T P - PBR^{-1}B^T P. \tag{A.14}$$

The LQG control problem differs from the LQR in that it concerns dynamical system affected by noise and for which the state is not accessible. The LQG problem is solved by applying the separation principle, stating that the control design and the estimator design can be carried out independently. In practice, the LQG results in a LQR and a Kalman filter, which is used for the estimation of the state from noisy outputs (measurements). The dynamical system in this case is described as[3]

$$\dot{x} = Ax + Bu + v \tag{A.15}$$

$$y = Cx + w, \tag{A.16}$$

where y is the system output, v is the system noise and w is the measurement noise. A fundamental assumption for optimality is that the noise (both v and w) is white and Gaussian. The estimate of the state $\hat{x}$ is given by the Kalman-Bucy filter

$$\dot{\hat{x}} = A\hat{x} + Bu + L(y - C\hat{x}) \tag{A.17}$$

with initial condition $\hat{x}(0) = E[x(0)]$. The Kalman gain L is calculated as $L = SC^T W^{-1}$ with $W = E[ww^T]$. S is the solution of the Riccati equation

$$0 = AS + SA^T - SC^T W^{-1} CS + V \tag{A.18}$$

where $V = E[vv^T]$.

By applying the separation principle, the gain K is calculated as in the LQR case, eq. (A.13), and by using the same Riccati equation in (A.14) for the calculation of P.

[2]Note: $K(t)$ is in general time-dependent

[3]Assumption to simplify explanation: system is time-invariant

Specific embodiment of theory we are applying – Controller model

The control system is designed as a single-input/single-output. However, the LQG allows the design of multi-input/multi-output controllers.

More specifically, the controller model is composed of a linear system (A_d, B_d, C_d) describing the heave dynamics, combined with a second linear system (A_e, B_e, C_e) describing the excitation, which is considered as colored system noise. The dynamic model in heave is

$$\dot{x}_d = A_d x_d + B_d u + B_d f_e \tag{A.19}$$
$$y = C_d x_d, \tag{A.20}$$

while the model of the excitation force is

$$\dot{x}_e = A_e x_e + B_e w \tag{A.21}$$
$$f_e = C_e x_e \tag{A.22}$$

The state vector of the system dynamics is composed as

$$x_d = \begin{bmatrix} z \\ \dot{z} \\ x_r \end{bmatrix}$$

where z is the heave position and x_r is the state of the radiation force model, while the input u is the PCC force and the output y is the heave velocity ($y = \dot{z}$). Thus, the matrices A_e, B_e, C_e are:

$$A_d = \begin{bmatrix} \dots \end{bmatrix} \tag{A.23}$$

The matrices of the augmented state space model are built as:

$$A = \begin{bmatrix} A_d & B_d C_e \\ \mathbf{0} & A_e \end{bmatrix} \qquad B' = \begin{bmatrix} B_d \\ \mathbf{0} \end{bmatrix} \qquad B_v = \begin{bmatrix} \mathbf{0} \\ B_e \end{bmatrix} \qquad C' = [C_d \;\; \mathbf{0}]$$

resulting in the dynamical system

$$\dot{x} = A x + B' u + B_w w \tag{A.24}$$
$$y = C' x. \tag{A.25}$$

The system is analogous to the model for the LQG problem in (A.15) and (A.16). However, the cost functional to be minimized is different. In fact, the objective is to maximize the expected value of the absorbed power $\bar{P}_{abs} = E[-v_{out}\, i]$. The instantaneous power can be written as (fig. A.4)

$$-v_{out}\, i = -(v + R i)\, I = -v i - R i^2.$$

Additionally, the force and velocity are related to the current and voltage as

$$f = K_i\, i \qquad\qquad v = K_v\, \dot{z},$$

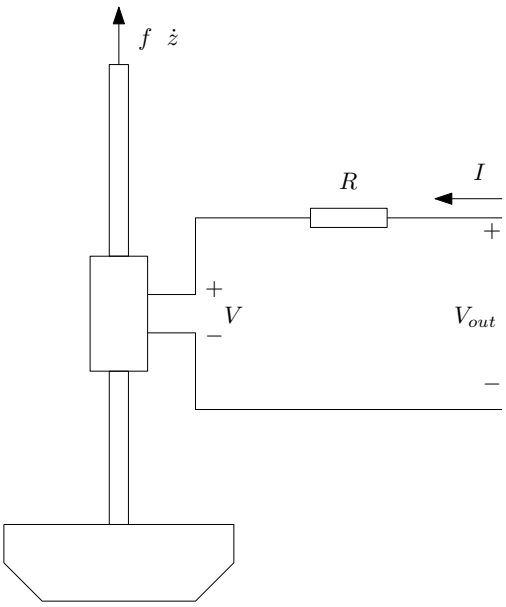

Figure A.4: Schematic

and the dynamical system can be redefined in terms of the current i and the input and the voltage v as the output by redefining B and C as

$$B = B' K_i \qquad\qquad C = K_v C' \tag{A.26}$$

resulting in

$$\dot{x} = Ax + Bi + B_w w \tag{A.27}$$
$$v = Cx. \tag{A.28}$$

Thus, the cost functional to be minimized is[4]

$$J = E\left[x^T H i + i^T R i\right], \tag{A.29}$$

which is written in the same form as the standard LQ problem in (A.11), with $Q = 0$ and $H = C^T$.

Particular ("non-standard") features when applied to wave energy conversion

In general the matrix Q is non-zero. When $Q = 0$ the Weakly Strictly Positive Real condition must be satisfied [27] otherwise a solution for the optimization problem may not exist. In our case this situation has not happened (solution has always been found, so far).

[4]LQ problems in standard forms solve a minimization problem, thus the sign is changed

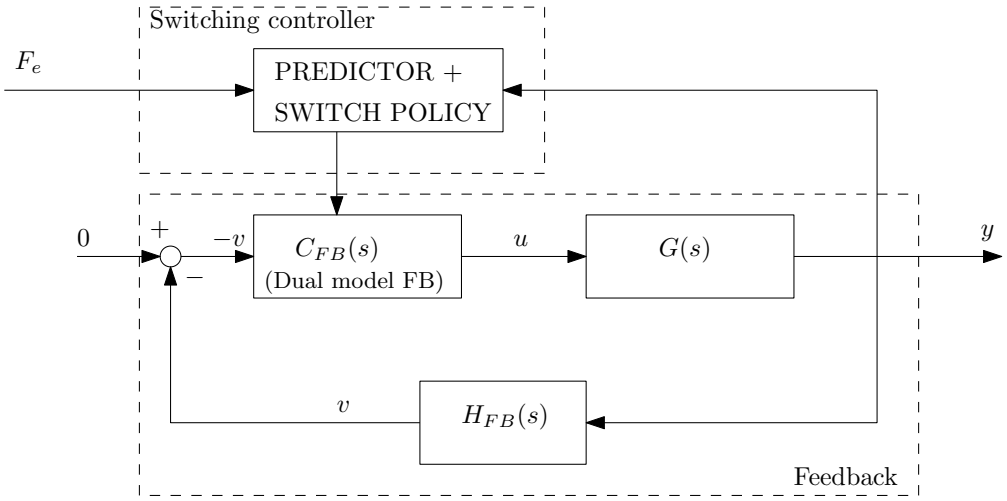

Figure A.5: Structure of latching control

A.5 PDC3 algorithm

A.6 Latching

Latching is a type of switching control (Figure A.5), the implementation of which is carried out by assuming that the force exerted by the linear generator is of the form

$$f_u = -(B_u + u(t)\,G)\dot{z}(t)$$

where $\dot{z}$ is the heave velocity of the buoy and B_u is the damping coefficient used for power absorption, such that the instantaneous absorbed power is $P_u(t) = -f_u(t)\,\dot{z}(t) = B\dot{z}(t)^2$. The control signal $u(t)$ is a switching binary function that takes the value of 0 when the device in unlatched (absorption mode), or 1 when the device is latched. When the device is in latched mode ($u(t) = 1$), then the total of the damping exerted by the PCC is equal to $B_u + G$, where G takes a value large enough to prevent, in practice, the device from moving. However, since the value of G is not infinite, the device moves with a very small velocity when in latching mode.

The optimal switching policy for $u(t)$ can be obtained by using Pontryagin principle [28]; however, this approach is not suitable for real-time implementation because of the high computational cost. The solution chosen for the switching policy is the empirical method described by Budal and Falnes in [30], where the device is being latched whenever it reaches zero velocity, and it is being released a quarter of the resonance period before the next predicted peak in the excitation force. Figure A.6 illustrates the working principle of latching control: by holding the device locked for an appropriate time interval so as the peak of the velocity matched with the peak of the excitation force, the oscillating body moves at considerably higher peak velocity and it absorbs more power.

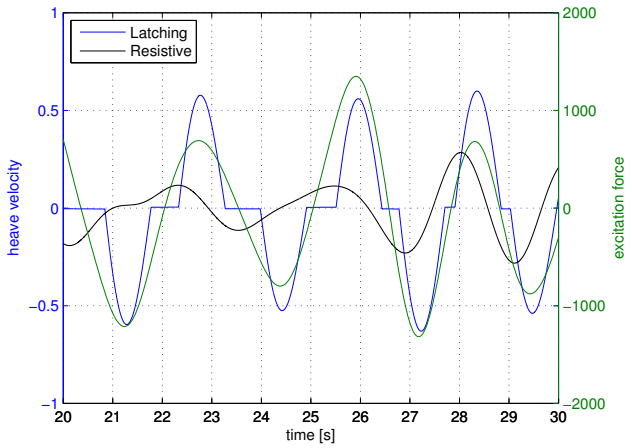

Figure A.6: Heave velocities of latching control vs resistive control

DISTRIBUTION:

1 MS 0899 Technical Library, 9536 (electronic copy)


Sandia National Laboratories